FEDERAL UNIVERSITY OF SANTA CATARINA
DEPARTMENT OF MECHANICAL ENGINEERING

Gonzalo Guillermo Moreno Contreras

A KINESTATIC MODEL FOR THE THREE-DIMENSIONAL STATIC ANALYSIS OF LONG COMBINATION VEHICLES

Florianópolis
2017

Gonzalo Guillermo Moreno Contreras

A KINESTATIC MODEL FOR THE THREE-DIMENSIONAL STATIC ANALYSIS OF LONG COMBINATION VEHICLES

Tese submetida ao Programa de Pós-Graduação em Engenharia Mecânica da Universidade Federal de Santa Catarina para a obtenção do título de Doutor em Engenharia Mecânica.

Orientador: Prof. Daniel Martins, Ph.D.
Coorientador: Prof. Rodrigo de Souza Vieira, Ph.D.

Florianópolis
2017

Ficha de identificação da obra elaborada pelo autor,
através do Programa de Geração Automática da Biblioteca Universitária da UFSC.

Moreno Contreras, Gonzalo Guillermo
A KINESTATIC MODEL FOR THE THREE-DIMENSIONAL STATIC ANALYSIS OF LONG COMBINATION VEHICLES / Gonzalo Guillermo Moreno Contreras ; orientador, Daniel Martins, coorientador, Rodrigo Vieira, 2017.
213 p.

Tese (doutorado) - Universidade Federal de Santa Catarina, Centro Tecnológico, Programa de Pós Graduação em Engenharia Mecânica, Florianópolis, 2017.

Inclui referências.

1. Engenharia Mecânica. 2. Dinâmica veicular. 3. Método de Davies. 4. Seguridade rodoviaria. 5. Combinações de veiculos de carga (CVC). I. Martins, Daniel. II. Vieira, Rodrigo. III. Universidade Federal de Santa Catarina. Programa de Pós-Graduação em Engenharia Mecânica. IV. Título.

Gonzalo Guillermo Moreno Contreras

A KINESTATIC MODEL FOR THE THREE-DIMENSIONAL STATIC ANALYSIS OF LONG COMBINATION VEHICLES

Esta Tese foi julgada aprovada para obtenção do Título de "Doutor em Engenharia Mecânica, Área de concentração Projeto de Sistemas Mecânicos", e aprovada em sua forma final pelo Programa de Pós-Graduação em Engenharia Mecânica da Universidade Federal de Santa Catarina.

Florianópolis, Junho de 13 de 2017.

Prof. Daniel Martins, Dr. Eng.
Orientador

Prof. Rodrigo de Souza Vieira, Dr. Eng.
Co-orientador

Prof. Jonny Carlos da Silva, Dr. Eng .
Coordenador do Programa de Pós Graduação em Engenharia Mecânica - POSMEC

Banca Examinadora:

Prof. Daniel Martins, Dr. Eng.
Presidente
Universidade Federal de Santa Catarina

Prof. Tarcisio Antonio Hess Coelho, Dr. Eng.
Universidade de São Paulo – (USP).

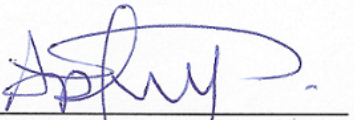

Prof. Anibal Alexandre Campos Bonilla, Dr. Eng.
UDESC- Joinville – Santa Catarina

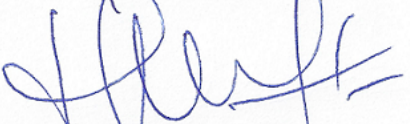

Prof. Edson de Pieri, Dr. Eng.
Universidade Federal de Santa Catarina

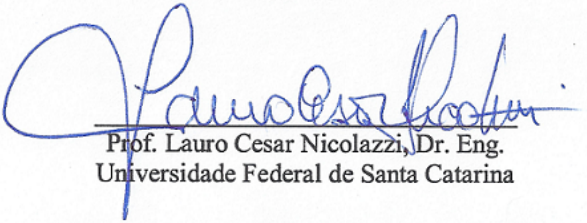

Prof. Lauro Cesar Nicolazzi, Dr. Eng.
Universidade Federal de Santa Catarina

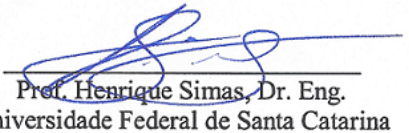

Prof. Henrique Simas, Dr. Eng.
Universidade Federal de Santa Catarina

RESUMO

A movimentação de carga no Brasil é amplamente dominada pelo transporte rodoviário, dentro do qual se destacam as Combinações de Veículos de Carga (*CVC's*). Estes tipos de veículos oferecem uma maior capacidade de carga, impactando em uma diminuição dos custos de transporte e assim, elevando a eficiência e competitividade das empresas e do país. Mas as *CVC's* possuem baixa estabilidade lateral, o que está causando o crescimento na incidência dos acidentes de tombamentos destes veículos. Em geral, as *CVC's* mostram um baixo desempenho com respeito à estabilidade, e isto tem sido o foco de muitos estudos em todo o mundo. Algumas características tais como, suspensão, pneus, chassis e quinta roda foram analisadas separadamente, para determinar a sua influência sobre a estabilidade lateral de veículos. A maioria dos modelos de estabilidade dos veículos não consideram aspectos longitudinais do veículo e da estrada, como a rigidez do chassis, a localização longitudinal do centro de gravidade e o ângulo de inclinação longitudinal da estrada. A utilização de modelos tridimensionais de veículos permitem uma análise mais rigorosa da estabilidade do veículos. Neste contexto, o objetivo deste estudo é o desenvolvimento de um modelo de mecanismo tridimensional para representação da última unidade de uma *CVC* (reboque) submetido a um carregamento lateral crescente até atingir o limiar de tombamento. O modelo proposto leva em conta o movimento do centro de gravidade do reboque, o qual é afetado pelos movimentos impostos na suspensão, pneus, sistema de engate e o chassi do reboque. O método de Davies tem demonstrado ser uma ferramenta importante na análise de mecanismos, e por isso é aplicado para a análise cinestática do mecanismo tridimensional do reboque.

Palavras-chave: Tombamento. Combinações de veículos de carga (*CVC's*). Estabilidade. Método de Davies. Segurança rodoviária.

RESUMO EXPANDIDO

Introdução

A segurança é uma preocupação comum para todos os usuários das estradas. Ela é desafiada pela densidade de tráfego, que aumentou consideravelmente nos últimos anos e é esperado que continuasse a aumentar no futuro. Além disso, a introdução de veículos mais longos e mais pesados é um desafio ainda maior em questões de segurança rodoviária. Estes veículos denominados combinações de veículos de carga (CVC's) oferecem uma maior capacidade de carga, impactando em uma diminuição dos custos de transporte. Mas as CVC's possuem baixa estabilidade lateral, o que está causando o crescimento na incidência dos acidentes de tombamentos destes veículos. Tendo em conta todos estes fatores, neste estudo e analisado o fenômeno da estabilidade em veículos pesados e é desenvolvido um mecanismo que permite avaliar o limiar de tombamento das combinações de veículos de carga.

Objetivos

O objetivo principal deste estudo é o desenvolvimento de um modelo de mecanismo tridimensional para representação da última unidade de uma CVC (reboque) submetido a um carregamento lateral crescente até atingir o limiar de tombamento. O modelo proposto leva em conta o movimento do centro de gravidade do reboque, o qual é afetado pelos movimentos impostos pelos sistemas de suspensão, pneus, quintaroda e o chassi.

Metodologia

Para o desenvolvimento do modelo proposto são estudados os principais modelos de estabilidade presentes na literatura; também são estudados os mecanismos que influenciam o movimento do centro de gravidade e os grãos de liberdade permitidos por cada um destes. Isto permite o desenvolvimento dos sub-mecanismos que conformam o mecanismo principal que representa a ultima unidade de uma CVC (reboque). A estática do modelo proposto é analisada com ajuda do método de Davies, o modelo é submetido a um carregamento lateral crescente até atingir o limiar de

tombamento, isto permite determinar a aceleração lateral máxima que suporta o veículo até o limiar de tombamento e a velocidade máxima com a qual o veículo pode percorrer uma curva.

Resultados e discussão

Neste documento são realizados diferentes casos de estudo: nos primeiros casos são comparado os resultados dados pelo modelo proposto e os resultados dados por os modelos desenvolvidos nos programas computacionais especializados Adams e Trucksim, isto permitio determinar que o modelo proposto aporta bom resultados em termos de estabilidade veícular. Nos seguintes casos de estudo são analisados vários veículos comuns nas estradas de Brasil, estes estudos permitirem determinar as velocidades máximas com a qual estes veículos podem percorrer diferentes curvas com segurança. Os resultados obtidos demostraram que os atuais limites de velocidades são altos, o qual ocasiona que em sertãs situações os veículos analisados estejam propensos ao tombamento.

Considerações finais

O modelo proposto permitira avaliar a estabilidade de diferentes combinações de veículos de carga só sertãs condições de carga, os resultados obtidos podem ser empregados para avaliar o desempenho dos veículos, o desempenho dos mecanismos que influenciam a estabilidade do veículo, e também se pode avaliar a logística de transporte de carga no Brasil.

Palavras-chave: Tombamento. Combinações de veículos de carga (*CVC's*). Estabilidade. Método de Davies. Segurança rodoviária.

ABSTRACT

The cargo transportation in Brazil is mostly dominated by road transport, using Long Combinations Vehicles (*LCV's*). These types of vehicles offer more load capacity, which reduce transport costs and thus increase the efficiency and competitiveness of companies and of the country. But the tradeoff of *LCV's* are their low lateral stability and propensity to rollover. In general, *LCV's* show poor performance with regard to stability, and this has been the focus of many studies around the world. Some characteristics such as the suspension topology, tires, chassis and fifth wheel have been analyzed, separately, to determine their influence on the lateral stability of vehicles. Most vehicle stability models do not consider the longitudinal aspects of the vehicle and the road such as the stiffness of the chassis, the gravity center location, and the longitudinal slope angle of the road. The use of three-dimensional models of vehicles allows a more rigorous analysis of the vehicle stability. In this context, the aim of this study is to develop a three-dimensional mechanism model to represent the last trailer unit of a *LCV* under an increasing lateral load until it reaches the rollover threshold. The proposed model takes into account the movement of the center of gravity of the trailer which is affected by the movements resulted by suspension, tires, fifth-wheel and chassis of the trailer. Davies method has proved to be an important tool in the kinetostatic analysis of mechanisms, and therefore it is employed for the kinetostatic analysis of the three-dimensional mechanism of the trailer.

Keywords: Rollover. Long combination vehicles (*LCV's*). Stability. Davies method. Road safety.

Este trabalho é dedicado aos meus pais
à minha esposa, à minha família,
meus amigos e a todos aqueles que me
apoiaram na minha trajetória até aqui.

ACKNOWLEDGEMENTS

Ao realizar uma retrospectiva do meu doutorado, vejo que todo caminho e todo projeto tem suas dificuldades; mas nossa fé e todas as pessoas que temos a nosso lado fizeram um importante aporte para a conclusão de nossos sonhos.

Começo a agradecer a Deus e a Nossa Senhora de Aparecida que guiaram meus passos e me deram forças para enfrentar diversas situações.

Aos meus pais Gonzalo Moreno e Marlene Contreras, às minhas irmãs, sobrinhos, e a toda minha família (CONTRERERIO.COM) pelo apoio, paciência, compressão e amor proporcionado ao longo da minha vida.

A minha esposa Nathaly García, pela paciência, apoio, esforço e amor, durante todo este tempo; pelos conselhos no momento oportuno, pelos momentos felizes e tristes (sempre se aprende algo); hoje eu acredito que todos nossos sonhos são importantes e possíveis quando se tem a nosso lado a companhia perfeita.

A minha sogra e as minhas cunhadas pelo apoio dado durante todo este tempo, muito obrigado.

Aos meus grandes e eternos amigos da Colômbia, especialmente a Nury, Sandra, Juan Pablo, Yesid e Renzo, este tempo na Ilha da Magia foi maravilhoso. Muito abrigado pela amizade e pelos momentos felizes compartilhados.

Ao Prof. Daniel Martins e ao Prof. Rodrigo de Souza Vieira por acreditar nas minhas capacidades, e que com sabedoria souberam lidar com todas as turbulências no desenvolvimento do projeto, muito obrigado pelas ideias e contribuições feitas.

Ao Prof. Lauro Nicolazzi, muito obrigado pelas ideias e contribuições feitas para o desenvolvimento deste projeto.

Às empresas Mechanical Simulation e Virtual CAE pela ajuda fornecida com a licença do software TruckSim.

Ao pessoal do Laboratório de Robótica (LAR), a Julio, Marcel, Thaís, Leonardo, Neider, Camilo, Estevan, Rodrigo, Elias, Fabiola, Leandro, Humberto, etc., como eu aprendi com vocês! Muito obrigado por se disponibilizarem e por toda a ajuda fornecida.

A Vangelo Manenti e a Thiago Rios, muito obrigado por se disponibilizarem e por toda a ajuda fornecida.

A CAPES, CNPq e a Universidade de Pamplona (Pamplona- Colômbia) pelo apoio financeiro fornecido.

"Deus é o dono de tudo. Devo a Ele a oportunidade
que tive de chegar aonde cheguei. Muitas pessoas
têm essa capacidade, mas não têm essa oportunidade.
Ele a deu para mim, não sei por quê.
Sei que não posso desperdiçá-la.
(Ayrton Senna)

LIST OF FIGURES

LIST OF TABLES

LIST OF SYMBOLS AND ABBREVIATIONS

Roman

A	Transformation matrix	
a	Distance from the front axle to the center of gravity	m
b	Lateral separation between the springs	m
c	Number of constraints	
d	Translation of the prismatic joint (Screw parameter)	m
E	Modulus of elasticity	$N.m^2$
e	Tangent of the bank angle	%
F	Force	N
G	Modulus of rigidity (or Shear Modulus)	Pa
g	Gravity acceleration	m/s^2
h	*CG* height	m
j	Number of mechanical joints	
k	Number of cuts	
L	Wheelbase of the trailer	m
l	Length of the leaf spring	m
LLT	Lateral load transfer	
M	Degrees of freedom (DoF)	
m	Mass of the vehicle	kg
n	Number of mechanical links	
P	Prismatic joint	

R	Revolute joint	
S	Spherical joint	
s	Unit vector along the direction of the screw axis	
T	Torque that act on the revolute joint	N.m
t	Vehicle track	m
V	Vehicle speed	km/h
W	Vehicle or trailer weight	N
x	Constant that allows to control the torque distribution of the chassis	

Greek

α	Linear coefficient of thermal expansion	$1/^{o}C$
δ	Elastic deformation	m/m
ε	Longitudinal tilt angle of the roll axis	^{o}
θ	Rotation angle of the revolution joint or roll angle	^{o}
λ	Degrees of freedom of the space in which the mechanism is intended to move	
ν	Number of independent loops in the mechanism	
τ	Torque	N.m
ϕ	Bank angle	%
φ	Slope angle	%
ψ	Trailer/trailer angle	^{o}
Ψ	Magnitude vector of the wrench	

Composed and constants

$\$^{A}$	Wrench
$\widehat{\$}^{A}$	Normalized wrench (screw)
$[A_N]$	Action matrix
$[A_d]$	Action matrix

$[\widehat{A}_{np}]$	Primary action matrix	
$[\widehat{A}_{ns}]$	Secondary action matrix	
A_b	Cross-sectional area of the bar	m^2
a_c	Regression coefficient	N/m
a_y	Lateral acceleration	m/s^2
b_1	Fifth-wheel width	m
b_l	Width of the leaf	m
C_i	System variable i	
d_1	Offset of the cargo, lateral CG displacement	m
d_2	Longitudinal CG displacement	m
d_3	Vertical CG displacement	m
E_s	Modulus of elasticity for a multiple leaf	$N.m^2$
F_{FWn}	Fifth-wheel normal load n	N
F_f	Normal force of the front mechanism	N
F_i	Force i	N
F_{LSn}	Spring normal load n	N
F_n	Normal load	N
F_p	Perpendicular load	N
F_r	Normal force of the rear mechanism	N
F_{Ti}	Instantaneous tire normal load i	N
F_{xi}	Tire traction or brake force i	N
F_{yi}	Tire lateral force i	N
F_{zi}	Tire normal load i	N
F_{zi}^{start}	Initial normal load i	N
f_{max}	Maximum side friction factor	

$\triangle F$	Algebraic change in the initial load	N
$\triangle F_z$	Rate of normal load transfer	N
G_A	Direc coupling graph	
h_0	*CR* height	m
h_1	Instantaneous lateral distance between the zero-reference frame and the trailer *CG*	m
h_2	Instantaneous *CG* height	m
h_5	Fifth-wheel height	m
$[I]$	Incident matrix	
J_f	Equivalent polar moment of the trailer front frame	m^4
J_r	Equivalent polar moment of the trailer rear frame	m^4
k_1	Stiffness of the helical spring	N/m
k_2	Spring's torsion coefficient	N.m/rad
k_f	Stiffness of the fifth-wheel	N/m
k_{Ls}	Equivalent stiffness of the suspension	N/m
k_s	Equivalent spring stiffness	N/m
k_{st}	Spring's torsion coefficient	N.m/rad
k_T	Equivalent vertical rubber stiffness	N/m
k_t	Vertical stiffness of rubber	N/m
k_θ	Roll stiffness of the suspension	N.m
$k_{\theta f}$	Roll stiffness of the front suspension	N.m
$k_{\theta r}$	Roll stiffness of the rear suspension	N.m
LLT_f	Lateral load transfer on the front axle	
LLT_r	Lateral load transfer on the rear axle	
L_b	Original lenght of the bar	m
l_{12}	*CG* height above the chassis	m

l_{13}	Distance between the fifth-wheel and the trailer front axle	m
l_c	Number of chords	
l_f	Instantaneous height of the fifth-wheel system (n = 5,6)	m
l_{fw}	Initial height of the fifth-wheel system (n = 5,6)	m
l_i	Instantaneous dynamic rolling radii of tire (i = 1,2,7,8)	m
l_n	Instantaneous height of the leaf spring (n = 3,4,9,10)	m
l_r	Initial dynamic rolling radius of tire i	m
l_{re}	Distance from the center of gravity to the rear axle	m
l_s	Initial height of the leaf spring (n = 3,4,9,10)	m
M_p	Moment of the prismatic joint	N.m
M_θ	Moment about the roll axis	Nm
n_l	Number of the leaves	
$[Q]$	Mechanism cut-set matrix	
P_1	System variable	
P_x	Component of force on x-axis	N
P_y	Component of force on y-axis	N
P_z	Component of force on z-axis	N
p_1	Reference position matrix	
p_2	Instantaneous position matrix	
p_i	System variable i	
R_c	Radius of curvature	m
R_{min}	Minimum radius of curvature	m
S_d	Spherical slider joint	
SRT_{2D-CB}	Static rollover threshold for the Chang model	
SRT_{2D}	Static rollover threshold for a rigid model	
SRT_{2D-B}	Static rollover threshold with bank angle	

SRT_{2D-R} Static rollover threshold for the Rill model

SRT_{2DTM} Static Rollover threshold for a two-dimensional trailer model in a road with bank angle

SRT_{2D-W} Static rollover threshold for the Winkler model

SRT_{3D-G} Static rollover threshold for the Gillespie model

SRT_{3D-N} Static rollover threshold for the Navin model

SRT_{3D} Static rollover threshold for a trailer model with all compliant

SRT_{off} Static rollover threshold for a trailer model with lateral offset of the cargo

SRT_t Static rollover threshold for a trailer model with tire influences

SRT_{ts} Static rollover threshold for a trailer model with tire and suspension influence

SRT_{rv} Static rollover threshold for a rigid trailer model

$SRT_{\psi\phi\varphi}$ Three-dimensional Static Rollover Threshold

s_0	Position vector of a point lying on the screw axis	
s_{0i}	Instantaneous position vector	
T_{CG}	Torque applied by the forces acting on the *CG*	N.m
T_f	Torque applied on the trailer front axle	N.m
T_{fx}	Torque applied on the trailer front axle in *x*-axis	N.m
T_{fy}	Torque applied on the trailer front axle in *y*-axis	N.m
T_r	Torque applied on the trailer rear axle	N.m
t_i	Front and rear track widths (i = 1,3)	m
t_{i+1}	Front and rear axle widths (i = 2,4)	m
t_l	Thickness of the leaf	m
$\triangle T$	Algebraic change in the temperature	^{o}C
$\triangle t$	Lateral position of the *CG* relative to the center of track	m
δ_F	Deformation by force	m/m

δ_{LS}	Leaf spring deformation	m/m
δ_S	Spring deformation	m/m
δ_T	Thermal deformation	m/m
δ_t	Vertical rubber or tire deformation	m/m
δ_{Total}	Total axial deformation	m/m
θ_{3D}	Total body roll angle of the trailer	^{o}
$[\Psi_p]$	Primary variable vector	
$[\Psi_s]$	Secondary variable vector	

Abbreviation

AASHTO American Association of State Highway and Transportation Officials

ABNT Associação Brasileira de Normas Técnicas

ABS Antilock Brake Systems

ANFAVEA Associação Nacional dos Fabricantes de Veículos Automotores

ANTT Agência Nacional de Transportes Terrestres

CG Center of gravity

CNT Confederação Nacional do Transporte

CONTRAN Conselho Nacional de Trânsito

CR Roll center

CVC Combinações de Veículos de Carga

DENATRAN Departamento Nacional de Trânsito

DoF Degrees of Freedom

ESC Electronic Stability Control

FEM Finite Element Method

LCV Long Combinations Vehicle

LLT Lateral load transfer

RA	Rearward Amplification
SRT	Static Rollover Threshold
VJM	Virtual Joint Method

CONTENTS

Chapter 1

INTRODUCTION

Safety is a common concern for all roads users. It is challenged by the traffic density, which has increased substantially over the past years and is expected to continue to rise in the future. Also the introduction of longer and heavier vehicles, challenges road safety.

In this contex, road transport has been the preference for overland transport of goods in Brazil. Figure 1 shows that such kind of transportation moves around 61% of the cargo in Brazil is carried by road (CAIXETA, 2003; CNT, 2016) and, considering only containerized cargo, this share reaches up to 90% (ARAUJO *et al.*, 2013).

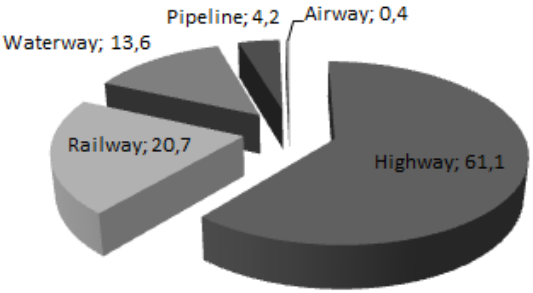

Figure 1 – Brazilian Transport Matrix.
Source: Adapted of CNT (2016).

While large territorial countries, such as the United States, Canada, China, Australia and Russia, use predominantly railway and waterway transport over road transport, exactly the opposite occurs in Brazil, where there is a predominance of the road mode, as shown in Fig. 2 .

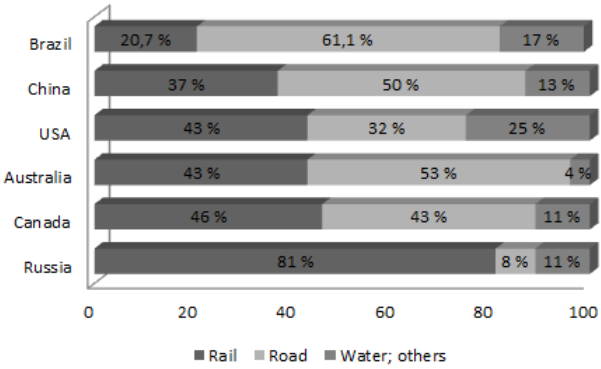

Figure 2 – World Transport Matrix.
Source: Adapted of Costa (2012).

In this context, long combination vehicles (*LCV's*) emerged as a solution to increase the volume of cargo transportation, as a low price solution. Many countries worldwide, including Brazil, approved the road traffic of this type of vehicle in order to be more competitive. Despite the advantages of this kind of transportation, there are some aspects of their stability that make them unreliable vehicles.

In the last years, Brazil has faced a strong increase of *LCV's* models. According to Lopes *et al.* (2008), DENATRAN (2009), and Petrassi (2010), in Brazil there are about three hundred thousand *LCV's*, divided into 61 different types of *LCV's* approved by the DENATRAN (2009) and ANTT (2016a) over Brazilian roads, such as the Semi-trailer, B-Train, Turnpike double (or Road-train) and the Triple-Trailer Combination.

Besides this complex scenario, the B-train and the Road-train are the most common in Brazil (GONCALVES, 2006), thanks to their advantages regarding other cargo vehicles, such as load capacity 45 % higher, and operating costs reductions of about 16 % less. Figure 3 shows typical configurations of three common types of *LCV's* operating in Brazil.

For the year 2017, the *LCV's* have become the primary way of cargo transportation in Brazil. According to the ANTT (2016a) there are about 2.24 million registered cargo vehicles on Brazilian roads, under several classifications made by the DENATRAN (2009) and ANTT (2016b).

In recent years, the incidence of the rollover crashes of *LCV's* has been increasing dramatically. This issue has encouraged the development of many static and dynamic studies looking for a better understanding

regards the factors involved in this type of incident.

The high rates of vehicle crashes and their consequences are the main reasons to do a study and a simulation of a three-dimensional model for lateral stability analysis of *LCV's*. According to IPEA (2015) in Brazil in the year 2014, there were about 167 thousand vehicle crashes, with a balance of 8233 people killed and 26 thousand wounded. The same research estimates that the country spends close to U$ 13 billion per year as hospital costs, loss of future incomes, traffic jams, damage to vehicles, etc.

According to Jabour (2004), the heavy vehicles were involved in 36 % of all accidents (about 10 % of rollover). Even though for this accident the rate is low, the number of people killed, wounded and economic loss are very high.

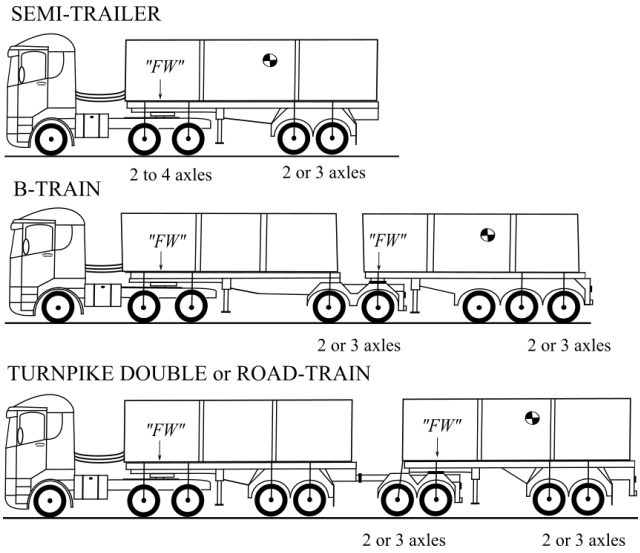

Figure 3 – Long combination vehicles (*LCV's*).

All *LCV's* are subjected to high inertial forces when performing evasive manoeuvres and turns. These forces influence directly the vehicle stability, and, when a limit is reached, they may cause the rollover. The rollover can be defined as any manoeuvre in which a vehicle rotates 90^o or more around its longitudinal axis and one side touches the ground (GILLESPIE, 1992).

According to Winkler and Ervin (1999), all rollover events in the

real world are dynamic events to some extent; no event is truly static. However, there is a very strong relationship between the basic static roll stability of the heavy vehicle and the actual occurrence of rollover in accidents.

The stability of *LCV's* has been the focus of research efforts in recent decades. A variety of measurements has been defined to parameterize the stability of *LCV's*. The *Static Rollover Threshold* (SRT) is one of the most important parameters used to define the stability of vehicles. This factor is highly dependent on the location of the vehicle center of gravity (*CG*), and it represents the maximum lateral acceleration - a_y (expressed in terms of gravity acceleration - g) in a quasi-static situation immediately before one tire loses contact with the ground (WINKLER, 1987; GILLESPIE, 1992; HAC, 2002).

Gillespie (1992), Winkler (2000), Chang (2001), Rill (2011) developed two-dimensional models to determine the SRT factor of heavy vehicles, but two-dimensional models implicitly consider that the vehicles have only two contact points to the road when making a turn (the inner and outer tire on the turn). However, vehicle models in general have at least four contact points (BLUNDELL; HARTY, 2004; RILL, 2011), which has a significant influence on the vehicle stability.

In the last decade, three-dimensional vehicle models have been developed (BOUTELDJA *et al.*, 2004; DAHLBERG; WIDEBERG, 2004; GASPAR *et al.*, 2005; HAC *et al.*, 2008; CHEN; CHEN, 2009), these models have analyzed different characteristics of the vehicles, such as: stiffness of the chassis, the fifth wheel location, inertial forces, rearward amplification (*RA*), adverse environmental conditions, etc.

In this context, according to Winkler (2000), Rill (2011), Kamnik *et al.* (2003), and Zhou and Zhang (2013), the chassis of the vehicle has a significant torsional compliance, which would allow its front and rear parts to roll almost independently.

Additionally, according to Jindra (1966), Rempel (2001), and Melo (2004) the last unit (trailer) of a *LCV* is subjected to a high lateral acceleration compared to the tractor unit, this acceleration is caused by the phenomenon known as rearward amplification (*RA*), impacting the rollover threshold of the last unit and the vehicle. For this reason, the last trailer of the *LCV's* is the critical unit and it is prone to rollover.

For these reasons, three-dimensional vehicle analysis offer a new rollover insight. As a consequence, more knowledge enables the SRT factor to be more precise, resulting in better road safety.

During the development of this research, we analyzed the last trailer of *LCV's* (MORENO *et al.*, 2015; MORENO *et al.*, 2016), and reported

that the SRT factor represents a three-dimensional phenomenon, and that longitudinal parameters and the lateral load transfer (*LLT*) play important roles in relation to the SRT factor calculation.

Other researchers have described that the bank angle and the longitudinal slope of the road (as show in Fig. 47) also influence the SRT factor calculation (CHANG, 2001; AASHTO, 2003; WOODROOFFE *et al.*, 2010).

Taking all these aspects into account, we developed a three-dimensional simplified mechanism model that represent the last trailer of a *LCV* (Fig. 4), this model considers the main characteristics of trailer, and the road such as: suspension, tires, fifth-wheel, chassis, bank angle, longitudinal slope angle and trailer/trailer angle, to calculate the three-dimensional SRT factor for a trailer in different situations. The results obtained with this research were published in Moreno *et al.* (2015), Moreno *et al.* (2016), Moreno *et al.* (2016a), Moreno *et al.* (2016c), Moreno *et al.* (2016b).

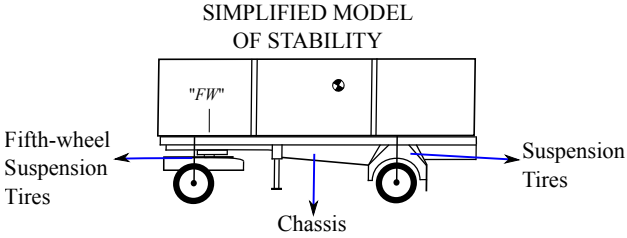

Figure 4 – Three-dimensional simplified model.

In this work the formalism described by Davies (1983b) is used as the primary mathematical tool to analyze the mechanisms statically. The Davies method appears in many publications and further details regarding its use can be found in the literature (DAVIES, 1983b; TSAI, 1999; ERTHAL, 2010; MEJIA *et al.*, 2013).

1.1 OBJECTIVE

The main objective of this work is to develop a three-dimensional mechanism model to evaluate the stability of *LCV's* taking into account different characteristics of the trailer and the road such as: suspension, tires, fifth-wheel, chassis, bank angle, longitudinal slope angle and trailer/-trailer angle. Some specific objectives are listed below:

(i) Understand how the characteristics of the trailer may influence stability performance.

(ii) Develop a mechanism model that represents a critical unit of the *LCV's* (trailer), and that includes different characteristics of the trailer and the road.

(iii) Analyze the influence of the characteristics of the vehicle and the road in the stability calculation.

(iv) Compare the new proposed model of stability with other approaches found in the literature.

1.2 MOTIVATION

As mentioned above, research efforts are currently being made worldwide to develop mathematical models that allow a better understanding of the rollover crashes of *LCV's*. The inclusion of vehicle and road characteristics allows to evaluate their influence on the static rollover threshold of the vehicle.

With an ever increasing number of vehicles on highways today, fatalities due to vehicle rollover are becoming a larger concern. Increased driver distraction, increased *LCV's*, along with increased speed in same cases all lead to more accidents. Automobile manufacturers have been developing and implementing better safety features, improving safety standards, and creating more rigorous manoeuvres for the testing of new vehicles. While these attitudes aided in crash avoidance and severity reduction, more can be done to further save lives and money.

Researcher interested in initiating study on rollover dynamics is left with the challenging task of identifying suitable vehicle models from the literature, comparing these models in their respective behaviour and in their ability to match experimental results, and determining suitable parameters for the models. This work seeks to address these issues via comparisons between the developed model and experimental and computational results so that this divide may be bridged.

In this context, this work was motivated by the possibility to contribute concurrently in the following fronts:

• Increase of the road safety in Brazil and worldwide.

• Developed a tool that can be used to improve the processes of: vehicle designers, road designers, insurance companies, transport companies, etc.

1.3 TESTS OF STABILITY

As mentioned above, the SRT factor is a one of the most important parameters used to define the stability of vehicles. In this context, the Steady State Circular Test (ISO-14792, 2011) was adapted and selected to analyze the static rollover threshold of the trailer model (DELANNE *et al.*, 2003; BARICKMAN *et al.*, 2011; LIMA *et al.*, 2011).

In the circular test, the vehicle is driven around a circle with a constant radius. Starting from rest, this manoeuvre increased the inertial force (ma_y) at a moderate rate proportionately with the square of velocity. Assuming that the vehicle in the limit of the rollover do not slip, the tests were completed, when the *LLT* coefficient in the rear axle become complete (the entire load is transferred from the rear inner tire to the rear outer tire when the trailer model makes a turn).

1.3.1 Load conditions

A total of three load conditions of the trailer were used in this work:

• the recommended load capacity (CONTRAN, 2011): the load is laterally centered and was tested the influence of the suspension, tires, fifth-wheel, chassis, trailer/trailer angle, bank angle and slope angle on the stability of the trailer,

• normal load with *CG* displacement: it was tested the influence of the load distributions on the stability of the trailer, and

• overweight: it was tested the influence of the overweight on the stability of the trailer.

1.4 THESIS OVERVIEW

This work is organized as summarized below.

Chapter 2 presents the vehicles stability problem and a literature review, Chapter 3 presents the static analysis tools used to develop the three-dimensional model of the vehicle, Chapter 4 presents the development of the two and three-dimensional model of the trailer, and the load distribution of the trailer model, Chapter 5 presents the static analysis of the two-dimensional trailer model using the Davies method, and the comparing with the approaches found in the literature, Chapter 6 presents the static analysis of the three-dimensional trailer model using the Davies method, and the comparing with the approaches found in the literature, Chapter 7 presents the comparison between a two-dimensional model developed with Adams and the two-dimensional model developed in the Chapter 5,

Chapter 8 presents the comparison between a three-dimensional model developed with TruckSim and the three-dimensional model developed in the Chapter 6, Chapter 9 presents a case study of stability, where the influence of the characteristics of the vehicle and the road were analyzed, nnd finally, Chapter 10 and 11 present the conclusions and the topics for further works.

Additionally to the eleven main chapters described previously, the list of publications generated by this work is included, and the description of the Davies method and two examples of the vehicles stability are included in the appendix.

Chapter 2

LITERATURE REVIEW

This chapter presents the factors that influence the rollover crash and the main models of heavy vehicle stability.

The stability of *LCV's* has been the focus of research efforts in recent decades. A variety of measurements have been defined to parameterize the stability of *LCV's*. The SRT factor is one of the most important parameters used to define the stability of vehicles.

2.1 CONTRIBUTING FACTORS IN ROLLOVER CRASH

Many factors related to heavy vehicle operation, as well as factors related to roadway design and road surface properties, can cause heavy vehicles to become yaw unstable or to roll. Described below are several real-world situations where roll or electronic stability control systems may prevent or lessen the severity of crashes (WOODROOFFE *et al.*, 2009; BARICKMAN *et al.*, 2011):

• **Speed too high to negotiate a curve** - speed of vehicle is too high to safely negotiate a curve. When the lateral acceleration of a vehicle during a manoeuvre exceeds the vehicle's roll stability threshold, a rollover is initiated. A driver typically cannot recover from the rollover once it begins.

• **Sudden steering manoeuvres to avoid a crash** - driver makes an abrupt steering manoeuvre, such as a single or double lane change manoeuvre, or attempts to perform an off-road recovery manoeuvre, generating a lateral acceleration that is sufficiently high to cause a rollover. Manoeuvring a vehicle on off-road, unpaved surfaces such as grass, gravel, or dirt may require a larger steering input (larger wheel slip angle) to achieve a given vehicle response, and this can lead to a large increase in lateral acceleration once the vehicle returns to the paved surface.

• **Loading conditions** - vehicle yaw due to over-steer is more likely to occur when a vehicle is in a lightly loaded condition and has a low center of gravity height. Heavy vehicle rollovers are much more likely to occur when the vehicle is in a loaded condition as a result of a high center of gravity height. Cargo that is placed off-center in the trailer will result in the vehicle being less stable in one direction than the other. It is also possi-

ble that improperly secured cargo can shift while the vehicle is negotiating a curve, thereby reducing the roll stability.

Sloshing can occur in tankers transporting liquid bulk cargoes. This condition is of particular concern when the tank is partially full because the vehicle may experience significantly reduced roll stability during certain manoeuvres.

• **Road surface conditions** - the road surface condition can also play a role in the loss of control of vehicle. On a dry, high friction asphalt or concrete surface, a tractor trailer combination vehicle executing a severe turning manoeuvre is likely to experience a high lateral acceleration, which may lead to a rollover. A similar manoeuvre performed on a wet or slippery road surface may result in vehicle yaw.

• **Road design configuration** - some drivers may misjudge the curvature of ramps and not brake sufficiently to safely negotiate the curve. This includes ramps with decreasing radius curves as well as curves and ramps with improper signage. A decrease in superelevation (banking) at the end of a ramp where it merges with the roadway causes an increase in vehicle lateral acceleration (and may be accompanied by the driver accelerating in preparation to merge) may result in rollover.

• **Braking manoeuvres** - most common heavy vehicle yaw (jackknife) events occur due to rear wheel lockup during braking. If the rear wheels are locked, they cannot generate any lateral force and only a very small side force (roadway crown or slight trailer angle) is needed to cause the tractor to lose directional control. Also, loss of steering control or "plow-out" can occur due to front wheel lockup, although this is most likely to happen on a heavy vehicle under light loading conditions and slippery road surfaces. Since most jackknife crashes are caused by lockup of the tractor's rear wheels during braking, the requirement for antilock brake systems (ABS) on truck tractors, effective since 1997, has largely addressed the loss of-control crashes due to wheel lockup. As a result, electronic stability control (ESC) is expected to reduce crashes other than braking-related jackknife crashes.

• **Vehicle factors** - The tires, suspension, fifth-wheel and chassis are directly responsible for the *CG* movements; these movements are dependent on the forces acting on the trailer *CG*, such as weight (W), disturbances forces imposed by the ground and lateral inertial force (ma_y) when the vehicle makes a turn.

Severely worn tires (e.g., tread depth below 1.58 mm) are more likely to contribute to vehicle yaw or under-steering under wet slippery conditions. The condition of the vehicle's brakes, including brake adjustment, is critical in enabling the driver to reduce speed for upcoming curves, and also

to prevent brake fade from occurring on long downhill grades. Replacing tires that have insufficient tread depth and maintaining the ABS in proper operating condition are critical in preventing jackknife events and trailer swing during panic braking.

2.2 STATIC ROLLOVER THRESHOLD FOR TWO-DIMENSIONAL MODELS

Some researchers have defined mathematical equations to calculate the SRT factor (GILLESPIE, 1992; HAC, 2002; WINKLER, 1987), some models are presented below.

2.2.1 Rigid model

The coefficient estimation originally supposes a completely rigid two dimensional vehicle supported in two tires, as presented in Fig. 5. During cornering (vehicle on a left curve), the lateral tire forces on the ground level (not shown) counterbalance the lateral inertial force acting on the vehicle gravity center, resulting in a roll moment. Considering the moments about the zero-reference frame - A point (Fig. 5):

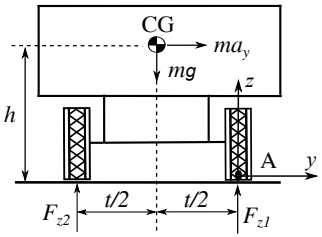

Figure 5 – Rigid vehicle model.

$$\sum M_A = mg\frac{t}{2} - ma_y h - F_{z2}t = 0 \tag{2.1}$$

where a_y is the lateral acceleration acting over the vehicle gravity center, g is the gravitational acceleration, m is the mass of the vehicle, h is the CG height, t is the vehicle track and F_{zi} is the tire normal load i.

Initially for the vehicle of the Fig. 5, the weight is equally distributed on both sides (RILL, 2011), then the initial normal load acting on the vehicle tires (F_{zi}^{start}) can be defined as:

$$F_{z1}^{start} = F_{z2}^{start} = \frac{1}{2}mg \tag{2.2}$$

On Figure 5, the tire load at the right is increased by the same amount as the left is decreased, as shown by Eq. (2.3):

$$F_{z1} = F_{z1}^{start} + \triangle F_z \quad and \quad F_{z2} = F_{z2}^{start} - \triangle F_z \tag{2.3}$$

At the rollover limit, these values, known as the *LLT* coefficient, became:

$$\triangle F_z = \frac{1}{2}mg \tag{2.4}$$

where $\triangle F_z$ is the rate of normal load transfer. The Eq. (2.3) is based on the *LLT* coefficient, proposed by Lui *et al.* (1997), which is an indicator of rollover stability (KAMNIK *et al.*, 2003; RILL, 2011; IMINE *et al.*, 2014).

This *LLT* coefficient is defined as the proportion of normal load that is transferred from a side of the vehicle to the other side of the vehicle in a transient manoeuvre, as presented by Eq. (2.5)

$$LLT = \frac{F_{z1} - F_{z2}}{F_{z1} + F_{z2}} \tag{2.5}$$

At the rollover threshold limit condition $\triangle F_z = \frac{1}{2}mg$, the normal load F_{z2} reaches zero, and thus the *LLT* coefficient is complete (*LLT* = 1). Hence, applying this condition in the Eq. (2.1), the static rollover threshold (SRT_{2D}) for a two-dimensional vehicle model (rigid model) can be calculated as:

$$SRT_{2Dm} = \frac{a_y}{g} = \frac{t/2}{h} \tag{2.6}$$

2.2.2 Rigid model in a road with bank angle

Figure 6 shows a rigid model in a road with bank angle (ϕ) (CHANG, 2001). Making the same analysis of the rigid vehicle, considering the moment about the A point:

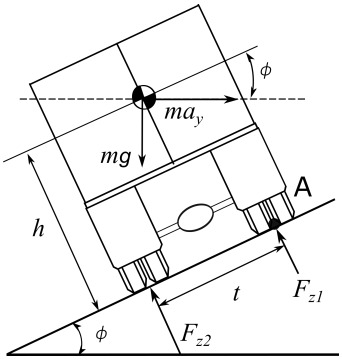

Figure 6 – Rigid vehicle model with bank angle.

$$F_{z2}t + ma_y h\cos(\phi) - mg(\frac{t\cos(\phi)}{2} + h\sin(\phi)) = 0 \tag{2.7}$$

At the rollover threshold limit condition, the normal load F_{z2} reaches zero, dividing by $\cos(\phi)$, and rearranging the equation, the static rollover threshold (SRT_{2D-B}) for a two-dimensional vehicle model with bank angle is represented by the Eq. (2.8):

$$SRT_{2D-B} = \frac{a_y}{g} = \frac{t/2}{h} + e \tag{2.8}$$

where e is the tangent of bank angle ($e = \tan(\phi)$).

2.2.3 Models with compliances of the suspension and tires

Several researchers have considered the influence of the suspension and tires on the lateral and vertical *CG* location, which affects the vehicle behavior (GILLESPIE, 1992; WINKLER *et al.*, 1992; CHANG, 2001; HAC, 2002; LAMBERT, 2007), some models are presented below.

2.2.3.1 Winkler model

Winkler *et al.* (1992) developed a two-dimensional model of the heavy vehicle (Fig. 7), this model takes into account the influence of the suspension and tires on the *CG* movement.

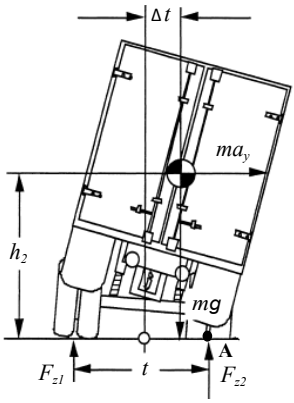

Figure 7 – Winkler model.
Source: Adapted of Winkler *et al.* (1992).

Making the same analysis of the rigid vehicle, and considering the moment about the A point:

$$F_{z1}t + ma_y h_2 - mg(\frac{t}{2} - \triangle t) = 0 \tag{2.9}$$

where $\triangle t$ is the lateral position of the *CG* relative to the center of track. At the rollover threshold limit condition, the normal load F_{z1} reaches zero, re-arranging the equation, the static rollover threshold for the Winkler model (SRT_{2D-W}) is represented by the Eq. (2.10).

$$SRT_{2D-W} = \frac{a_y}{g} = \frac{t/2 - \triangle t}{h_2} \tag{2.10}$$

2.2.3.2 Rill model

Rill (2011) presents a similar model (Fig. 8) as in the previous case, which includes the roll stiffness of the suspension (k_θ) (as shown in Eq. (2.11)), and the equivalent vertical rubber stiffness of the tire (k_T):

$$k_\theta = \frac{k_{Ls} b^2}{2} \tag{2.11}$$

where k_{Ls} is the equivalent leaf stiffness of the suspension, and b is the lateral separation between the springs.

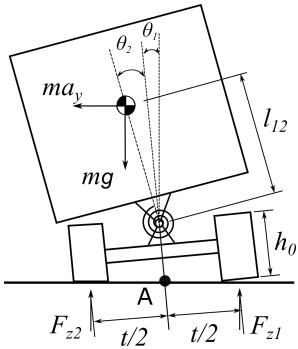

Figure 8 – Rill model.
Source: Adapted of Rill (2011).

In Fig. 8, h_0 is the *CR* height, l_{12} is the *CG* height above the chassis, and θ_1 and θ_2 are the roll angles of the suspension and the tires respectively. Assuming that for small angles, $\cos(\theta_i)$ may be assumed as unity, and $\sin(\theta_i) = \theta_i$, and considering the moment about the A point:

$$(F_{z2} - F_{z1})\frac{t}{2} - ma_y h - mg[h\theta_1 + l_{12}\theta_2] = 0 \tag{2.12}$$

where $h = h_0 + l_{12}$. At the rollover threshold limit condition, the wheel load at the right will vanish ($F_{z1} = 0$), whereas the left wheel carries the vehicle weight ($F_{z2} = mg$), replacing and rearranging:

$$\frac{a_y}{g} = \frac{t/2}{h} - \theta_1 - \frac{l_{12}}{h}\theta_2 \tag{2.13}$$

At the tilting limit and taking into account the Eq. (2.4), the tire deflection (δ_t) is represented by the Eq. (2.14)

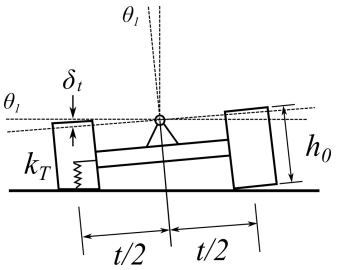

Figure 9 – Tire deflection.
Source: Adapted of Rill (2011).

$$\delta_t = \frac{\triangle F_z}{k_T} = \frac{mg}{2k_T} \tag{2.14}$$

Of the Fig. 9 and Eq. (2.14), the roll angle of the axle is defined by:

$$\theta_1 = \frac{\delta_t}{t/2} = \frac{mg}{tk_T} \tag{2.15}$$

In analogy with Eq. (2.12), the balance of torques at the body roll center (CR)(Fig. 9) is represented by the Eq. (2.16)

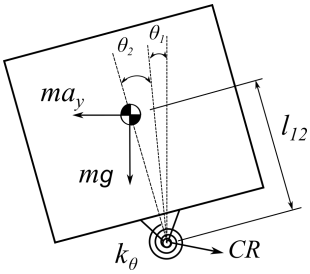

Figure 10 – Body roll center.
Source: Adapted of Rill (2011).

$$k_\theta \theta_2 = ma_y l_{12} + mgl_{12}(\theta_1 + \theta_2) = 0 \tag{2.16}$$

rearranging the Eq. (2.16):

$$\theta_2 = \frac{a_y}{g}\frac{mgl_{12}}{k_\theta - mgl_{12}} + \frac{mgl_{12}}{k_\theta - mgl_{12}}\theta_1 \tag{2.17}$$

Not allowing the vehicle overturn at $a_y = 0$, demands a minimum roll stiffness of $k_\theta > mgl_{12}$. With Eqs. (2.15) and (2.17), the overturning condition in Eq. (2.13) reads as:

$$\begin{gathered}\frac{a_y}{g}h = \frac{t}{2} - \frac{mgh}{tk_T} - l_{12}\left[\frac{a_y}{g}\frac{mgl_{12}}{k_\theta - mgl_{12}} + \frac{mgl_{12}}{k_\theta - mgl_{12}}\frac{mg}{tk_T}\right] \\ \frac{a_y}{g}h = \frac{t}{2} - \frac{h}{k_T^*} - l_{12}\left[\frac{a_y}{g}\frac{1}{k_\theta^* - 1} + \frac{1}{k_\theta^* - 1}\frac{1}{k_T^*}\right]\end{gathered} \tag{2.18}$$

where, for abbreviation purposes, the dimensionless quantities have been introduced.

$$k_T^* = \frac{tk_T}{mg} \quad k_\theta^* = \frac{k_\theta}{mgl_{12}} \tag{2.19}$$

Of the Eq. (2.18), the static rollover threshold for the Rill model (SRT_{2D-R}) is represented by the Eq. (2.20).

$$SRT_{2D-R} = \frac{a_y}{g} = \frac{t/2}{h + \dfrac{l_{12}}{k_\theta^* - 1}} - \frac{1}{k_T^*} \tag{2.20}$$

2.2.3.3 Chang model

Chang (2001) developed a two-dimensional model of the heavy vehicle (Fig. 11), this model takes into account the influence of the suspension and the bank angle on the SRT factor calculation.

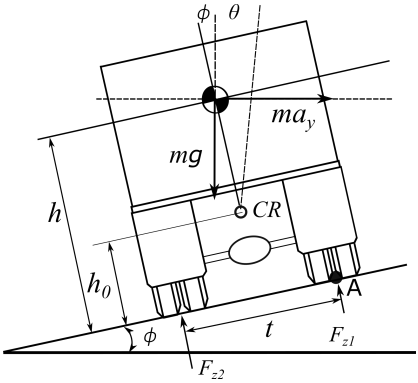

Figure 11 – Chang model with bank angle.
Source: Adapted of Chang (2001).

Making the same analysis of the rigid vehicle with bank angle, assuming that for small angles, $\cos(\theta - \phi)$ may be assumed as unity, and $\sin(\theta - \phi) = \theta - \phi$, and considering the moment about the A point:

$$F_{z2}t + ma_y h - mg\left[\frac{t}{2} - (h - h_0)(\theta - \phi)\right] = 0 \tag{2.21}$$

At the rollover threshold limit condition, the normal load F_{z2} reaches zero, rearranging the equation, the static rollover threshold for the Chang model (SRT_{2D-CB}) is represented by the Eq. (2.22).

$$SRT_{2D-CB} = \frac{a_y}{g} = \frac{t/2}{h} + (1 - \frac{h_0}{h})(\phi - \theta) \tag{2.22}$$

2.3 STATIC ROLLOVER THRESHOLD FOR THREE DIMENSIONAL MODELS

Although, most models to calculate the SRT factor are two-dimensional, some researchers have developed three-dimensional models to represent this factor, some models are presented below.

2.3.1 Gillespie model

Taking into account the roll stiffness of the suspension (k_θ) (Eq. (2.11)), Gillespie (1992) presents a model of stability (Fig. 12). The moment about the point A is represented by:

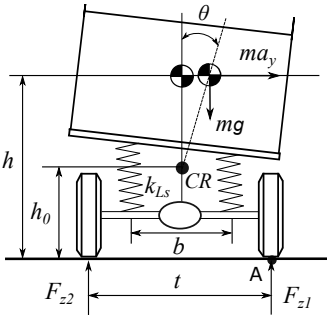

Figure 12 – Gillespie model.
Source: Adapted of Gillespie (1992).

$$F_{z2}t - mg\left[\frac{t}{2} - (h - h_0)\theta\right] + ma_y h = 0 \tag{2.23}$$

The three-dimensional model of Fig. 13 defines a virtual roll axis from the *CR* at front of the vehicle to the *CR* at rear of the vehicle.

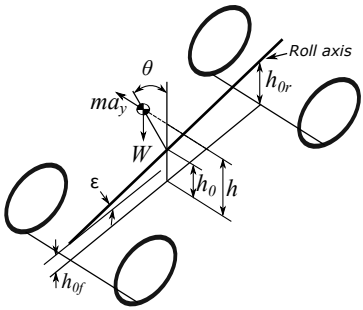

Figure 13 – Gillespie model.
Source: Adapted of Gillespie (1992).

The moment M_θ about the roll axis is represented by:

$$M_\theta = [W(h-h_0)\sin(\theta) + ma_y(h-h_0)\cos(\theta)]\cos(\varepsilon) \tag{2.24}$$

where ε is the longitudinal tilt angle of the roll axis. For small angles, $\cos(\theta)$ and $\cos(\varepsilon)$ may be assumed as unity, and $\sin(\theta) = \theta$. Then:

$$\begin{gathered} M_\theta = W(h-h_0)\theta + ma_y(h-h_0) \\ M_\theta = W(h-h_0)\left[\theta + \frac{a_y}{g}\right] \end{gathered} \tag{2.25}$$

but:

$$M_\theta = M_{\theta f} + M_{\theta r} = (k_{\theta f} + k_{\theta r})\theta \tag{2.26}$$

where $k_{\theta f}$ and $k_{\theta r}$ are the roll stiffness of the front and rear suspension respectively (as shown in Eq. (2.11)). From Eqs. (2.25) and (2.26) can be solved the roll angle (θ),

$$\theta = \frac{W(h-h_0)}{k_{\theta f} + k_{\theta r} - W(h-h_0)}\frac{a_y}{g} \tag{2.27}$$

From Eqs. (2.23), at the rollover threshold limit condition, the normal load F_{z2} reaches zero, and replacing the roll angle of Eq. (2.27), the

static rollover threshold for the Gillespie model (SRT_{3D-G}) is represented by:

$$SRT_{3D-G} = \frac{a_y}{g} = \frac{\frac{t}{2h}}{1+(1-\frac{h_0}{h})\left[\frac{W(h-h_0)}{k_{\theta f}+k_{\theta r}-W(h-h_0)}\right]} \tag{2.28}$$

Regarding to this aspect, Winkler (2000), Rill (2011), and Zhou and Zhang (2013) reported that the chassis has a significant torsional compliance, which would allow that its front and rear parts roll almost independently. In this regard, Kamnik *et al.* (2003) reported that the *LLT* coefficient is different for the front and the rear axles of the trailer.

2.3.2 Navin model

Taking into account that the last unit of the *LCV's* is the critical unit, Navin (1992) developed a three-dimensional model, this model defines a virtual roll axis from fifth-wheel to rear outside trailer tire, as shown in Fig. 14.

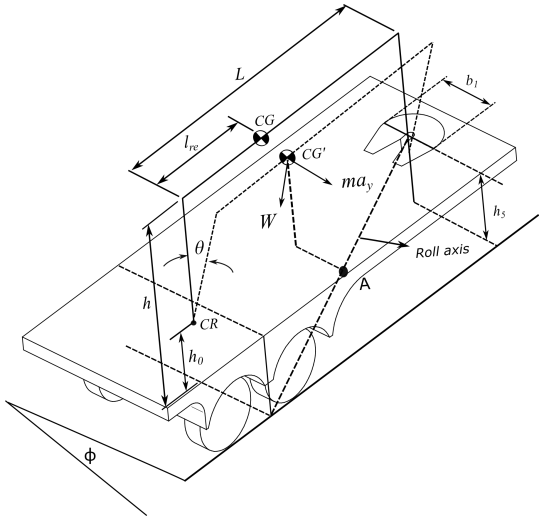

Figure 14 – Navil model.
Source: Adapted of Navin (1992).

Assuming that for small angles, $\cos(\theta)$ and $\cos(\phi)$ may be assumed as unity, and $\sin(\theta) = \theta$ and $\sin(\phi) = \phi$, and considering the moment about the A point on the roll axis:

$$\begin{aligned}&(ma_y - mg\phi)(h - \frac{h_5 l_{re}}{L})\\ -&(ma_y\phi + mg)(\frac{t}{2} - \frac{tl_{re}}{2L}) - (h - h_0)\theta) = 0\end{aligned} \tag{2.29}$$

where L is the wheelbase of the trailer, l_{re} is the distance from the *CG* to the rear axle, and h_5 is the fifth-wheel height.

Rearranging the equation, and eliminating the second-order terms, the static rollover threshold for the Navin model (SRT_{3D-N}) is represented by the Eq. (2.30).

$$SRT_{3D-N} = \frac{a_y}{g} = \frac{\frac{t}{2}(1 - \frac{l_{re}}{L}) + h(\phi - \theta) - \frac{h_5 l_{re}\phi}{L} + h_0\theta}{\frac{t\phi}{2}(\frac{l_{re}}{L} - 1) + h - h_5\frac{l_{re}}{L}} \tag{2.30}$$

2.4 OTHERS MODELS OF LATERAL STABILITY

Using Lagrange and Newton methods, two- and three-dimensional models have been developed to determine the influence of different characteristics of the vehicle on the lateral stability (FANCHER; WINKLER, 1992; BOUTELDJA *et al.*, 2004; GASPAR *et al.*, 2005; DAHLBERG; WIDEBERG, 2004), these models are very important, but don't define a mathematical equation for the SRT factor. Besides the characteristics above mentioned, these models taking into account the inertial forces, the longitudinal location of the *CG*, the fifth-wheel, the steering angle, the trailer/trailer angle, among other characteristics to determine the lateral stability or the rearward amplification (*RA*) of the vehicles, as shown in Figs. 15 and 16.

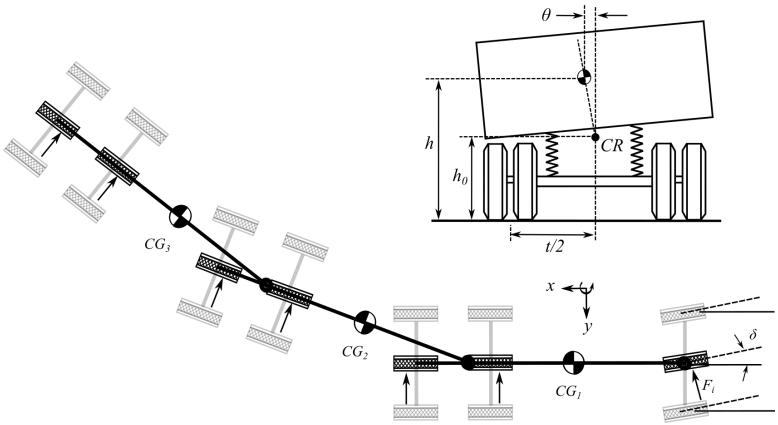

Figure 15 – Bicycle model together with planar model.

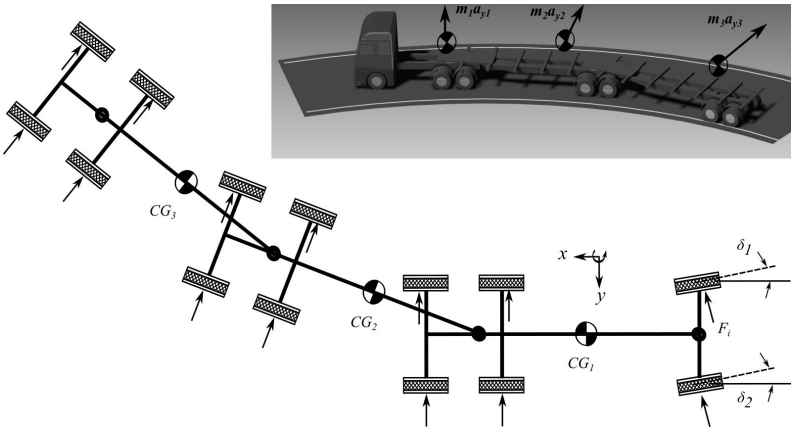

Figure 16 – Three-dimensional model.

2.5 NEW APPROACH

Many studies had successfully demonstrated the applicability of the Davies method and the screw theory to solve the kinematics and statics of mechanisms. In this context, Erthal (2010) developed a vehicle model (with suspension McPherson) to analyze the stability (Fig. 17), and Lee

(2001), Bidaud *et al.* (2006), Lee and Han (2008) used the screw theory to analyze the dynamic behaviour characteristics of vehicles (Fig. 18).

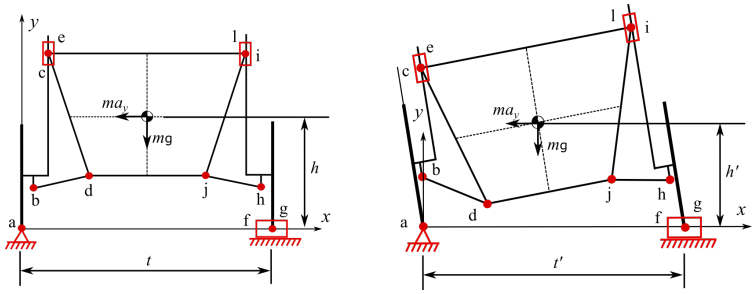

Figure 17 – Erthal model.
Source: Adapted of Erthal (2010).

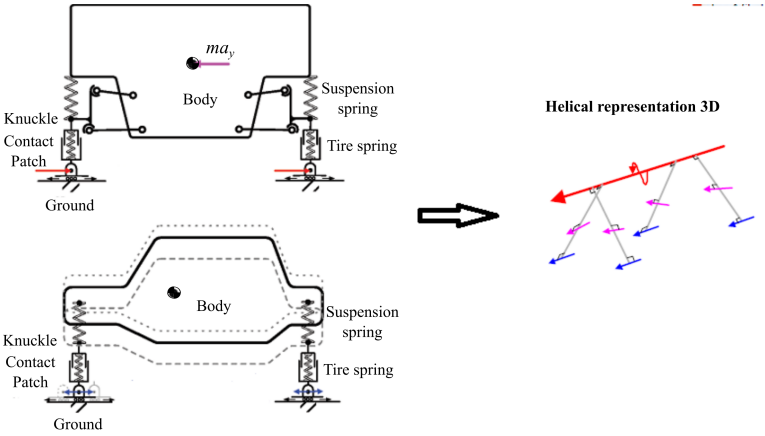

Figure 18 – Lee model (LEE; HAN, 2008).
Source: Adapted of Lee and Han (2008).

Table 1 shows the main stability and lateral models of *LCV's* and their characteristics.

Table 1 – Stability models.

	Characteristics																						
	2D	3D	Bicycle model	*CG* height (h_2)	*CR* height	Bank angle (ϕ)	Slope angle (φ)	Vehicle track (t)	Suspension	Tires	Steering angle	Trailer/trailer angle (ψ)	Fifth-wheel	Inertial forces	*LLT* coefficient	Longitudinal location of *CG*	Stiffness of the chassis	Active suspension	Liquid loads	Load distribution	Wind force	Roll angle (θ_{al})	Rearward amplification (RA)
Models of SRT factor																							
Gillespie (1992)	x	x		x	x			x	x					x								x	
Winkler *et al.* (1992)	x			x	x			x	x	x				x								x	
Navin (1992)		x		x	x	x		x	x				x	x		x						x	
Ranganathan (1993)	x			x	x			x	x					x					x			x	
Winkler (2000)		x		x	x			x	x	x			x	x	x	x	x		x	x		x	
Chang (2001)	x			x	x	x			x					x								x	
Jung *et al.* (2009)	x			x	x	x		x	x					x	x							x	
Rill (2011)	x			x	x			x	x	x				x	x							x	
Other models of lateral stability																							
Fancher and Winkler (1992)	x		x								x	x	x	x		x						x	x
Rempel (2001)		x		x				x	x		x	x	x	x		x							x
Takano and Nagai (2001)	x		x	x	x			x	x		x			x		x	x					x	
Miege and Cebon (2002)	x			x				x	x					x				x	x			x	
Kamnik *et al.* (2003)		x		x	x			x	x		x	x	x	x	x	x	x					x	
Sampson and Cebon (2003)		x		x				x	x				x	x		x		x				x	
Sanchez *et al.* (2004)		x		x	x			x	x		x	x	x	x		x						x	
Whitehead *et al.* (2004)	x		x	x				x	x		x			x		x						x	
Bouteldja *et al.* (2004)		x		x	x			x	x		x	x	x	x		x						x	
Dahlberg and Wideberg (2004)	x		x								x	x	x	x		x						x	x
Gaspar *et al.* (2005)		x		x	x			x	x		x			x	x	x		x				x	
Prem *et al.* (2006)		x		x		x		x	x	x				x	x	x			x				
Pinxteren (2010)		x		x				x	x		x	x	x	x		x							
Ricalde *et al.* (2008)		x		x	x			x	x		x	x	x	x		x						x	
Hac *et al.* (2008)			x								x	x	x	x		x							x
Chen and Chen (2009)	x			x	x	x		x	x		x			x	x							x	
Ryu *et al.* (2010)		x		x	x			x	x		x			x		x		x				x	
Islam and He (2013)	x		x								x	x	x	x		x						x	

Table 1 – Stability models.

	Characteristics	2D	3D	Bicycle model	*CG* height (h_2)	*CR* height	Bank angle (ϕ)	Slope angle (φ)	Vehicle track (t)	Suspension	Tires	Steering angle	Trailer/trailer angle (ψ)	Fifth-wheel	Inertial forces	*LLT* coefficient	Longitudinal location of *CG*	Stiffness of the chassis	Active suspension	Liquid loads	Load distribution	Wind force	Roll angle (θ_{all})	Rearward amplification (*RA*)
Malviya and Mishra (2014)			x		x		x	x	x						x	x	x					x	x	
Imine *et al.* (2014)		x		x	x	x			x	x	x	x			x		x		x					
Huston and Kelly (2014)		x			x	x			x						x		x						x	
He *et al.* (2015)			x		x				x	x	x				x	x	x					x	x	

Chapter 3

STATIC ANALYSIS TOOLS

Stiffness and deformation analysis are the most important indicators in performance evaluation of mechanical systems. These parameters are important for designing mechanical components and control systems where the performance of the mechanism in certain critical position is important.

Prismatic joints "*P*" are frequently used in the description of the stiffness and the elastic deformations of the links; this technique is also known as the Virtual Joint Method (*VJM*), which is based on the extension of the traditional rigid model by adding virtual joints (localized passive prismatic joint) (PASHKEVICH *et al.*, 2011) for the static analysis of mechanisms.

This method is based on the stiffness matrix, which uses the inverse of the Jacobian matrix. But in several cases, generally to get the inverse of the Jacobian matrix is a hard task, and it takes a long computational time (NAKAMURA; HANAFUSA, 1986; HU *et al.*, 2002; KIM; RYU, 2003; MERLET, 2006; SARIYILDIZ *et al.*, 2011).

On the other hand, when it is analyzed the buckling of columns, the bar under the action of a force can have two kinds of deformation: a substantial axial deformation and a smaller but not negligible shear deformation; these deformations are very important for the static solution of the mechanisms. In the theory of buckling of columns, the axial deformation and the small shear deformation are associated to a helical spring and a torsion spring at the base, respectively (WOOD, 1974; POPOV, 1998; ADMAN; SAIDANI, 2014).

Making an analogy between stability of columns and the static analysis of flexible bodies, the technique mentioned above is applied to the modeling and static analysis of mechanisms with locally flexible bodies; and the formalism described by Davies (DAVIES, 1983b) was used as the primary mathematical tool to analyze the mechanisms statically.

The Davies method was selected since it allows the static model for the mechanism to be obtained in a straightforward manner and it is also easily adapted using this approach. More details on the Davies method can be found in Davies (1983b), Tsai (1999), Erthal (2010), Mejia *et al.* (2013), Moreno *et al.* (2015), Moreno *et al.* (2016). Other kinematic

static methods may be used instead. However, in the author's opinion, they would be more cumbersome or lack generality.

These fundamentals are briefly described as follows.

3.1 DEFORMATION MODEL

Elastic and plastic deformations of different components of the mechanisms can be caused by the internal or external forces that act on the mechanism, or by changes in temperature.

For the representation of the axial deformation in mechanical components, passive prismatic joints are used frequently (PASHKEVICH *et al.*, 2011), but some mechanical components have a relatively small shear deformation that other methods commonly ignore. This deformation, generally small, is however crucial for the solution of mechanisms with flexible bodies, such as: suspensions, tires, hydraulic and pneumatic systems.

Taking into account all these aspects, the following model was developed: using a column where the buckling mode adopted has one end fixed and one end free (Fig. 19(a)), the bar under the action of the force F has an axial deformation and a small shear deformation (Fig. 19(b)); these deformations allow two degrees of freedom (2 DoF) of the bar: displacement of the point A in the longitudinal y-axis and a roll rotation around the z-axis.

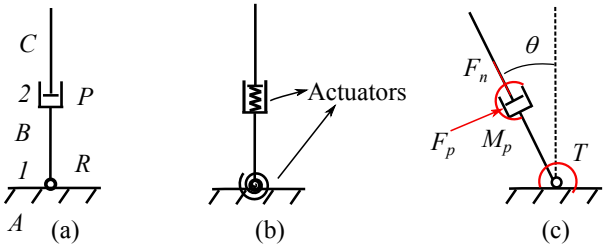

Figure 19 – Deformation model of a buckling column.

Further, these deformations can be associated to a helical spring and a torsion spring at the base respectivelly (WOOD, 1974; POPOV, 1998; ADMAN; SAIDANI, 2014), as shown in Fig. 19(c).

In Fig. 19(c) k_1 and k_2 are the stiffness of the compression spring and the torsional spring respectively ($k_2 >> k_1$) (POPOV, 1998), and θ is the rotation angle of the bar.

Using mechanism theory, and taking into account that the mechanism of the Fig. 19(b) has two degree of freedom, the helical spring of the Fig. 19(c) is represented by a prismatic joint and the torsional spring is represented by a revolute joint at the base, as shown in Fig. 20(a)

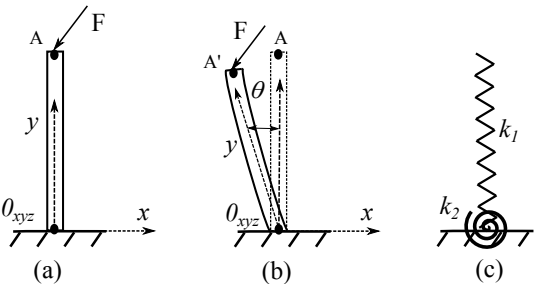

Figure 20 – Proposed kinematic chain of a buckling column with $M = 2$.

Figure 20(a) shows the proposed kinematic chain of the bar, which is composed of three links ($n = 3$) identified by the letters A (the base) and B-C (the bar), and the two joints ($j = 2$) identified by numbers as follow: a revolute joint "*R*" (1), and a prismatic joint "*P*" (2).

The mechanism of the Fig. 20(a) has 2-DoF, and it requires two actuators to control its movements, but, the movements are dependent on the forces acting on it. Therefore the mechanism has two passive actuators that controls the following movements of the bar: the first actuator is a prismatic joint with helical spring, which controls the axial deformation of the bar, and the second actuator is a revolute joint with torsional spring, which controls the rotation of the bar, as shown in Fig. 20(b).

Figure 20(c) shows the forces that act on the joints of the mechanism: F_n and F_p are the axial and perpendicular loads in the passive prismatic joint respectively, M_p is the moment that act on the prismatic joint, and T is the torque that act on the revolute joint with torsional spring.

From the general equations of mobility (Eq. (3.1) and Eq. (3.2)) (KUTZBACH, 1929; CROSSLEY, 1964; TSAI, 2001), the proposed mechanism of the Fig. 20(a) with three links ($n = 3$) and two joints ($j = 2$) in a planar space ($\lambda = 3$) has two degrees of freedom (2 DoF), and it has the same movements that the mechanism of the Fig. 20(b):

$$M = \lambda(n - j - 1) + j \tag{3.1}$$

$$\nu = j - n + 1 \tag{3.2}$$

where M is the number of degrees of freedom (DoF) or mobility of the mechanism, λ is the number of degrees of freedom of the space in which the mechanism is intended to move, n is the number of mechanism links, including the fixed link, j is the number of mechanism joints, and ν is the number of independent loops in the mechanism.

On the other hand, in a continuous body, a strain field results from a displacement field induced by applied forces or to changes in the temperature field inside the body. In a mechanism, the total axial deformation of structural members (δ_{Total}) is influenced by the deformation induced by forces (δ_F) and deformation induced by the changes in temperature (δ_T), as shown in Eq. (3.3).

$$\delta_{Total} = \delta_F + \delta_T \tag{3.3}$$

The main mechanisms of deformation by force and temperature are briefly summarized in Table 2, where all notations are adapted to those used in this work.

In Table 2 δ is the elastic deformation, δ_S is the spring deformation, δ_{LS} is the leaf spring deformation, δ_t is the rubber deformation, δ_T is the thermal deformation, L_b is the original length of the bar, A_b is the cross-sectional area of the bar, E is the modulus of elasticity for the material, $\triangle F$ is the algebraic change in the initial load, F^{start} is the initial normal load, k_s is the equivalent vertical spring stiffness, l is the length of the leaf spring, n_l is the number of leaves, b_l is the width of the leaf, t_l is the thickness of the leaf, E_s is the modulus of elasticity for a multiple leaf, k_{Ls} is the equivalent leaf stiffness, k_t is the vertical or radial stiffness of the rubber or tire, a_c is the regression coefficient, k_T is the equivalent rubber stiffness, $\triangle T$ is the algebraic change in the temperature, α is the linear coefficient of thermal expansion, τ is the torque, and k_{st} is the spring torsional coefficient.

Table 2 – Summary of the related works and expressions for the deformation of mechanical members.

Publications	Element	Deformation by	Model
Huang *et al.* (2004), Hibbeler (2011)	Links	Force	$\delta = -\frac{F_n L_b}{A_b E}$
Hibbeler (2011) Mirzaeifar *et al.* (2011) Bakhshesh and Bakhshesh (2012)	Spring	Force	$\delta_S = \frac{\triangle F}{k_s} = \frac{F^{start} - F_n}{k_s}$
Rill (2006) Dhoshi *et al.* (2011)	Leaf Spring	Force	$\delta_{LS} = \frac{3 \triangle F l^3}{8 E_s n_l b_l t_l^3} = \frac{\triangle F}{k_{Ls}}$
Taylor *et al.* (2000) Rill (2011)	Rubber - Tires	Force	$\delta_t = \frac{3 \triangle F}{k_t + a_c} = \frac{\triangle F}{k_T}$
Fang *et al.* (1999) Hibbeler (2011)	Links	Temperature	$\delta_T = \alpha \triangle T L$
Popov (1998) Farley and Morgenroth (1999) Wang and Howard (2004)	Torsional spring	Torque	$\theta = \frac{\tau}{k_{st}}$

3.2 MECHANISM STATICS

Several methodologies allow us to obtain a complete static analysis of a mechanism. In this study, the formalism described by Davies (1983b) was used as the primary mathematical tool to analyze the mechanisms statically.

The Davies method provides a systematic way to relate the joint forces and moments in closed kinematic chains (DAVIES, 1983a; DAVIES, 1983b; DAVIES, 1995). This method is based on graph theory, screw theory and the Kirchhoff cut-set law and it can be used to obtain the statics of a mechanism as a matrix expression. The Davies method for static analysis can be briefly described through the following steps:

1. Given a mechanism, draw its kinematic chain identifying all of its "n" links, "f" external loads, and "j" direct couplings (joints).

2. Draw the direct coupling graph "G_A" for the mechanism with the links of the mechanism as the vertices of the graph, and the joints and external loads of the mechanism as the edges of the graph. Assign positive directions to each edge with an arrow pointing from the minor to the major vertex.

3. Write the incidence matrix of the direct coupling graph $[I]_{n,j+f}$.

4. Generate the cut-set matrix $[Q]_{k;j+f}$ from $[I]_{n,j+f}$ using the Gauss-Jordan elimination method, where the number of cuts ($k = n-1$) (identity matrix), and the number of chords ($l_c = j+f-n+1$) are defined and depicted in the action graph.

5. Write the expanded cut-set matrix $[Q]_{k;c}$, where c is the number of constraints at the joints and external loads of the mechanism.

6. Write a wrench $\$_{J_{\lambda;c}}$ for each constraint or external force of the mechanism, as follows:

$$\begin{aligned}\$_{J_{\lambda;c}} = &\begin{bmatrix} 0 \\ z \\ -y \\ 1 \\ 0 \\ 0 \end{bmatrix} J_{F_x} + \begin{bmatrix} -z \\ 0 \\ x \\ 0 \\ 1 \\ 0 \end{bmatrix} J_{F_y} + \begin{bmatrix} y \\ -x \\ 0 \\ 0 \\ 0 \\ 1 \end{bmatrix} J_{F_z} \\ &+ \begin{bmatrix} 1 \\ 0 \\ 0 \\ 0 \\ 0 \\ 0 \end{bmatrix} J_{M_x} + \begin{bmatrix} 0 \\ 1 \\ 0 \\ 0 \\ 0 \\ 0 \end{bmatrix} J_{M_y} + \begin{bmatrix} 0 \\ 0 \\ 1 \\ 0 \\ 0 \\ 0 \end{bmatrix} J_{M_z}\end{aligned} \tag{3.4}$$

where λ is the degrees of freedom of the space in which the mechanism is intended to move.

7. Replace each wrench $\$_{J_{\lambda;c}}$ in the expanded cut-set matrix $[Q]_{k;c}$ in order to obtain the generalized action matrix $[A_N]_{\lambda k;c}$.

8. Operate algebraically the generalized action matrix $[A_N]_{\lambda k;c}$ in order to statically solve the system.

These fundamentals are briefly described in Appendix A.

3.3 PUBLICATION SUBMITTED

The developed model of deformation has the following publication:

• Moreno, G. G., Nicolazzi, L., Vieira, R. S., Martins, D. *Stiffness and deformation of mechanisms locally flexible bodies: a general method using expanded passive joints*. Submitted to Mechanism and Machine Theory.

Chapter 4

VEHICLE MODEL FOR LATERAL STABILITY

According to Jindra (1966), Rempel (2001), and Melo (2004) the last unit of a *LCV* (trailer) is subjected to a high lateral acceleration compared to the tractor unit, this acceleration is caused by the phenomenon known as rearward amplification (*RA*), impacting the rollover threshold of the the vehicle. For this reason, the last trailer of the *LCV's* is the critical unit and it is prone to rollover; taking into consideration this aspect, a simplified trailer model (Figs. 4 and 21) is modeled and analyzed to calculate the SRT factor for *LCV's*.

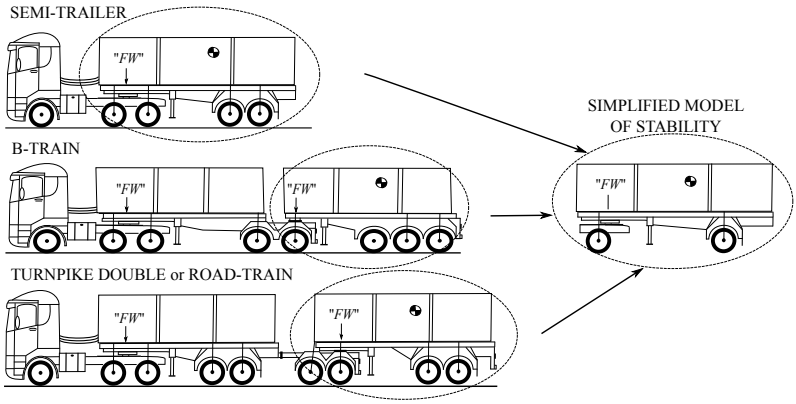

Figure 21 – Simplified trailer model.

As previously mentioned, the SRT factor is highly dependent on the location of the vehicle center of gravity (*CG*) and in this sense, the tires, suspension, fifth-wheel and chassis are directly responsible for the *CG* movements; these movements are dependent on the forces acting on the trailer *CG*, such as weight (*W*), disturbances forces imposed by the ground and lateral inertial force (ma_y) when the vehicle makes a turn or evasive manoeuvres.

4.1 TIRES SYSTEM

The tires system (tires and axle) maintains contact with the ground, and it filters the disturbances imposed by road imperfections (LEDESMA; SHIH, 1999).

When a vehicle goes around a corner, the friction between the tires and roadway pulls the truck and trailer around the curve. If the tire grip is inadequate, the vehicle will slide sideways. If the tire grip is good, the vehicle might 'pivot' over the outer tires (HART, 2012).

Hence, at the static rollover threshold calculation, the tires system allows two motions of the vehicle: displacement in the vertical z-axis and a roll rotation around the longitudinal x-axis (RILL, 2011), as shown in Fig. 22.

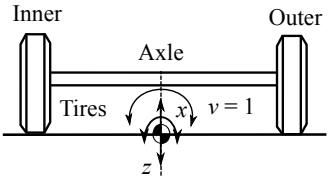

Figure 22 – Tires system.

4.1.1 Kinematic chain of the tires system

Mechanical systems can be represented by kinematic chains composed of links and joints, which facilitates their modeling and analysis, (KUTZBACH, 1929; CROSSLEY, 1964; TSAI, 2001); to model the tire kinematic chain the mobility equations Eqs. (3.1) and (3.2) were used.

For the model, the tires are assumed as flexible mechanical components with only radial deflection (as it was described in section 3.1), then the kinematic chain of tires system in Fig. 22, has 2-DoF (M = 2), the workspace is planar ($\lambda = 3$) and the number of independent loops is one ($\nu = 1$); using the mobility equations, the kinematic chain of tires system should be composed of five links ($n = 5$) and five joints ($j = 5$).

In order to model this system the following considerations were taken into account:

• there are up to three different components of forces, acting on the tire-road contact i of the vehicle (SMITH, 2004; PACEJKA, 2012; JAZAR, 2014; GARCIA-POZUELO *et al.*, 2014), as shown in Fig. 23, where F_{xi} is the traction or brake force on the tire i, F_{yi} is the tire lateral force i and F_{zi} is the tire normal load i,

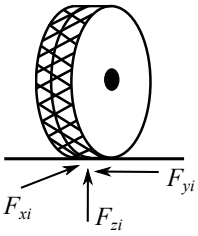

Figure 23 – Constraints of tire-road contact.

• however, at rollover threshold, the tire-road contact of the tires 1 and 4 (outer tires in the turn, Fig. 24) receives greater normal and lateral forces than the inner tires 2 and 3, and thus tires 1 and 4 are not prone to slide laterally (HART, 2012). We consider that the tire-road contact of the outer tires 1 and 4 only allows vehicle rotation along the longitudinal x-axis. Therefore, tire-road contact was modeled as a pure revolute joint "R" along the longitudinal x-axis,

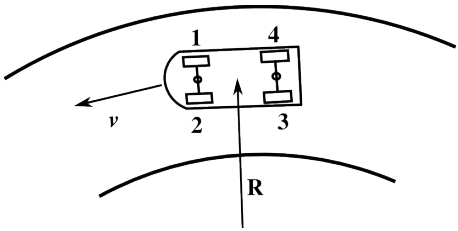

Figure 24 – Vehicle on a curved path.

• while, at the rollover threshold, the inner tires 2 and 3 may slide laterally, producing a track width change of their respective axles. As a consequence, the tire-road contact of the tires 2 and 3 has only a constraint on the vertical z-axis. Therefore, the tire-road contact was modeled as a prismatic joint "P" in the lateral y-axis, and

• in vehicles with rigid suspension, the tires remain perpendicular to the axle (JAZAR, 2014).

Applying these constraints to the kinematic chain of the tires system, a model with the configuration shown in Fig. 25(a) is proposed.

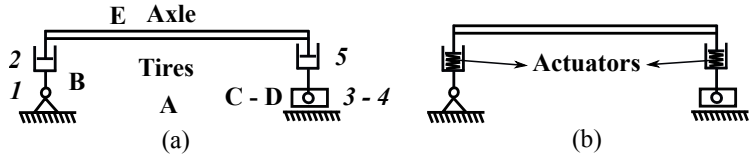

Figure 25 – a) Kinematic chain of the tires system. b) Tires system including actuators.

The kinematic chain of the tires system (Fig. 25(a)) is composed of five links identified by letters A (road), B (outer tire in the turn), C and D (inner tire in the turn), and E (the vehicle axle); and the five joints are identified by numbers as follow: the revolute joint *1* is the tire-road contact of the outer tire in the turn, the prismatic joint *3* and the revolute joint *4* are the tire-road contact of the inner tire in the turn, and the prismatic joints *2* and *5* represent the radial deflection of the tires.

The mechanism of Fig. 25(a) has 2-DoF, and it requires two actuators to control its movement, but, the movements of the tires system are dependent on the forces acting on it. Therefore the mechanism has a passive actuator (spring) in each prismatic joint of tires (*2* and *5* - radial deflection of the tires), as shown in Fig. 25(b); these actuators control the movement in longitudinal x-axis and the vertical z-axis.

In the proposed model of the Fig. 25(a), the revolute joint *3* and the prismatic joint *4* can be changed by a spherical slider joint (S_d), with constraint in the z-axis (Fig. 26), which does not modify the operation of the mechanism.

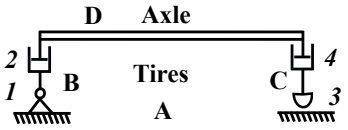

Figure 26 – Tires system model.

4.1.2 Kinematic of the tires system

Given the pose (position and orientation) of the tires system, the kinematic problem consists in finding the corresponding rotation angle or displacement of all joints (active and passive) to achieve this position. The movement of the tires system is orientated by the forces acting on the mechanism (the trailer weight (W) and the inertial force (ma_y)). These forces affect the passive actuators of the mechanism, as shown in Figs. 27 and 28.

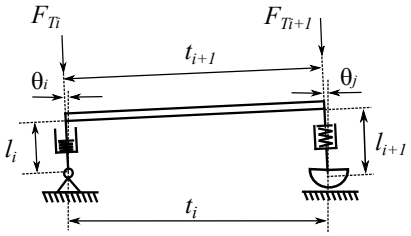

Figure 27 – Movement of the tires system.

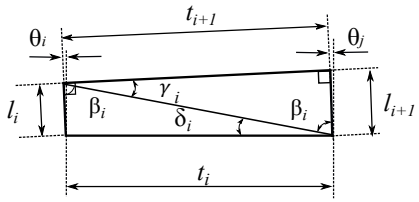

Figure 28 – Movement of the tires system.

Using the Table 2 and Fig. 28, the kinematic of the tires system is defined by the Eqs.(4.1) to (4.5).

$$l_i = \delta_t + l_r = \frac{3 \triangle F}{k_t + a_c} + l_r \approx \frac{-F_{Ti} + F_{zi}^{start}}{k_T} + l_r \tag{4.1}$$

$$\beta_i = 90^o - \arcsin\left(\frac{l_{i+1}}{\sqrt{t_{i+1}^2 + l_{i+1}^2}}\right) \tag{4.2}$$

$$t_i = \sqrt{t_{i+1}^2 + l_{i+1}^2 + l_i^2 - 2\left(\sqrt{t_{i+1}^2 + l_{i+1}^2}\right) l_i \cos(\beta_i)} \tag{4.3}$$

$$\delta_i = \arcsin\left(l_i \sin(\beta_i)/t_i\right) \tag{4.4}$$

$$\theta_i = \theta_j = 90^o - \delta_i - \beta_i \tag{4.5}$$

where δ_t is the vertical deformation of the tire, $\triangle F$ is the algebraic change in the load, k_t is the vertical stiffness of tire, a_c is the regression coefficient, l_i is the instantaneous dynamic rolling radius per tire i, F_{Ti} is the instantaneous tire normal load i, F_{zi}^{start} is the initial normal load i, k_T is

the equivalent tire vertical stiffness, l_{ri} is the initial dynamic rolling radius of the tire i, t_i is the track width i, t_{i+1} is the axle width, and $\theta_{i,j}$ are the rotation angles of the revolution joints i and j respectively.

4.2 SUSPENSION SYSTEM

The suspension system comprises the linkage between the sprung and unsprung masses of a vehicle, which reduces the movement of the sprung mass, allowing tires to maintain contact with the ground, and filtering disturbances imposed by the ground (LEDESMA; SHIH, 1999). There are several types of suspensions, but the most commonly used by *LCV's* is the leaf spring suspension (RILL *et al.*, 2003), as shown in Fig. 29. For developing the simplified trailer model Fig. 21, it is assumed that the vehicle has rigid suspension on front and rear axles.

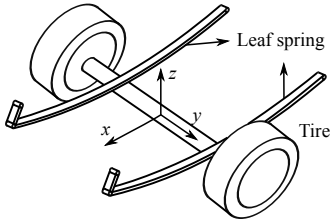

Figure 29 – Solid axle with leaf spring suspension.
Source: Adapted from Rill *et al.* (2003).

The leaf spring suspension is a mechanism that allows three motions of the vehicle's body under the action of the forces acting on the mechanism, displacements in the vertical z-axis and the lateral y-axis, and a roll rotation about the longitudinal x-axis (JAZAR, 2014; REMPEL, 2001), as shown in Figs. 30(a) and 30(b).

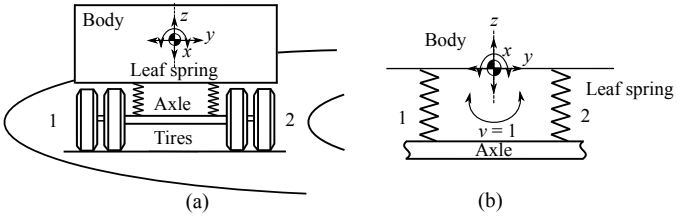

Figure 30 – a) Body motion. b) Suspension system.

4.2.1 Kinematic chain of the suspension system

The kinematic chain of the suspension system of the Fig. 31(a) has 3-DoF (M = 3), the workspace is planar ($\lambda = 3$), and the number of independent loops is one ($\nu = 1$). From the mobility equations (Eqs. (3.1) and (3.2)), the kinematic chain of the suspension system should be composed of six links ($n = 6$) and six joints ($j = 6$).

In order to model this system the following considerations are taken into account:

• leaf spring is assumed as flexible mechanical component with axial deformation and a small rotation, and it is can be represented by a prismatic joint "*P*" supported in a revolute joint "*R*" (as it was described in section 3.1), and

• to allow the rotation of the body in the *z*-axis, the link between the body and the leaf springs are made with revolute joints. Applying these concepts into the kinematic chain of the suspension system, a model with the configuration shown in Fig. 31(b) is proposed.

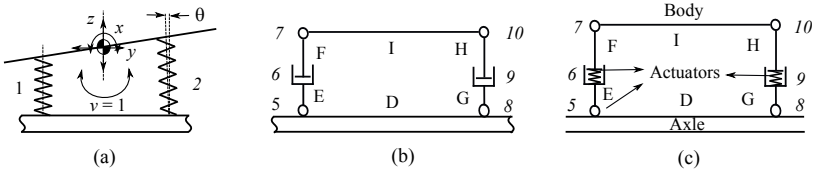

Figure 31 – a) Movement of suspension system. b) Kinematic chain of suspension system. c) Suspension system including actuators.

The kinematic chain of the suspension system is composed of six links identified by letters D (the vehicle axle), E and F (the leaf spring 1), G and H (the leaf spring 2) and I (the vehicle's body); and the six joints are identified by the following numbers: four revolute joints (*5, 7, 8* and *10*), and two prismatic joints that represent the leaf springs of the system (*6* and *9*), as shown in Fig. 31(b).

The mechanism of Fig. 31(b) has 3-DoF, and it requires three actuators to control its movement, but, the movements of the suspension system are dependent on the forces acting on it. Applying the technique developed in section 3.1, the kinematic chain of the suspension system has a passive actuator in the prismatic joints *6* and *9* (axial deformation of the leaf spring), and a passive actuator in the joints *5* and *8* (torsion spring - shear deformation of the springs); but the mechanism with four passive actuators is overconstrained, in this case only one equivalent passive actu-

ator is used in the joint *5*, as shown in Fig. 31(c).

4.2.2 Kinematic of the suspension system

The movement of the suspension is orientated first by the movement of the tires system, and second by the forces acting on the mechanism (trailer weight (W) and the inertial force (ma_y)). These forces affect the passive actuators of the mechanism, as shown in Figs. 32 and 33.

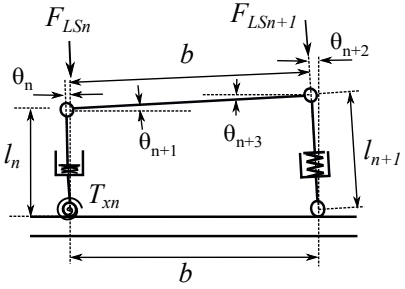

Figure 32 – Movement of suspension system.

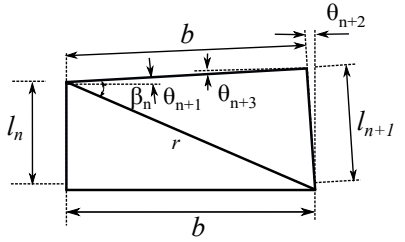

Figure 33 – Movement of suspension system.

Using the Table 2 and Fig. 33, the kinematic of the suspension system is defined by the Eqs. (4.6) to (4.12).

$$\theta_n = \frac{T_{xn}}{k_{st}} \tag{4.6}$$

$$l_n = \delta_{LS} + l_s = \frac{3 \triangle F l^3}{8 E_s n_l b_l t_l^3} + l_s \approx \frac{-F_{LSn} + F_{zi}^{start}}{k_{Ls}} + l_s \tag{4.7}$$

$$r = \sqrt{l_n^2 + b^2 - 2 l_n b \cos(\frac{\pi}{2} + \theta_n)} \tag{4.8}$$

$$\beta_n = \arccos\left((b^2 + r^2 - l_{n+1}^2)/(2br)\right) \tag{4.9}$$

$$\theta_{n+1} = \beta_n + \arcsin\left(\frac{b}{r}\sin(\frac{\pi}{2} + \theta_n)\right) - \frac{\pi}{2} \tag{4.10}$$

$$\theta_{n+2} = \theta_n + \arcsin\left(\frac{b}{r}\sin(\frac{\pi}{2} + \theta_n)\right) - \arcsin\left(\frac{b}{l_{n+1}}\sin(\beta_n)\right) \tag{4.11}$$

$$\theta_{n+3} = \frac{\pi}{2} - \beta_n - \arcsin\left(\frac{b}{l_{n+1}}\sin(\beta_n)\right) \tag{4.12}$$

where T_{xn} is the torque around the x-axis on the joint n, k_{st} is the spring's torsion coefficient, δ_{LS} is the leaf spring deformation, $\triangle F$ is the algebraic change in the initial load, l is the length of the leaf spring, n_l is the number of leaves, b_l is the width of the leaf, t_l is the thickness of the leaf, E_s is the modulus of elasticity for a multiple leaf, l_n is the instantaneous height of the leaf spring n, F_{LSn} is the spring normal load n, l_s is the initial suspension height, b is the lateral separation between the springs, k_{Ls} is the equivalent stiffness of the suspension, and θ_n is the rotation angle of the revolute joint n.

4.3 THE FIFTH-WHEEL SYSTEM

The fifth-wheel is a coupling device. Its purpose is to connect a tractive unit to a towed unit. The tractive unit is normally a tractor, but in the case of a multiple trailer train, the fifth-wheel also can be located on a lead trailer. The fifth-wheel allows an articulation between the tractive and the towed units.

The fifth-wheel consists of a wheel-shaped deck plate usually designed to tilt or oscillate on mounting pins. The assembly is bolted to the frame of the tractive unit. A sector is cut away in fifth-wheel plate (sometimes called a throat), allowing a trailer kingpin to engage with locking jaws in the center of the fifth-wheel. The trailer kingpin is mounted in the trailer upper coupler assembly. The upper coupler consists of the kingpin and the bolster plate, (BENNETT, 2011).

When the vehicle makes different manoeuvres (starting go uphill or downhill, and during cornering) (CHEN; TOMIZUKA, 1995; SAF-HOLLAND, 2006), the fifth-wheel allows the free movement of the trailer and more flexibility of the chassis, as shown in Figs. 34 to 36.

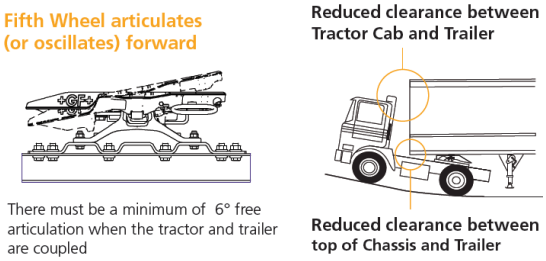

Figure 34 – Movement of fifth-wheel - starting uphill.
Source: Adapted from SAF-HOLLAND (2006).

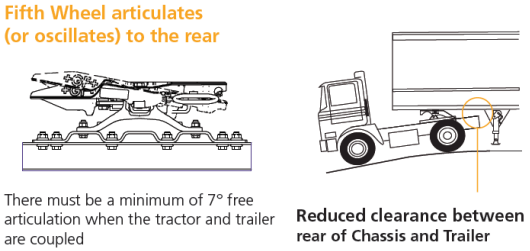

Figure 35 – Movement of fifth-wheel - starting downhill.
Source: Adapted from SAF-HOLLAND (2006).

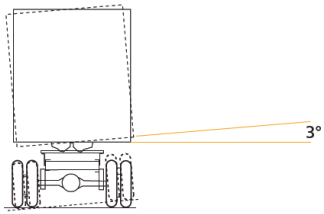

Figure 36 – Movement of fifth-wheel - rotation x-axis.
Source: Adapted from SAF-HOLLAND (2006).

Rotation about the longitudinal x-axis of up 3^o of movement between the tractor and trailer is permitted. On a standard fifth-wheel this occurs as result of clearance in fifth-wheel to bracket fit, compression of the rubber bushes and also vertical movement between the kingpin and locks may allow some lift of the trailer one side.

Taking into account the movements of the body car, the mechanism that represent the fifth-wheel was designed similar to the suspension mechanism, with 3 degrees of freedom (3-DoF)(Fig. 37), and it is located over the front suspension mechanism.

4.3.1 Kinematic of the fifth-wheel system

The movement of the fifth-wheel system is orientated by the forces acting on the mechanism (trailer weight (W) and the inertial force (ma_y)). These forces affect the passive actuators of the mechanism, as shown in Fig. 37.

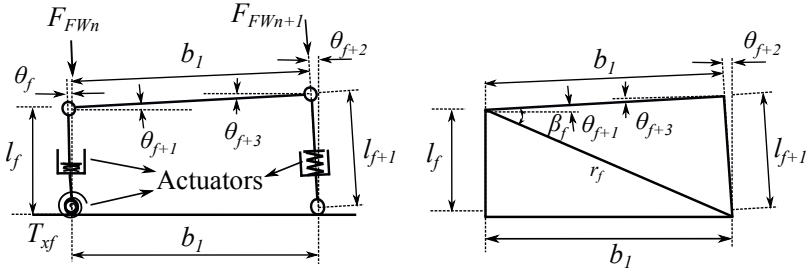

Figure 37 – Kinematic chain of fifth-wheel system.

Using the Table 2 and Fig. 37, the kinematic of the fifth-wheel system is defined by the Eqs. (4.13) to (4.19).

$$\theta_f = \frac{T_{xf}}{k_{st}} \tag{4.13}$$

$$l_f = \delta_S + l_{fw} \approx \frac{-F_{FWn} + F_{zi}^{start}}{k_{Ls}} + l_{fw} \tag{4.14}$$

$$r_f = \sqrt{l_f^2 + b_1^2 - 2 l_f b_1 \cos(\frac{\pi}{2} + \theta_f)} \tag{4.15}$$

$$\beta_f = \arccos\left((b_1^2 + r_f^2 - l_{f+1}^2)/(2 b_1 r_f)\right) \tag{4.16}$$

$$\theta_{f+1} = \beta_f + \arcsin\left(\frac{b_1}{r_f}\sin(\frac{\pi}{2} + \theta_f)\right) - \frac{\pi}{2} \tag{4.17}$$

$$\theta_{f+2} = \theta_f + \arcsin\left(\frac{b_1}{r_f}\sin(\frac{\pi}{2} + \theta_f)\right) - \arcsin\left(\frac{b_1}{l_{f+1}}\sin(\beta_f)\right) \tag{4.18}$$

$$\theta_{f+3} = \frac{\pi}{2} - \beta_f - \arcsin\left(\frac{b_1}{l_{f+1}}\sin(\beta_f)\right) \tag{4.19}$$

from Fig. 37 T_{xf} is the torque around the x-axis on the joint f, k_{st} is the spring's torsion coefficient, δ_S is the spring deformation, l_f is the instantaneous height of the fifth-wheel, F_{FWn} is the fifth-wheel normal load, l_{fw} is the initial fifth-wheel height, b_1 is the fifth-wheel width, k_{Ls} is the stiffness of the spring, and θ_f is the rotation angle of the revolute joint f.

4.4 THE CHASSIS

The chassis is the backbone of the trailer and it integrates the main truck component systems such as the axles, suspension, power train and cab. The chassis is also an important part that contributes to the dynamic performance of the whole vehicle. One of the important dynamic properties of truck is the torsional stiffness, which causes different lateral load transfers on the axles of the vehicle (KURDI *et al.*, 2014).

According to Winkler (2000), Rill (2011), and Zhou and Zhang (2013), the chassis of the vehicle has a significant torsional compliance, which would allow its front and rear parts to roll almost independently. Therefore, the lateral load transfer is different on the front and rear axles of the vehicle. Then, applying the torsion theory, the vehicle frame has a similar behavior with a statically indeterminate torsional shaft, as shown in Fig. 38.

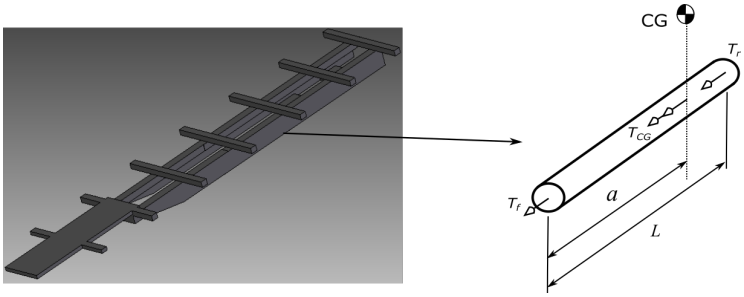

Figure 38 – Kinematic chain of the chassis.

where T_{CG} is the torque applied by the forces acting on the CG, T_f (T_{28}) is the torque applied on the front axle of the trailer, T_r (T_{27}) is the torque applied on the rear axle of the trailer, a is the distance from the front axle to the center of gravity, and L is the wheelbase of the trailer. Applying

torsion theory to the statically indeterminate shaft, the next equation is defined:

$$\frac{T_f a}{J_f G} = \frac{T_r (L-a)}{J_r G} \tag{4.20}$$

where J_f and J_r are the equivalent polar moments on the front and rear sections of the vehicle frame respectively, and G is the modulus of rigidity (or Shear Modulus).

According to Kamnik *et al.* (2003) when a articulated vehicle makes a spiral manoeuvre, the *LLT* coefficient on the rear axle is greater than the *LLT* coefficient on the front axle; therefore the equivalent polar moment on the rear (J_r) is greater than the equivalent polar moment on the front (J_f). Then, the polar moment of the trailer rear frame can be expressed as $J_r = xJ_f$ (where x is the constant that allows to control the torque distribution of the chassis); replacing and simplifying the Eq. (4.20):

$$T_f + T_r \left(\frac{a-L}{ax} \right) = 0 \tag{4.21}$$

However, when a trailer model makes a turn, the torque applied on the front axle has two components, as shown in Fig. 39 and Eqs. (4.22) and (4.23).

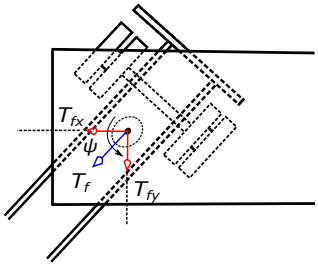

Figure 39 – Torque components.

$$T_{fx} = T_f \cos \psi \tag{4.22}$$

$$T_{fy} = T_f \sin \psi \tag{4.23}$$

where T_{fx} (T_{x28}) is the torque applied in the longitudinal x-axis (this torque acts on the lateral load transfer on the front axle), T_{fy} (T_{y28}) is the torque applied in the lateral y-axis, and ψ is the trailer/trailer angle.

4.5 TWO-DIMENSIONAL TRAILER MODEL

In this section a two-dimensional vehicle model that represent the last axle of the trailer is proposed (Fig. 40(a)). The model is simplified having only one equivalent axle; then, the model is composed of a mechanism that represents the tire movements (tire system), a mechanism that represents the suspension system and, finally, the vehicle body, as shown in Fig. 40(b).

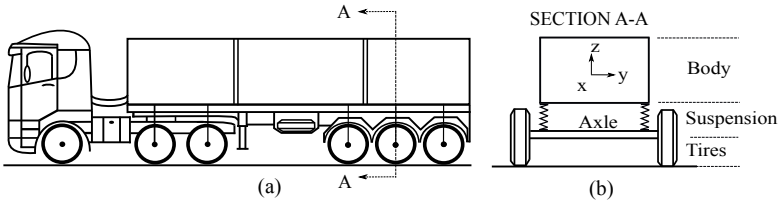

Figure 40 – (a) Heavy vehicle. (b)Vehicle model.

Taking into account the models developed for tires and suspension, the mechanism that represent a two-dimensional trailer model is shown in Fig. 41.

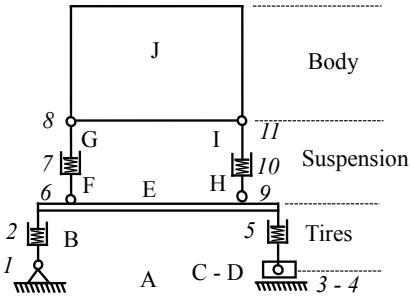

Figure 41 – Two-dimensional vehicle model.

The kinematic chain of the trailer model is composed of 11 joints (j = 11; 6 - revolute joints "R" and 5 - prismatic joints "P") and 10 links (n = 10), and the workspace is planar ($\lambda = 3$); according to mobility equation Eq. (3.1) the system has 5-DoF (M = 5).

4.6 THREE-DIMENSIONAL TRAILER MODEL

Using the simplified model of the last trailer (Fig. 21) with one equivalent axle on front and one equivalent axle on rear; and taking into account the models developed, the three-dimensional model (Fig. 42) is composed by the following mechanisms:

- the first mechanism is located at the front of the trailer, and it is composed of sub-mechanisms that represent the tires (tires system), the suspension (suspension system), and the fifth-wheel (fifth-wheel system),
- the second mechanism is located at the rear of the trailer, and it is composed of sub-mechanisms that represent the tires (tires system), and the suspension (suspension system), and
- the third mechanism represents the vehicle body (chassis), and links the front and rear trailer mechanisms.

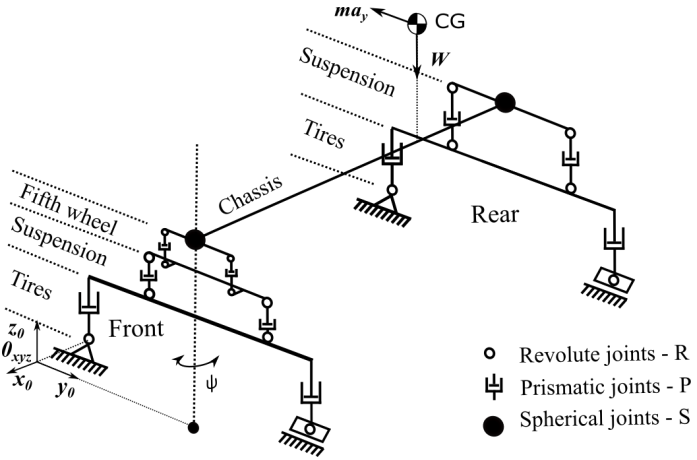

Figure 42 – Trailer model.

The kinematic chain of the trailer model (Fig. 42) is composed of twenty-eight joints (j = 30; 16 - revolute joints "R", 12 - prismatic joints "P", and 2 spherical joints "S", and twenty-five links (n = 25). But, making the expansion of the spherical joint the kinematic chain is composed of thirty-four joints (j = 34) and twenty-nine links (n = 29), and the workspace is planar ($\lambda = 3$); according to mobility equation Eq. (3.1) the system has 16-DoF (M = 16).

Making the simplification of the model, according to the Fig. 26 the kinematic chain of the trailer model (Fig. 43) is composed of twenty-

eight joints (j = 28; 14 - revolute joints "R", 10 - prismatic joints "P", 2 spherical joints "S", and 2 spherical slider joints "S_d"), and twenty-three links (n = 23).

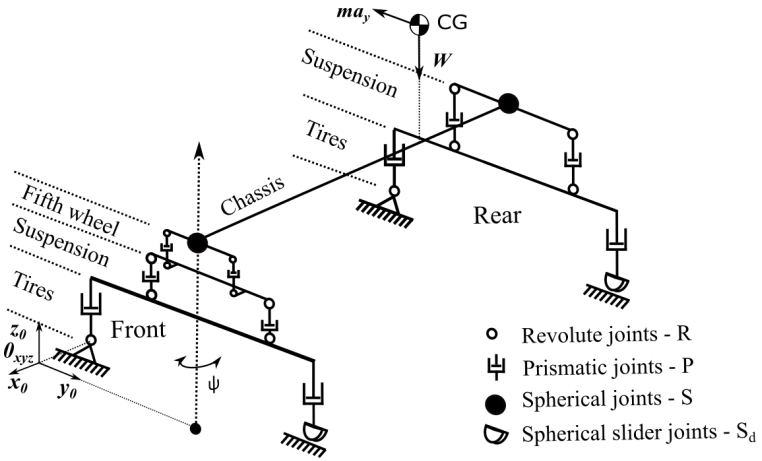

Figure 43 – Trailer simplified model.

4.7 LOAD DISTRIBUTION

Load distribution is a key factor in many stability-related crashes. Drivers must make sure that there is enough weight over all axles to provide adequate brake balance (NZTA, 2008).

The tests were obtained using the next loading conditions (BARICKMAN *et al.*, 2011):

• for the two-dimensional model, the load condition using is a load laterally centered, and

• for the three-dimensional model the loading conditions included a load laterally centered, load with *CG* displacement, and overweight with *CG* displacement.

Normally the national regulation boards establish the maximum load capacity of the axles of *LCV's*, therefore based on the design load capacity of the pavement and bridges, so each country has its own regulations. In this scope, the designers develop their products considering that the vehicle is loaded uniformly, causing the load distribution on the axles be in accordance with the laws. Figure 44 shows the example of the normal load distribution.

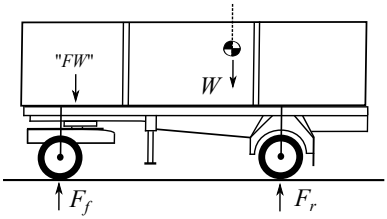

Figure 44 – Normal load distribution.

However, some loading does not properly distribute the load, which ultimately changes the center of gravity of the trailer forward or backward, as shown in Fig. 45 respectively.

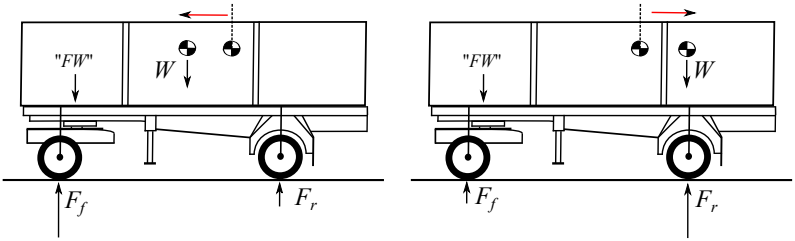

Figure 45 – Longitudinal *CG* displacement.

In Figures 44 and 45, F_f and F_r are the normal forces acting on the front and rear mechanisms of the trailer model respectively.

Generally, the *CG* position is dependent on the type of cargo and the load distribution on the trailer and it varies in three directions: longitudinal (x-axis), lateral (y-axis) and vertical (z-axis), as shown Fig. 46:

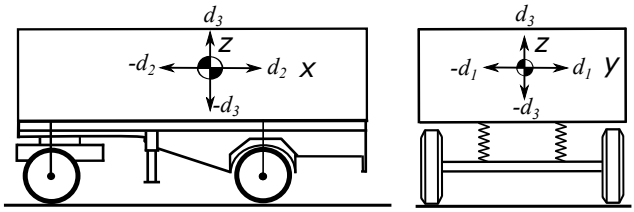

Figure 46 – *CG* displacements.

where d_1 denotes the lateral *CG* displacement, d_2 denotes the longitudinal

CG displacement, and d_3 denotes the vertical *CG* displacement.

Furthermore Figs. 47(a) and 47(b) show that only the weight (W) and the lateral inertial force (ma_y) act on the trailer center of gravity, but when the model takes into account the longitudinal slope angle (φ) and the bank angle (ϕ) of the road, these forces have three components, as represented in Eqs. (4.24) to (4.26) (BONNESON, 2000):

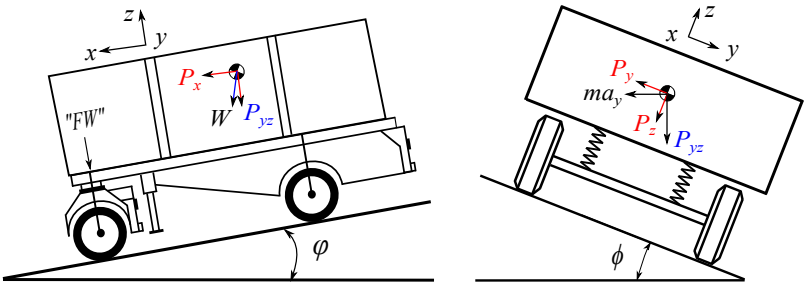

Figure 47 – a) Longitudinal slope of the road. b) Banked road

$$P_x = W \sin\varphi \tag{4.24}$$

$$P_y = -W \sin\phi \cos\varphi + ma_y \cos\phi \tag{4.25}$$

$$P_z = W \cos\phi \cos\varphi + ma_y \sin\phi \tag{4.26}$$

where P_x is the force acting on the longitudinal x-axis, P_y is the force acting on the lateral y-axis, and P_z is the force acting on the vertical z-axis.

Finally, when the trailer model makes a turn on a road with bank angle and slope angle (Fig. 48), considering the moments about the point A, the normal force acting on the rear mechanism of the trailer model (F_r) is given by the Eq. (4.27):

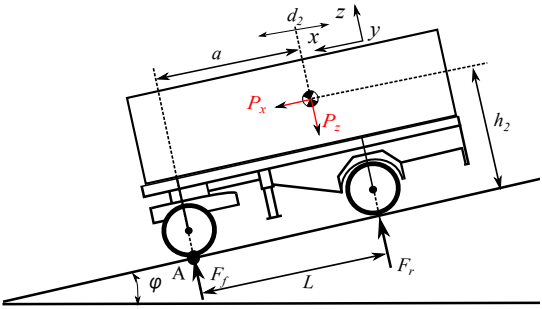

Figure 48 – Load distribution of the trailer model.

$$P_x h_2 - P_z(a \pm d_2) + F_r L = 0 \tag{4.27}$$

where h_2 is the instantaneous CG height, L is the wheelbase of the trailer, a is the distance from the front axle to the center of gravity, and d_2 denotes the longitudinal CG displacement.

Chapter 5

STATIC ANALYSIS OF THE TWO-DIMENSIONAL MODEL

To check that the proposed model provides consistent results, a two-dimensional model of the trailer was analyzed (it was described in Section 4.5).

5.1 SCREW THEORY OF THE MECHANISM

Screw theory enables the representation of the instantaneous position of the mechanism in a coordinate system and the representation of the forces and moments, as it was described in Section A.1. All these fundamentals are briefly presented below.

5.1.1 Method of successive screw displacements of the mechanism

In the kinematic model for a mechanism, the successive screws displacement method is used ((TSAI, 1999))(Section A.1.1). Figure 49 and Table 3 show the screw parameters of the mechanism, where s is the unit vector along the direction of the screw axis, s_0 is the position vector of a point lying along the screw axis, θ_i is the rotation angle, and d_i is the translation of the prismatic joint.

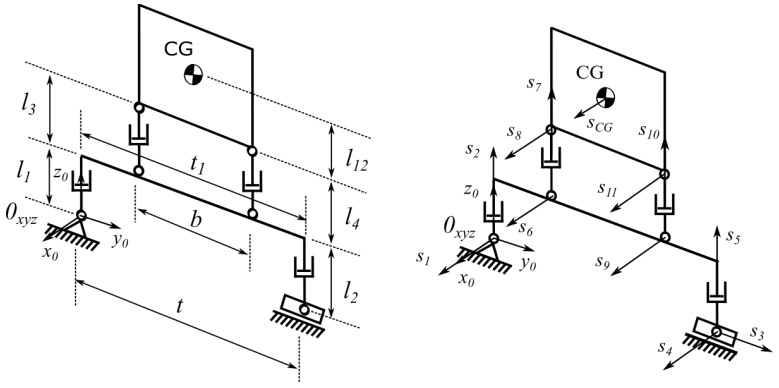

Figure 49 – Variables of the mechanism position.

The tests of the two-dimensional model were obtained using load laterally centered and, thus the initial lateral position of the center of gravity is centered.

Table 3 – Screw parameters of the mechanism.

Joints and points	s			s_0			θ	d
	s_x	s_y	s_z	s_{0x}	s_{0y}	s_{0z}		
Joint 1	1	0	0	0	0	0	θ_1	0
Joint 2	0	0	1	0	0	0	0	l_1
Joint 3	0	1	0	0	0	0	0	t
Joint 4	1	0	0	0	0	0	θ_4	0
Joint 5	0	0	1	0	0	0	0	l_2
Joint 6	1	0	0	0	$(t_1-b)/2$	0	θ_6	0
Joint 7	0	0	1	0	$(t_1-b)/2$	0	0	l_3
Joint 8	1	0	0	0	$(t_1-b)/2$	0	θ_8	0
Joint 9	1	0	0	0	$(t_1+b)/2$	0	θ_9	0
Joint 10	0	0	1	0	$(t_1+b)/2$	0	0	l_4
Joint 11	1	0	0	0	$(t_1+b)/2$	0	θ_{11}	0
CG	1	0	0	0	$t_1/2$	l_{12}	0	0

Table 4 – Instantaneous position matrix.

Joints and points	Instantaneous position matrix
Joint 1	$p_1' = A_1 p_1$
Joint 2	$p_2' = A_1 A_2 p_2$
Joint 4	$p_4' = A_3 A_4 p_4$
Joint 5	$p_5' = A_3 A_4 A_5 p_5$
Joint 6	$p_6' = A_1 A_2 A_6 p_6$
Joint 7	$p_7' = A_1 A_2 A_6 A_7 p_7$
Joint 8	$p_8' = A_1 A_2 A_6 A_7 A_8 p_8$
Joint 9	$p_9' = A_1 A_2 A_9 p_9$
Joint 10	$p_{10}' = A_1 A_2 A_9 A_{10} p_{10}$
Joint 11	$p_{11}' = A_1 A_2 A_9 A_{10} A_{11} p_{11}$
CG (12)	$p_{CG}' = A_1 A_2 A_6 A_7 A_8 A_{CG} p_{CG}$

Table 5 – Instantaneous position vector s_{0i}.

Joints and points	s_{0i}		
	s_{0ix}	s_{0iy}	s_{0iz}
Joint 1	0	0	0
Joint 2	0	$-l_1 \sin\theta_1$	$l_1 \cos\theta_1$
Joints 3, 4	0	t	0
Joint 5	0	$t - l_2 \sin\theta_4$	$l_2 \cos\theta_4$
Joint 6	0	$((t_1 - b)\cos\theta_1)/2$ $-l_1 \sin\theta_1$	$((t_1 - b)\sin\theta_1)/2$ $+l_1 \cos\theta_1$
Joints 7, 8	0	$((t_1 - b)\cos\theta_1)/2$ $-l_1 \sin\theta_1 - l_3 \sin(\theta_1 + \theta_6)$	$(t_1 - b)\sin\theta_1/2$ $+l_1 \cos\theta_1 + l_3 \cos\theta_1$
Joint 9	0	$((t_1 + b)\cos\theta_1)/2 - l_1 \sin\theta_1$	$((t_1 + b)\sin\theta_1)/2 + l_1 \cos\theta_1$
Joints 10, 11	0	$((t_1 + b)\cos\theta_1)/2 - l_1 \sin\theta_1$ $-l_4 \sin(\theta_1 + \theta_9)$	$((t_1 + b)\sin\theta_1)/2 + l_1 \cos\theta_1$ $+l_4 \cos(\theta_1 + \theta_9)$
CG	0	h_1	h_2

In Tables 3, 4 and 5, t is the vehicle track width, t_1 is the vehicle axle width, b is the lateral separation between the springs, θ_i is the rotation angle of the revolute joint i, l_1 and l_2 are the instantaneous dynamic rolling radius of the tires 1 and 2 respectively, l_3 and l_4 are the instantaneous height of the leaf spring 3 and 4 respectively, A is the transformation matrix of the point i, and l_{12} is the height of the CG above the chassis, h_1 is the instantaneous lateral distance between the zero-reference frame and the center of gravity (Eq. (5.1)), and h_2 is the instantaneous CG height (Eq. (5.2)).

$$h_1 = \frac{t_1 \cos\theta_1}{2} + \frac{b(\cos\theta_{1+6+8} - \cos\theta_1)}{2} - l_{12} \sin\theta_{1+6+8} - l_1 \sin\theta_1 - l_3 \sin\theta_{1+6} \tag{5.1}$$

$$h_2 = \frac{t_1 \sin\theta_1}{2} + \frac{b(\sin\theta_{1+6+8} - \sin\theta_1)}{2} + l_{12} \cos\theta_{1+6+8} + l_1 \cos\theta_1 + l_3 \cos\theta_{1+6} \tag{5.2}$$

This method enables the determination of the displacement of the mechanism and the instantaneous position vector s_{0i} of the joints, and the center of gravity (CG) (The vectors s_{0i} (Table 5) are obtained from the

first three terms of the last column of equations shown in Table 4), as it was described in Section A.1.1.

5.1.2 Wrench - forces and moments

In the static analysis, all forces and moments of the mechanism are represented by wrenches ($\$^A$) (DAVIES, 1983b; CAZANGI, 2008; MEJIA *et al.*, 2013). According to the orientation of the mechanism, the wrenches (forces and moments) applied (or sustained) can be represented by the vector $\$^A = \begin{bmatrix} M_x & F_y & F_z \end{bmatrix}^T$ (two-dimensional space), where F denotes the forces, and M denotes the moments (Section A.1.2).

The proposed model (Fig. 50) represents a vehicle making a turn with bank angle. To simplify the model, the following considerations were made:

- for the x-direction a steady state model was used in the analysis;
- disturbances imposed by the road and the lateral friction forces (F_y) (tire-ground contact) in joint 3 were neglected; and
- the forces P_z (Eq. (4.26)) and P_y (Eq. (4.25)) are the only external forces acting on the center of gravity CG.

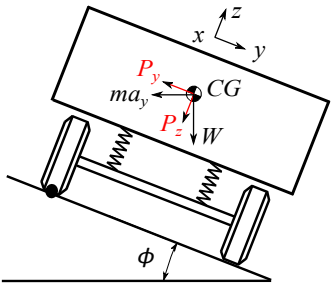

Figure 50 – Two-dimensional model in a road with bank angle.

Considering a static analysis in a two-dimensional space (TSAI, 2001), the corresponding wrenches of each joint and the external forces are defined by the parameters in Table 6, where s_i represents the orientation vector of each wrench i.

Table 6 – Wrench parameters of the mechanism.

Joints and points	Constraints and forces	s_i			Inst. position vector s_{0i} (Table 5)
		s_{ix}	s_{iy}	s_{iz}	
Revolute joints 1, 4, 8, 9 and 11	F_{yi}	0	1	0	Revolute joints 1, 4, 8, 9 and 11
	F_{zi}	0	0	1	
Prismatic joint 3	M_{xi}	1	0	0	Prismatic joint 3
	F_{zi}	0	0	1	
Revolute joints 6	F_{yi}	0	1	0	Revolute joints 6.
	F_{zi}	0	0	1	
	T_{xi}	1	0	0	
Prismatic joints 2, 5, 7 and 10	F_{pi}	0	$\cos\theta_{i-1}$	$\sin\theta_{i-1}$	Prismatic joints 2, 5, 7 and 10
	M_{xi}	1	0	0	
Prismatic joints 2 and 5	F_{Ti}	0	$-\sin\theta_{i-1}$	$\cos\theta_{i-1}$	Prismatic joints 2 and 5
Prismatic joints 7 and 10	F_{LSi}	0	$-\sin\theta_{i-1}$	$\cos\theta_{i-1}$	Prismatic joints 7 and 10
CG (12).	P_y	0	-1	0	*CG* (12).
	P_z	0	0	-1	

All of the wrenches of the mechanism together comprise the action matrix $[A_d]$ given by Eq. (5.3).

$$[A_d]_{3\times 29} = \begin{bmatrix} 0 & 0 & \cdots & p_1F_{y11} & p_2F_{z11} & h_2P_y & -h_1P_z \\ F_{y1} & 0 & \cdots & F_{y11} & 0 & -P_y & 0 \\ 0 & F_{z1} & \cdots & 0 & F_{z11} & 0 & -P_z \end{bmatrix} \tag{5.3}$$

where p_i are system variables.

The wrench can be represented by a normalized wrench and a magnitude (Eq. (A.8)). Therefore, from the Eq. (5.3) the unit action matrix and the magnitude action vector are obtained, as represented by Eqs. (5.4) and (5.5).

$$\left[\widehat{A}_d\right]_{3\times 29} = \begin{bmatrix} 0 & 0 & \cdots & p_1 & p_2 & h_2 & -h_1 \\ 1 & 0 & \cdots & 1 & 0 & -1 & 0 \\ 0 & 1 & \cdots & 0 & 1 & 0 & -1 \end{bmatrix} \tag{5.4}$$

$$[\Psi]_{29\times 1} = \begin{bmatrix} F_{y1} & F_{z1} & \cdots & F_{y11} & F_{z11} & P_y & P_z \end{bmatrix}^T \tag{5.5}$$

5.1.3 Graph theory

Kinematic chains and mechanisms are comprised of links and joints, which can be represented in a more abstract approach by graphs, as it was

describe in Section A.2. Figure 51 shows the direct coupling graph which represents the mechanism of Fig. 41. The graph has 10 vertices (links) and 13 edges (joints and external forces (P_y and P_z).

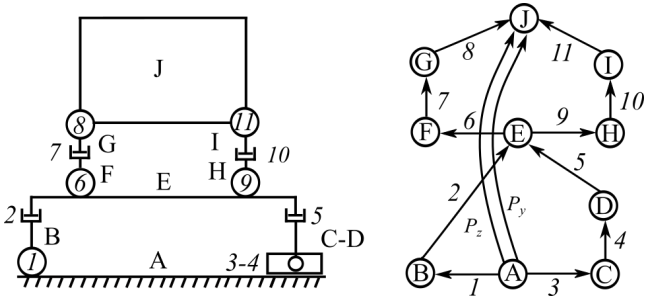

Figure 51 – Direct coupling graph representing the mechanism.

The direct coupling graph (Fig. 51) can be represented by the incidence matrix $[I]_{10\times13}$ (DAVIES, 1995) (Eq. (5.6)). Solving the system in Eq. (5.6), using the Gauss-Jordan elimination method, the incidence matrix provides the cut-set matrix $[Q]_{9\times13}$ (DAVIES, 1995; ERTHAL, 2010; MORENO *et al.*, 2016c; MORENO *et al.*, 2016) (Eq. (5.7)) for the mechanism, where each line represents a cut of the graph and the columns represent the joints and the external forces. In addition, this matrix is rearranged, allowing 9 branches (edges *1-4, 6-10* and *27* - identity matrix) and 4 chords (edges *5, 11*, P_y and P_z) to be defined, as shown in Fig. 52(a).

$$[I]_{10\times13} = \begin{array}{c} \\ A \\ B \\ C \\ D \\ E \\ F \\ G \\ H \\ I \\ J \end{array} \begin{array}{c} \begin{array}{ccccccccccc} 1 & 2 & 3 & 4 & \cdots & 9 & 10 & 11 & P_y & P_z \end{array} \\ \begin{bmatrix} 1 & 0 & 1 & 0 & \cdots & 0 & 0 & 0 & 1 & 1 \\ -1 & 1 & 0 & 0 & \cdots & 0 & 0 & 0 & 0 & 0 \\ 0 & 0 & -1 & 1 & \cdots & 0 & 0 & 0 & 0 & 0 \\ 0 & 0 & 0 & -1 & \cdots & 0 & 0 & 0 & 0 & 0 \\ 0 & -1 & 0 & 0 & \cdots & 1 & 0 & 0 & 0 & 0 \\ 0 & 0 & 0 & 0 & \cdots & 0 & 0 & 0 & 0 & 0 \\ 0 & 0 & 0 & 0 & \cdots & 0 & 0 & 0 & 0 & 0 \\ 0 & 0 & 0 & 0 & \cdots & -1 & 1 & 0 & 0 & 0 \\ 0 & 0 & 0 & 0 & \cdots & 0 & -1 & 1 & 0 & 0 \\ 0 & 0 & 0 & 0 & \cdots & 0 & 0 & -1 & -1 & -1 \end{bmatrix} \end{array} \tag{5.6}$$

$$[Q]_{9\times13} = \begin{array}{c} \\ Cut\ 1 \\ Cut\ 2 \\ Cut\ 3 \\ Cut\ 4 \\ Cut\ 5 \\ Cut\ 6 \\ Cut\ 7 \\ Cut\ 8 \\ Cut\ 9 \end{array} \begin{array}{c} \begin{array}{ccccccccccc} 1 & 2 & 3 & 4 & \cdots & 9 & 10 & 11 & P_y & P_z \end{array} \\ \begin{bmatrix} 1 & 0 & 0 & 0 & \cdots & 0 & 0 & 0 & 1 & 1 \\ 0 & 1 & 0 & 0 & \cdots & 0 & 0 & 0 & 1 & 1 \\ 0 & 0 & 1 & 0 & \cdots & 0 & 0 & 0 & 0 & 0 \\ 0 & 0 & 0 & 1 & \cdots & 0 & 0 & 0 & 0 & 0 \\ 0 & 0 & 0 & 0 & \cdots & 0 & 0 & 1 & 1 & 1 \\ 0 & 0 & 0 & 0 & \cdots & 0 & 0 & 1 & 1 & 1 \\ 0 & 0 & 0 & 0 & \cdots & 0 & 0 & 1 & 1 & 1 \\ 0 & 0 & 0 & 0 & \cdots & 1 & 0 & -1 & 0 & 0 \\ 0 & 0 & 0 & 0 & \cdots & 0 & 1 & -1 & 0 & 0 \end{bmatrix} \end{array} \tag{5.7}$$

All of the constraints are represented as edges. Which allows the amplification of the cut-set graph and the cut-set matrix. Additionally, the tire normal loads ($F_{T2,5}$), leaf spring normal loads ($F_{LS7,10}$), and the passive torsional moment (T_{x6}) are included.

Figure 52b presents the cut-set action graph and the Eq. (5.8) presents the expanded cut-set matrix ($[Q]_{9\times29}$), where each line represents a cut of the graph, and the columns represents the constraints of the joints as well as the external forces acting on the mechanism.

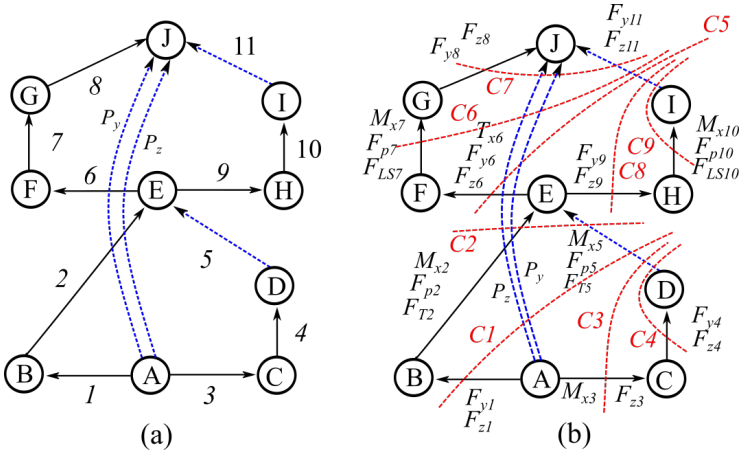

Figure 52 – (a) Cut-set graph. (b) Cut-set action graph.

$$[Q]_{9\times29} = \begin{array}{c} \begin{matrix} F_{y1} & F_{z1} & M_{x2} & F_{p2} & \cdots & F_{y11} & F_{z11} & P_y & P_z \end{matrix} \\ \begin{bmatrix} 1 & 1 & 0 & 0 & \cdots & 0 & 0 & 1 & 1 \\ 0 & 0 & 1 & 1 & \cdots & 0 & 0 & 1 & 1 \\ 0 & 0 & 0 & 0 & \cdots & 0 & 0 & 0 & 0 \\ 0 & 0 & 0 & 0 & \cdots & 0 & 0 & 0 & 0 \\ 0 & 0 & 0 & 0 & \cdots & 1 & 1 & 1 & 1 \\ 0 & 0 & 0 & 0 & \cdots & 1 & 1 & 1 & 1 \\ 0 & 0 & 0 & 0 & \cdots & 1 & 1 & 1 & 1 \\ 0 & 0 & 0 & 0 & \cdots & -1 & -1 & 0 & 0 \\ 0 & 0 & 0 & 0 & \cdots & -1 & -1 & 0 & 0 \end{bmatrix} \end{array} \tag{5.8}$$

5.1.4 Equation system solutions

Using the *Cut-set law* (DAVIES, 2000), the algebraic sum of the normalized wrenches Eqs. (5.4) and (5.5), that belong to the same cut $[Q]_{9\times29}$ (Fig. 52(b) and Eq. (5.8)) must be equal to zero. Thus, the statics of the mechanism can be defined, as exemplified in Eq. (5.9) (or the

amplified matrix of the Eq. (5.10)):

$$\left[\widehat{A}_n\right]_{27\times 29}[\Psi]^T_{29\times 1} = [0]_{27\times 1} \tag{5.9}$$

$$\begin{array}{l}
\\
\text{Cut 1} \\
\\
\\
\text{Cut 2} \\
\\
\vdots \\
\\
\text{Cut 9} \\
\\
\end{array}
\begin{bmatrix}
0 & 0 & 0 & \cdots & 0 & h_2 & -h_1 \\
1 & 0 & 0 & \cdots & 0 & -1 & 0 \\
0 & 1 & 0 & \cdots & 0 & 0 & -1 \\
0 & 0 & 1 & \cdots & 0 & h_2 & -h_1 \\
0 & 0 & 0 & \cdots & 0 & -1 & 0 \\
0 & 0 & 0 & \cdots & 0 & 0 & -1 \\
\vdots & \vdots & \vdots & \vdots & \vdots & \vdots & \vdots \\
0 & 0 & 0 & \cdots & -p_{10} & 0 & 0 \\
0 & 0 & 0 & \cdots & 0 & 0 & 0 \\
0 & 0 & 0 & \cdots & -1 & 0 & 0
\end{bmatrix}
\cdot
\begin{bmatrix}
F_{y1} \\ F_{z1} \\ M_{x2} \\ \vdots \\ F_{z11} \\ P_y \\ P_z
\end{bmatrix}
= [0]_{27\times 1} \tag{5.10}$$

It is necessary to identify the set of primary variables $[\Psi_p]$ (known variables), among the variables of Ψ. Once identified, the system of the Eq. (5.9) is rearranged and dividing into two sets, as shown by Eq. (5.11):

$$\left[\widehat{A}_{ns}\right]_{27\times 27}[\Psi_s]^T_{27\times 1} + \left[\widehat{A}_{np}\right]_{27\times 2}[\Psi_p]^T_{2\times 1} = [0]_{27\times 1} \tag{5.11}$$

where $[\Psi_p]$ is the primary variable vector, $[\Psi_s]$ is the secondary variable vector (unknown variables), $\left[\widehat{A}_{np}\right]$ are the columns corresponding to the primary variables and $\left[\widehat{A}_{ns}\right]$ are the columns corresponding to the secondary variables.

In this case, the primary variable vector is:

$$[\Psi_p]_{2\times 1} = \begin{bmatrix} P_y & P_z \end{bmatrix}^T \tag{5.12}$$

and the secondary variable vector is:

$$[\Psi_s]_{27\times 1} = \begin{bmatrix} F_{y1} & M_{x2} & F_{p2} & \cdots & F_{T2} & F_{LS7} & F_{z1} & F_{z3} \end{bmatrix}^T \tag{5.13}$$

Solving the system in Eq. (5.11) using the Gauss-Jordan elimination method provides the system Eq. (5.14). All secondary variables of

the systems in Eq. (5.14) are functions of the primary variables.

$$\left[\begin{array}{c|cc} & 0 & -1 \\ & C_1 & C_{22} \\ & C_2 & C_{23} \\ & 0 & 0 \\ & 0 & 0 \\ & -h_1/t & h_2/t \\ & C_3 & C_{24} \\ & C_4 & C_{25} \\ & C_5 & C_{26} \\ & C_6 & C_{27} \\ & C_7 & C_{16} \\ & C_8 & C_{28} \\ & C_9 & C_{29} \\ [I]_{27} & C_{10} & C_{30} \\ & C_{11} & C_{31} \\ & C_{12} & C_{32} \\ & C_{13} & C_{33} \\ & C_{14} & C_{34} \\ & C_{15} & C_{35} \\ & C_{16} & C_{36} \\ & C_{17} & C_{37} \\ & C_{18} & C_{38} \\ & C_{19} & C_{39} \\ & C_{20} & C_{40} \\ & C_{21} & C_{41} \\ & (h_1-t)/t & -h_2/t \\ & -h_1/t & h_2/t \end{array}\right] . \left[\begin{array}{c} F_{y1} \\ M_{x2} \\ F_{p2} \\ M_{x3} \\ F_{y4} \\ F_{z4} \\ F_{y6} \\ F_{z6} \\ M_{x7} \\ F_{p7} \\ F_{y8} \\ F_{z8} \\ F_{y9} \\ F_{z9} \\ M_{x10} \\ F_{p10} \\ M_{x5} \\ F_{p5} \\ F_{y11} \\ F_{z11} \\ T_{x6} \\ F_{T2} \\ F_{LS7} \\ F_{T5} \\ F_{LS10} \\ F_{z1} \\ F_{z3} \\ P_z \\ P_y \end{array}\right] = [0]_{27\times 1} \tag{5.14}$$

where C_i are system variables.

5.2 RESULT

The system of the Eq. (5.14) shows all forces of the mechanism; as the model does not have into account frictional forces on the tire-ground interface, the lateral force (F_{y4}) on the tire 2 is equal to zero (5^{th} row).

For this analysis only the forces acting on the suspension and the tires are taken into account; the last seven rows of Eq. (5.14) show the next equations: the moment of the joint 6 (T_{6x}), the normal forces of the

tire ($F_{T2,5}$), the normal forces of the leaf spring ($F_{LS7,10}$), and the normal loads of the tires (F_{z1} and F_{z3}).

$$T_{x6} + C_{17}P_z + C_{37}P_y = 0 \tag{5.15}$$

$$F_{T2} + C_{18}P_z + C_{38}P_y = 0 \tag{5.16}$$

$$F_{T5} + C_{20}P_z + C_{40}P_y = 0 \tag{5.17}$$

$$F_{LS7} + C_{19}P_z + C_{39}P_y = 0 \tag{5.18}$$

$$F_{LS10} + C_{21}P_z + C_{41}P_y = 0 \tag{5.19}$$

$$F_{z1} + ((h_1 - t)/t)P_z - (h_2/t)P_y = 0 \tag{5.20}$$

$$F_{z3} - (h_1/t)P_z + (h_2/t)P_y = 0 \tag{5.21}$$

From Eqs. (5.15) to (5.21) the instantaneous forces acting on mechanism can be obtained. These forces modifying the configuration of the tires and suspension systems, as shown in chapter 4.

At the rollover limit condition, the normal load, F_{z3}, reaches zero, applying this condition in Eq. (5.21) and replacing the forces P_z (Eq. (4.26)) and P_y (Eq. (4.25)), the SRT factor can be calculated as:

$$SRT_{2DTM} = \frac{a_y}{g} = \frac{h_1 + h_2 e}{h_2 - h_1 e} \tag{5.22}$$

where e is the tangent of the bank angle ($e = \tan(\phi)$) and SRT_{2DTM} is the static rollover threshold for a two-dimensional trailer model in a road with bank angle.

Table 7 shows a comparison between the SRT factors of the two-dimensional models presented in the Chapter 2 and the SRT factor of the developed model.

Table 7 – SRT factors of two-dimensional models.

Model	SRT factors of 2D models
Rigid model (Eq. (2.6))	$SRT_{2D} = \dfrac{t/2}{h}$
Rigid model in a road with bank angle (Eq. (2.8))	$SRT_{2D-B} = \dfrac{t/2}{h} + e$
Winkler model (Eq. (2.10))	$SRT_{2D-W} = \dfrac{t/2 - \triangle t}{h_2}$
Rill model (Eq. (2.20))	$SRT_{2D-R} = \dfrac{t/2}{h + \dfrac{l_{12}}{k_\theta^* - 1}} - \dfrac{1}{k_T^*}$
Chang model (Eq. (2.22))	$SRT_{2D-CB} = \dfrac{t}{2h} + (1 - \dfrac{h_0}{h})(\phi - \theta)$
Developed 2D-model (Eq. (5.22))	$SRT_{2DTM} = \dfrac{h_1 + h_2 e}{h_2 - h_1 e}$

Table 7 shows that the SRT factor of the developed 2D-model (Eq. (5.22)) is more complete, since the model takes into account all the characteristics considered by the other models.

5.3 PUBLICATIONS

The two-dimensional model of the trailer has the following publications:

• Moreno, G. G., Nicolazzi, L., Vieira, R. S., Martins, D. *Suspension and tires: the stability of heavy vehicles*. International Journal of Heavy vehicle Systems, (in press). 2016.

• Moreno, G. G., Nicolazzi, L., Vieira, R. S., Martins, D. *Modeling and analysis of solid axle suspension and its impact on the heavy vehicles stability*. In: CONEM 2016 Congresso Nacional de Engenharia Mecânica. Fortaleza - Brasil. 2016.

Chapter 6

STATIC ANALYSIS OF THE THREE-DIMENSIONAL MODEL

In this chapter a three-dimensional model of the trailer was analyzed (it was described in Section 4.6).

6.1 METHOD OF SUCCESSIVE SCREW DISPLACEMENTS OF THE MECHANISM

The tests of the three-dimensional model were obtained using three loading conditions. Loading conditions included a load laterally centered, load with *CG* displacement, and overweight with *CG* displacement; for these reasons the position of the center of gravity includes small displacements (d_1 - lateral *CG* displacement, d_2 - longitudinal *CG* displacement, and d_3 - vertical *CG* displacement)(it was described in Section 4.7).

In the kinematic model for a mechanism the successive screws displacement method is used (Section A.1.1). Figures 53 to 57 and Table 8 present the screw parameters of the mechanism.

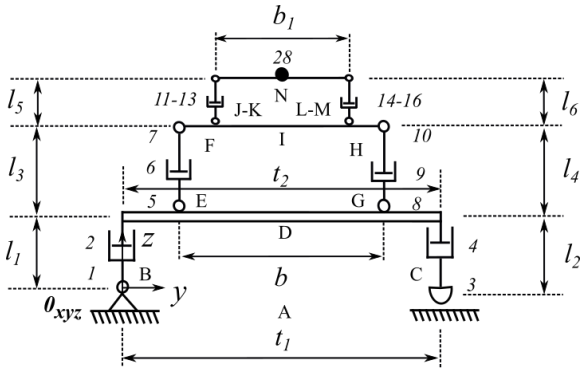

Figure 53 – Variables of the mechanism position (Front view of the trailer).

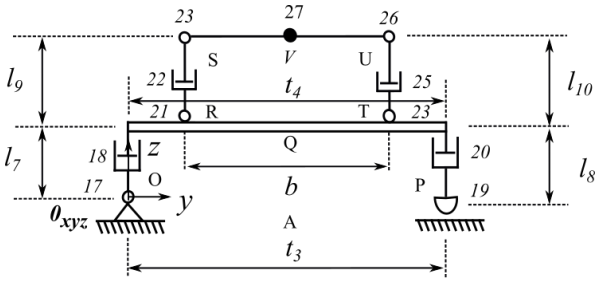

Figure 54 – Variables of the mechanism position (Rear view of the trailer).

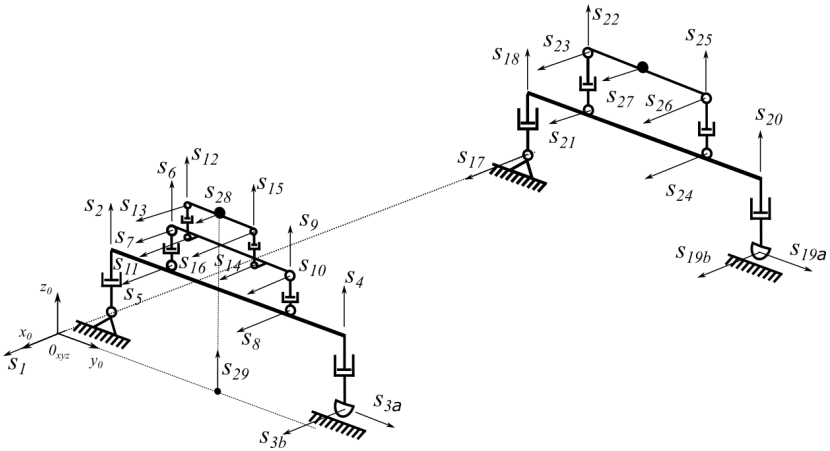

Figure 55 – Vectors along the direction of the screws axis (Front and rear views of the trailer).

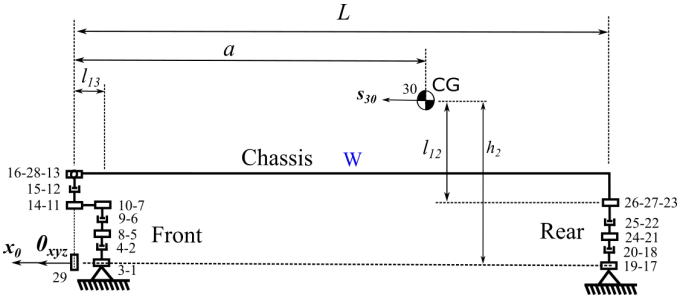

Figure 56 – Variables of the mechanism position (Right side view of the vehicle)

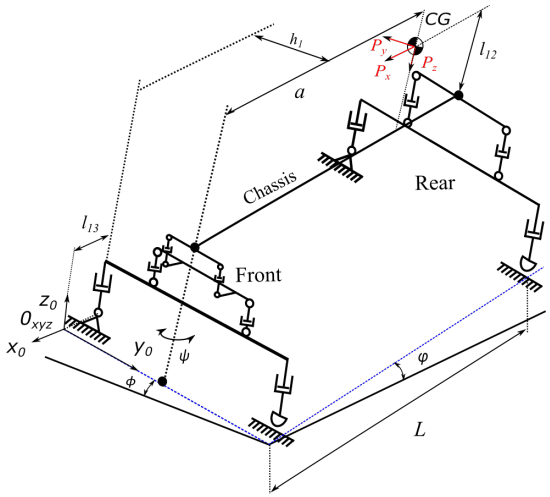

Figure 57 – Variables of the mechanism position (Three-dimensional model)

In Figures 53 to 57 and Table 8, l_{13} is the distance between the fifth-wheel and the front axle, $l_{1,2,7,8}$ are the dynamic rolling radii of tires, $t_{1,3}$ are the front and rear track widths of the trailer respectively, $t_{2,4}$ are the front and rear axle width of the trailer respectively, b is the lateral separation between the springs, b_1 is the fifth-wheel width, θ_i is the revolution joint angle rotation i, $l_{3,4,9,10}$ are the instantaneous heights of the leaf spring, l_{12} is the height of the CG above the chassis, and ψ is the trailer/trailer angle.

This method enables the determination of the displacement of the mechanism and the instantaneous position vector s_{0i} of the joints, and the center of gravity (The vectors s_{0i} (Table 10) are obtained from the first three terms of the last column of equations shown in Table 9), as it was described in Section A.1.1.

Table 8 – Screw parameters of the mechanism.

Joints and points	s			s_0			θ	d
	s_x	s_y	s_z	s_{0x}	s_{0y}	s_{0z}		
Joint 1	1	0	0	$-l_{13}$	0	0	θ_1	0
Joint 2	0	0	1	$-l_{13}$	0	0	0	l_1
Joint 3a	0	1	0	$-l_{13}$	0	0	0	t_1
Joint 3b	1	0	0	$-l_{13}$	0	0	θ_3	0
Joint 4	0	0	1	$-l_{13}$	0	0	0	l_2
Joint 5	1	0	0	$-l_{13}$	$(t_2-b)/2$	0	θ_5	0
Joint 6	0	0	1	$-l_{13}$	$(t_2-b)/2$	0	0	l_3
Joint 7	1	0	0	$-l_{13}$	$(t_2-b)/2$	0	θ_7	0
Joint 8	1	0	0	$-l_{13}$	$(t_2+b)/2$	0	θ_8	0
Joint 9	0	0	1	$-l_{13}$	$(t_2+b)/2$	0	0	l_4
Joint 10	1	0	0	$-l_{13}$	$(t_2+b)/2$	0	θ_{10}	0
Joint 11	1	0	0	0	$(t_2-b_1)/2$	0	θ_{11}	0
Joint 12	0	0	1	0	$(t_2-b_1)/2$	0	0	l_5
Joint 13	1	0	0	0	$(t_2-b_1)/2$	0	θ_{13}	0
Joint 14	1	0	0	0	$(t_2+b_1)/2$	0	θ_{14}	0
Joint 15	0	0	1	0	$(t_2+b_1)/2$	0	0	l_6
Joint 16	1	0	0	0	$(t_2+b_1)/2$	0	θ_{16}	0
Joint 17	1	0	0	$-L$	0	0	θ_{17}	0
Joint 18	0	0	1	$-L$	0	0	0	l_7
Joint 19a	0	1	0	$-L$	0	0	0	t_3
Joint 19b	1	0	0	$-L$	0	0	θ_{19}	0
Joint 20	0	0	1	$-L$	0	0	0	l_8
Joint 21	1	0	0	$-L$	$(t_4-b)/2$	0	θ_{21}	0
Joint 22	0	0	1	$-L$	$(t_4-b)/2$	0	0	l_9
Joint 23	1	0	0	$-L$	$(t_4-b)/2$	0	θ_{23}	0
Joint 24	1	0	0	$-L$	$(t_4+b)/2$	0	θ_{24}	0
Joint 25	0	0	1	$-L$	$(t_4+b)/2$	0	0	l_{10}
Joint 26	1	0	0	$-L$	$(t_4+b)/2$	0	θ_{26}	0
Joint 27	1	0	0	$-L$	$t_4/2$	0	θ_{27}	0
Joint 28	1	0	0	0	$t_2/2$	0	θ_{28}	0
Point 29	0	0	1	0	$t_2/2$	0	ψ	0
CG (30)	1	0	0	$-a\pm d_2$	$(t_4/2)\pm d_1$	$l_{12}\pm d_3$	0	0

Table 9 – Instantaneous position matrix.

Joints and points	Instantaneous position matrix
Joint 1	$p_1^{'} = A_{29}A_1p_1$
Joint 2	$p_2^{'} = A_{29}A_1A_2p_2$
Joint 3	$p_3^{'} = A_{29}A_{3a}A_{3b}p_3$
Joint 4	$p_4^{'} = A_{29}A_{3a}A_{3b}A_4p_4$
Joint 5	$p_5^{'} = A_{29}A_1A_2A_5p_5$
Joint 6	$p_6^{'} = A_{29}A_1A_2A_5A_6p_6$
Joint 7	$p_7^{'} = A_{29}A_1A_2A_5A_6A_7p_7$
Joint 8	$p_8^{'} = A_{29}A_1A_2A_8p_8$
Joint 9	$p_9^{'} = A_{29}A_1A_2A_8A_9p_9$
Joint 10	$p_{10}^{'} = A_{29}A_1A_2A_8A_9A_{10}p_{10}$
Joint 11	$p_{11}^{'} = A_{29}A_1A_2A_5A_6A_7A_{11}p_{11}$
Joint 12	$p_{12}^{'} = A_{29}A_1A_2A_5A_6A_7A_{11}A_{12}p_{12}$
Joint 13	$p_{13}^{'} = A_{29}A_1A_2A_5A_6A_7A_{11}A_{12}A_{13}p_{13}$
Joint 14	$p_{14}^{'} = A_{29}A_1A_2A_5A_6A_7A_{14}p_{14}$
Joint 15	$p_{15}^{'} = A_{29}A_1A_2A_5A_6A_7A_{14}A_{15}p_{15}$
Joint 16	$p_{16}^{'} = A_{29}A_1A_2A_5A_6A_7A_{14}A_{15}A_{16}p_{16}$
Joint 17	$p_{17}^{'} = A_{17}p_{17}$
Joint 18	$p_{18}^{'} = A_{17}A_{18}p_{18}$
Joint 19	$p_{19}^{'} = A_{19a}A_{19b}p_{19}$
Joint 20	$p_{20}^{'} = A_{19a}A_{19b}A_{20}p_{20}$
Joint 21	$p_{21}^{'} = A_{17}A_{18}A_{21}p_{21}$
Joint 22	$p_{22}^{'} = A_{17}A_{18}A_{21}A_{22}p_{22}$
Joint 23	$p_{23}^{'} = A_{17}A_{18}A_{21}A_{22}A_{23}p_{23}$
Joint 24	$p_{24}^{'} = A_{17}A_{18}A_{24}p_{24}$
Joint 25	$p_{25}^{'} = A_{17}A_{18}A_{24}A_{25}p_{25}$
Joint 26	$p_{26}^{'} = A_{17}A_{18}A_{24}A_{25}A_{26}p_{26}$
Joint 27	$p_{27}^{'} = A_{17}A_{18}A_{21}A_{22}A_{23}A_{27}p_{27}$
Joint 28	$p_{28}^{'} = A_{29}A_1A_2A_5A_6A_7A_{11}A_{12}A_{13}A_{28}p_{28}$
CG (30)	$p_{CG}^{'} = A_{17}A_{18}A_{21}A_{22}A_{23}A_{27}A_{CG}p_{CG}$

Table 10 – Instantaneous position vector s_{0i}.

Joints and points	s_{0i}		
	s_{0ix}	s_{0iy}	s_{0iz}
Joint 1	$\frac{t_2 s_{29} - 2l_{13}c_{29}}{2}$	$-\frac{2l_{13}s_{29} + t_2 c_{29} - t_2}{2}$	0
Joint 2	$\frac{(2l_1 s_1 + t_2)s_{29} - 2l_{13}c_{29}}{2}$	$-\frac{(2l_1 s_1 + t_2)c_{29} + 2l_{13}s_{29} - t_2}{2}$	$l_1 c_1$
Joint 3	$\frac{(t_2 - 2t_1)s_{29} - 2l_{13}c29}{2}$	$-\frac{2l_{13}s_{29} + (t_2 - 2t_1)c_{29} - t_2}{2}$	0
Joint 4	$\frac{(2l_2 s_3 + t_2 - 2t_1)s_{29} - 2l_{13}c_{29}}{2}$	$-\frac{2l_{13}s_{29} + (2l_2 s_3 + t_2 - 2t_1)c_{29} - t_2}{2}$	$l_2 c_3$
Joints 5 to 16	$\vdots$	$\vdots$	$\vdots$
Joint 17	$-L$	0	0
Joint 18	$-L$	$-l_7 s_{17}$	$l_7 c_{17}$
Joint 19	$-L$	t_3	0
Joint 20	$-L$	$t_3 - l_8 s_{19}$	$l_8 c_{19}$
Joint 21	$-L$	$-\frac{2l_7 s_{17} + (b - t_4)c_{17}}{2}$	$\frac{(t_4 - b)s_{17} + 2l_{17}c_{17}}{2}$
Joints 22-23	$-L$	$\frac{-2l_9 s_{21+17} - 2l_7 s_{17} + (b - t_4)c_{17}}{2}$	$\frac{2l_9 c_{21+17} + 2l_7 c_{17} + (t_4 - b)s_{17}}{2}$
Joints 24 to 28	$\vdots$	$\vdots$	$\vdots$
CG	$-a \mp d_2$	h_1	h_2

$s_i = \sin\theta_i \quad c_i = \cos\theta_i$

from the Table 10 h_1 is the instantaneous lateral distance between the zero-reference frame and the center of gravity (Eq. (6.1)), and h_2 is the instantaneous *CG* height (Eq. (6.2)).

$$h_1 = -(l_{12} \pm d_3)s_{27+23+21+17} \mp d_1 c_{27+23+21+17} + \frac{b}{2}c_{23+21+17}$$

$$- l_9 s_{21+17} - l_7 s_{17} - \frac{b - t_4}{2}c_{17} \tag{6.1}$$

$$h_2 = \mp d_1 s_{27+23+21+17} + (l_{12} \mp d_3)c_{27+23+21+17} + \frac{b}{2}s_{23+21+17}$$

$$+ l_9 c_{21+17} + \frac{t_4 - b}{2}s17 + l_7 c_{17} \tag{6.2}$$

6.1.1 Wrench - forces and moments

In the static analysis, all forces and moments of the mechanism are represented by wrenches ($\$^A$) (DAVIES, 1983b; CAZANGI, 2008; MEJIA *et al.*, 2013). According to the orientation of the mechanism, the wrenches (forces and moments) applied (or sustained) can be represented by the vector $\$^A = \begin{bmatrix} M_x & M_y & M_z & F_x & F_y & F_z \end{bmatrix}^T$ (three-dimensional space), where F denotes the forces, and M denotes the moments (Section A.1.2).

The proposed model (Fig. 57) represents a vehicle making a turn. To simplify the model, the following considerations were made:

- for the x-direction a steady state model was used in the analysis;
- accelerating, braking and aerodynamics forces were neglected;
- disturbances imposed by the road and the lateral friction forces (F_y) (tire-ground contact) in joints 3 and 19 were neglected; and
- the components of the total weight of the trailer (W) and the inertial force (ma_y) are the only external forces acting on the center of gravity *CG* (Eqs. (4.24) to (4.26)).

Considering a static analysis in a three-dimensional space (TSAI, 2001), the corresponding wrenches of each joint and the external forces are defined by the parameters in Table 11, where s_i represents the orientation vector of each wrench i.

Table 11 – Wrench parameters of the mechanism.

Joints and points	Constraints and forces	s_i			Inst. position vector s_{0i} (Table 10)
		s_{ix}	s_{iy}	s_{iz}	
Revolute joints 1, 7, 8, 10, 13, 14, 16, 17, 23, 24 and 26.	F_{xi}	1	0	0	Revolute joints 1, 7, 8, 10, 13, 14, 16, 17, 23, 24 and 26.
	F_{yi}	0	1	0	
	F_{zi}	0	0	1	
	M_{yi}	0	1	0	
	M_{zi}	0	0	1	
Spherical slider joints 3 and 19.	F_{xi}	1	0	0	Spherical slider joints 3 and 19.
	M_{yi}	0	1	0	
	F_{zi}	0	0	1	
Revolute joints 5, 11 and 21.	F_{xi}	1	0	0	Revolute joints 5, 11 and 21.
	F_{yi}	0	1	0	
	F_{zi}	0	0	1	
	T_{xi}	1	0	0	
	M_{yi}	0	1	0	
	M_{zi}	0	0	1	
Prismatic joints 2, 4, 6, 9, 12, 15, 18, 20, 22 and 25.	F_{xi}	1	0	0	Prismatic joints 2, 4, 6, 9, 12, 15, 18, 20, 22 and 25.
	F_{pi}	0	$\cos\theta_{i-1}$	$\sin\theta_{i-1}$	
	M_{xi}	1	0	0	
	M_{yi}	0	1	0	
	M_{zi}	0	0	1	
Prismatic joints 2, 4, 18 and 20.	F_{Ti}	0	$-\sin\theta_{i-1}$	$\cos\theta_{i-1}$	Prismatic joints 2, 4, 18 and 20.
Prismatic joints 6, 9, 22 and 25.	F_{LSi}	0	$-\sin\theta_{i-1}$	$\cos\theta_{i-1}$	Prismatic joints 6, 9, 22 and 25.
Prismatic joints 12 and 15.	F_{FWi}	0	$-\sin\theta_{i-1}$	$\cos\theta_{i-1}$	Prismatic joints 12 and 15.
Spherical joints 27 and 28.	F_{xi}	1	0	0	Spherical joints 27 and 28.
	F_{yi}	0	1	0	
	F_{zi}	0	0	1	
	T_{xi}	1	0	0	
CG (30).	P_x	1	0	0	*CG* (30).
	P_y	0	-1	0	
	P_z	0	0	-1	

All of the wrenches of the mechanism together comprise the action matrix $[A_d]$ given by Eq. (6.3)(or the amplified matrix of the Eq. (6.4)) .

$$[A_d]_{6\times 150} = \begin{bmatrix} \$^A_{F_{x1}} & \$^A_{F_{y1}} & \cdots & \$^A_{P_x} & \$^A_{P_y} & \$^A_{P_z} \end{bmatrix} \tag{6.3}$$

$$[A_d] = \begin{bmatrix} 0 & 0 & \cdots & 0 & h_2P_y & -h_1P_z \\ 0 & 0 & \cdots & h_2P_x & 0 & (-a\pm d_2)P_z \\ p_1F_{x1} & p_2F_{y1} & \cdots & -h_1P_x & -(-a\pm d_2)P_y & 0 \\ F_{x1} & 0 & \cdots & P_x & 0 & 0 \\ 0 & F_{y1} & \cdots & 0 & -P_y & 0 \\ 0 & 0 & \cdots & 0 & 0 & -P_z \end{bmatrix} \tag{6.4}$$

where p_i are system variables.

The wrench can be represented by a normalized wrench and a magnitude (Eq. (A.8)). Therefore, from the Eq. (6.4) the *unit action matrix* and the *magnitude action vector* are obtained, as represented by Eqs. (6.5) and (6.6).

$$\left[\widehat{A}_d\right]_{6\times 150} = \begin{bmatrix} 0 & 0 & \cdots & 0 & h_2 & -h_1 \\ 0 & 0 & \cdots & h_2 & 0 & (-a\pm d_2) \\ p_1 & p_2 & \cdots & -h_1 & -(-a\pm d_2) & 0 \\ 1 & 0 & \cdots & 1 & 0 & 0 \\ 0 & 1 & \cdots & 0 & -1 & 0 \\ 0 & 0 & \cdots & 0 & 0 & -1 \end{bmatrix} \tag{6.5}$$

$$[\Psi]_{150\times 1} = \begin{bmatrix} F_{x1} & F_{y1} & \cdots & P_x & P_y & P_z \end{bmatrix}^T \tag{6.6}$$

6.1.2 Graph theory

Figure 58 shows the direct coupling graph which represents the mechanism of Fig. 57. The graph has twenty-three vertices (links) and thirty-one edges (joints and the external forces P_x, P_y and P_z).

The direct coupling graph (Fig. 58) can be represented by the incidence matrix $[I]_{23\times 31}$ (Eq. (6.7)). Solving the system in Eq. (6.7) using the Gauss-Jordan elimination method, the incidence matrix provides the cut-set matrix $[Q]_{22\times 31}$ (Eq. (6.8)) for the mechanism, where each line represents a cut of the graph and the columns represent the joints and the external forces. In addition, this matrix is rearranged, allowing twenty-two branches (edges *1-3, 5-9, 11-15, 17-19, 21-25* and *27* - identity matrix) and nine chords (edges *4, 10, 16, 20, 26, 28*, P_x, P_y and P_z) to be defined, as shown in Fig. 59.

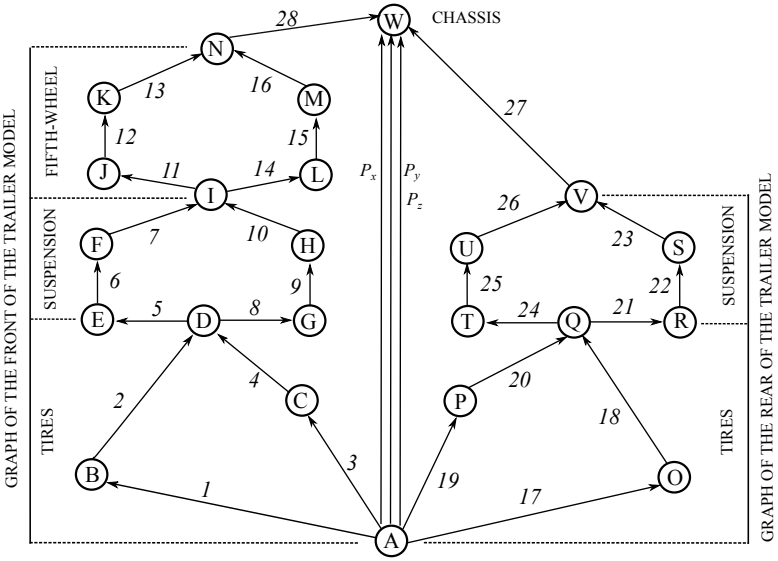

Figure 58 – Direct coupling graph of the mechanism.

$$
[I]_{23\times 31} = \begin{array}{c} \\ A \\ B \\ C \\ D \\ E \\ F \\ G \\ H \\ I \\ J \\ K \\ L \\ M \\ N \\ O \\ P \\ Q \\ R \\ S \\ T \\ U \\ V \\ W \end{array}
\begin{array}{c}
\begin{array}{cccccccccccccccc} 1 & 2 & 3 & 4 & 5 & 6 & 7 & 8 & \cdots & 25 & 26 & 27 & 28 & P_x & P_y & P_z \end{array} \\
\left[\begin{array}{cccccccccccccccc}
1 & 0 & 1 & 0 & 0 & 0 & 0 & 0 & \cdots & 0 & 0 & 0 & 0 & 1 & 1 & 1 \\
-1 & 1 & 0 & 0 & 0 & 0 & 0 & 0 & \cdots & 0 & 0 & 0 & 0 & 0 & 0 & 0 \\
0 & 0 & -1 & 1 & 0 & 0 & 0 & 0 & \cdots & 0 & 0 & 0 & 0 & 0 & 0 & 0 \\
0 & -1 & 0 & -1 & 1 & 0 & 0 & 1 & \cdots & 0 & 0 & 0 & 0 & 0 & 0 & 0 \\
0 & 0 & 0 & 0 & -1 & 1 & 0 & 0 & \cdots & 0 & 0 & 0 & 0 & 0 & 0 & 0 \\
0 & 0 & 0 & 0 & 0 & -1 & 1 & 0 & \cdots & 0 & 0 & 0 & 0 & 0 & 0 & 0 \\
0 & 0 & 0 & 0 & 0 & 0 & 0 & -1 & \cdots & 0 & 0 & 0 & 0 & 0 & 0 & 0 \\
0 & 0 & 0 & 0 & 0 & 0 & 0 & 0 & \cdots & 0 & 0 & 0 & 0 & 0 & 0 & 0 \\
0 & 0 & 0 & 0 & 0 & 0 & 0 & 0 & \cdots & 0 & 0 & 0 & 0 & 0 & 0 & 0 \\
0 & 0 & 0 & 0 & 0 & 0 & 0 & 0 & \cdots & 0 & 0 & 0 & 0 & 0 & 0 & 0 \\
0 & 0 & 0 & 0 & 0 & 0 & 0 & 0 & \cdots & 0 & 0 & 0 & 0 & 0 & 0 & 0 \\
0 & 0 & 0 & 0 & 0 & 0 & 0 & 0 & \cdots & 0 & 0 & 0 & 0 & 0 & 0 & 0 \\
0 & 0 & 0 & 0 & 0 & 0 & 0 & 0 & \cdots & 0 & 0 & 0 & 0 & 0 & 0 & 0 \\
0 & 0 & 0 & 0 & 0 & 0 & 0 & 0 & \cdots & 0 & 0 & 0 & 1 & 0 & 0 & 0 \\
0 & 0 & 0 & 0 & 0 & 0 & 0 & 0 & \cdots & 0 & 0 & 0 & 0 & 0 & 0 & 0 \\
0 & 0 & 0 & 0 & 0 & 0 & 0 & 0 & \cdots & 0 & 0 & 0 & 0 & 0 & 0 & 0 \\
0 & 0 & 0 & 0 & 0 & 0 & 0 & 0 & \cdots & 0 & 0 & 0 & 0 & 0 & 0 & 0 \\
0 & 0 & 0 & 0 & 0 & 0 & 0 & 0 & \cdots & 0 & 0 & 0 & 0 & 0 & 0 & 0 \\
0 & 0 & 0 & 0 & 0 & 0 & 0 & 0 & \cdots & 0 & 0 & 0 & 0 & 0 & 0 & 0 \\
0 & 0 & 0 & 0 & 0 & 0 & 0 & 0 & \cdots & 1 & 0 & 0 & 0 & 0 & 0 & 0 \\
0 & 0 & 0 & 0 & 0 & 0 & 0 & 0 & \cdots & -1 & 1 & 0 & 0 & 0 & 0 & 0 \\
0 & 0 & 0 & 0 & 0 & 0 & 0 & 0 & \cdots & 0 & -1 & 1 & 0 & 0 & 0 & 0 \\
0 & 0 & 0 & 0 & 0 & 0 & 0 & 0 & \cdots & 0 & 0 & -1 & -1 & -1 & -1 & -1
\end{array}\right]
\end{array}
\qquad (6.7)
$$

$$
[Q]_{22\times 31} = \begin{array}{c} \\ Cut\ 1 \\ Cut\ 2 \\ Cut\ 3 \\ Cut\ 4 \\ Cut\ 5 \\ Cut\ 6 \\ Cut\ 7 \\ Cut\ 8 \\ Cut\ 9 \\ Cut\ 10 \\ Cut\ 11 \\ Cut\ 12 \\ Cut\ 13 \\ Cut\ 14 \\ Cut\ 15 \\ Cut\ 16 \\ Cut\ 17 \\ Cut\ 18 \\ Cut\ 19 \\ Cut\ 20 \\ Cut\ 21 \\ Cut\ 22 \end{array}
\begin{array}{c}
\begin{array}{ccccccccccccccccccc} 1 & 2 & 3 & 4 & 5 & 6 & 7 & 8 & \cdots & 25 & 26 & 27 & 28 & P_x & P_y & P_z \end{array} \\
\left[\begin{array}{ccccccccccccccccc}
1 & 0 & 0 & 1 & 0 & 0 & 0 & 0 & \cdots & 0 & 0 & 0 & -1 & 0 & 0 & 0 \\
0 & 1 & 0 & 1 & 0 & 0 & 0 & 0 & \cdots & 0 & 0 & 0 & -1 & 0 & 0 & 0 \\
0 & 0 & 1 & -1 & 0 & 0 & 0 & 0 & \cdots & 0 & 0 & 0 & 0 & 0 & 0 & 0 \\
0 & 0 & 0 & 0 & 1 & 0 & 0 & 0 & \cdots & 0 & 0 & 0 & -1 & 0 & 0 & 0 \\
0 & 0 & 0 & 0 & 0 & 1 & 0 & 0 & \cdots & 0 & 0 & 0 & -1 & 0 & 0 & 0 \\
0 & 0 & 0 & 0 & 0 & 0 & 1 & 0 & \cdots & 0 & 0 & 0 & -1 & 0 & 0 & 0 \\
0 & 0 & 0 & 0 & 0 & 0 & 0 & 1 & \cdots & 0 & 0 & 0 & 0 & 0 & 0 & 0 \\
0 & 0 & 0 & 0 & 0 & 0 & 0 & 0 & \cdots & 0 & 0 & 0 & 0 & 0 & 0 & 0 \\
0 & 0 & 0 & 0 & 0 & 0 & 0 & 0 & \cdots & 0 & 0 & 0 & -1 & 0 & 0 & 0 \\
0 & 0 & 0 & 0 & 0 & 0 & 0 & 0 & \cdots & 0 & 0 & 0 & -1 & 0 & 0 & 0 \\
0 & 0 & 0 & 0 & 0 & 0 & 0 & 0 & \cdots & 0 & 0 & 0 & -1 & 0 & 0 & 0 \\
0 & 0 & 0 & 0 & 0 & 0 & 0 & 0 & \cdots & 0 & 0 & 0 & 0 & 0 & 0 & 0 \\
0 & 0 & 0 & 0 & 0 & 0 & 0 & 0 & \cdots & 0 & 0 & 0 & 1 & 1 & 1 & 1 \\
0 & 0 & 0 & 0 & 0 & 0 & 0 & 0 & \cdots & 0 & 0 & 0 & 1 & 1 & 1 & 1 \\
0 & 0 & 0 & 0 & 0 & 0 & 0 & 0 & \cdots & 0 & 0 & 0 & 0 & 0 & 0 & 0 \\
0 & 0 & 0 & 0 & 0 & 0 & 0 & 0 & \cdots & 0 & 1 & 0 & 1 & 1 & 1 & 1 \\
0 & 0 & 0 & 0 & 0 & 0 & 0 & 0 & \cdots & 0 & 1 & 0 & 1 & 1 & 1 & 1 \\
0 & 0 & 0 & 0 & 0 & 0 & 0 & 0 & \cdots & 0 & 1 & 0 & 1 & 1 & 1 & 1 \\
0 & 0 & 0 & 0 & 0 & 0 & 0 & 0 & \cdots & 0 & -1 & 0 & 0 & 0 & 0 & 0 \\
0 & 0 & 0 & 0 & 0 & 0 & 0 & 0 & \cdots & 1 & -1 & 0 & 0 & 0 & 0 & 0 \\
0 & 0 & 0 & 0 & 0 & 0 & 0 & 0 & \cdots & 0 & 0 & 1 & 1 & 1 & 1 & 1
\end{array}\right]
\end{array}
\tag{6.8}
$$

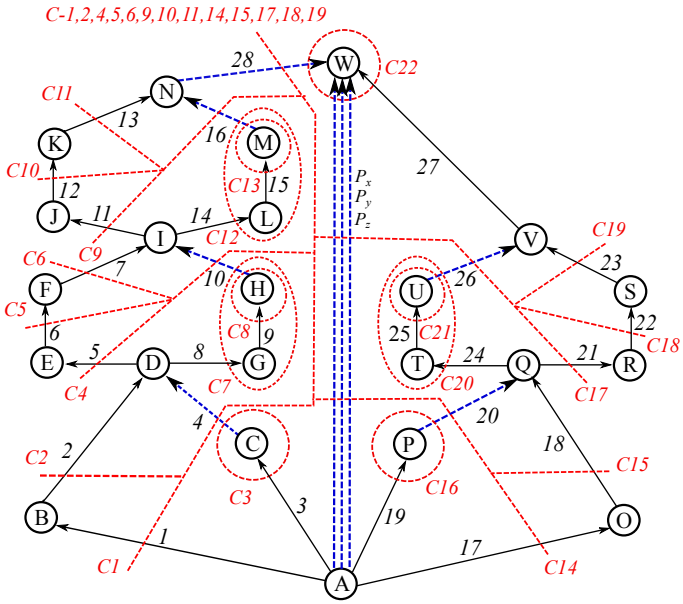

Figure 59 – Cut-set action graph of the mechanism.

All of the constraints are represented as edges. Which allows the amplification of the cut-set graph and the cut-set matrix. Additionally, the tire normal loads ($F_{T2,4,18,20}$), leaf spring normal loads ($F_{LS6,9,22,25}$), fifth-wheel normal loads ($F_{FW12,15}$), and the passive torsional moments ($T_{x5,11,21,27,28}$) are included.

Figure 59 presents the cut-set action graph and the Eq. (6.9) presents the expanded cut-set matrix ($[Q]_{22\times150}$), where each line represents a cut of the graph, and the columns represents the constraints of the joints as well as the external forces acting on the mechanism.

$$
[Q]_{22\times 150} = \begin{array}{c}
\begin{array}{ccccccccccccccccc}
F_{x1} & F_{y1} & F_{z1} & M_{y1} & M_{z1} & F_{x2} & F_{p2} & F_{T2} & \cdots & F_{x28} & F_{y28} & F_{z28} & T_{x28} & P_x & P_y & P_z
\end{array} \\
\left[\begin{array}{ccccccccccccccccc}
1 & 1 & 1 & 1 & 1 & 0 & 0 & 0 & \cdots & 0 & -1 & -1 & -1 & 0 & 0 & 0 \\
0 & 0 & 0 & 0 & 0 & 1 & 1 & 1 & \cdots & 0 & -1 & -1 & -1 & 0 & 0 & 0 \\
0 & 0 & 0 & 0 & 0 & 0 & 0 & 0 & \cdots & 0 & 0 & 0 & 0 & 0 & 0 & 0 \\
0 & 0 & 0 & 0 & 0 & 0 & 0 & 0 & \cdots & 0 & -1 & -1 & -1 & 0 & 0 & 0 \\
0 & 0 & 0 & 0 & 0 & 0 & 0 & 0 & \cdots & 0 & -1 & -1 & -1 & 0 & 0 & 0 \\
0 & 0 & 0 & 0 & 0 & 0 & 0 & 0 & \cdots & 0 & -1 & -1 & -1 & 0 & 0 & 0 \\
0 & 0 & 0 & 0 & 0 & 0 & 0 & 0 & \cdots & 0 & 0 & 0 & 0 & 0 & 0 & 0 \\
0 & 0 & 0 & 0 & 0 & 0 & 0 & 0 & \cdots & 0 & 0 & 0 & 0 & 0 & 0 & 0 \\
0 & 0 & 0 & 0 & 0 & 0 & 0 & 0 & \cdots & 0 & -1 & -1 & -1 & 0 & 0 & 0 \\
0 & 0 & 0 & 0 & 0 & 0 & 0 & 0 & \cdots & 0 & -1 & -1 & -1 & 0 & 0 & 0 \\
0 & 0 & 0 & 0 & 0 & 0 & 0 & 0 & \cdots & 0 & -1 & -1 & -1 & 0 & 0 & 0 \\
0 & 0 & 0 & 0 & 0 & 0 & 0 & 0 & \cdots & 0 & 0 & 0 & 0 & 0 & 0 & 0 \\
0 & 0 & 0 & 0 & 0 & 0 & 0 & 0 & \cdots & 0 & 0 & 0 & 0 & 0 & 0 & 0 \\
0 & 0 & 0 & 0 & 0 & 0 & 0 & 0 & \cdots & 0 & 1 & 1 & 1 & 1 & 1 & 1 \\
0 & 0 & 0 & 0 & 0 & 0 & 0 & 0 & \cdots & 0 & 1 & 1 & 1 & 1 & 1 & 1 \\
0 & 0 & 0 & 0 & 0 & 0 & 0 & 0 & \cdots & 0 & 0 & 0 & 0 & 0 & 0 & 0 \\
0 & 0 & 0 & 0 & 0 & 0 & 0 & 0 & \cdots & 0 & 1 & 1 & 1 & 1 & 1 & 1 \\
0 & 0 & 0 & 0 & 0 & 0 & 0 & 0 & \cdots & 0 & 1 & 1 & 1 & 1 & 1 & 1 \\
0 & 0 & 0 & 0 & 0 & 0 & 0 & 0 & \cdots & 0 & 1 & 1 & 1 & 1 & 1 & 1 \\
0 & 0 & 0 & 0 & 0 & 0 & 0 & 0 & \cdots & 0 & 0 & 0 & 0 & 0 & 0 & 0 \\
0 & 0 & 0 & 0 & 0 & 0 & 0 & 0 & \cdots & 0 & 0 & 0 & 0 & 0 & 0 & 0 \\
0 & 0 & 0 & 0 & 0 & 0 & 0 & 0 & \cdots & 1 & 1 & 1 & 1 & 1 & 1 & 1
\end{array}\right]
\end{array}
\tag{6.9}
$$

6.2 EQUATION SYSTEM SOLUTIONS

Using the *Cut-set law* (DAVIES, 2000), the algebraic sum of the normalized wrenches Eqs. (6.5) and (6.6), that belong to the same cut $[Q]_{22\times150}$ (Fig. 59 and Eq. (6.9)) must be equal to zero. Thus, the statics of the mechanism can be defined, as exemplified in Eq. (6.10) (or the amplified matrix of the Eq. (6.11)):

$$\left[\widehat{A}_n\right]_{132\times150}[\Psi]^T_{150\times1} = [0]_{132\times1} \tag{6.10}$$

$$\begin{array}{l}
\\
\text{Cut 1} \\
\\
\\
\\
\\
\vdots \\
\\
\\
\\
\text{Cut 22} \\
\\
\\
\\
\end{array}
\begin{bmatrix}
0 & 0 & \cdots & 0 & 0 \\
0 & 0 & \cdots & 0 & 0 \\
p_1 & p_2 & \cdots & 0 & 0 \\
1 & 0 & \cdots & 0 & 0 \\
0 & 1 & \cdots & 0 & 0 \\
0 & 0 & \cdots & 0 & 0 \\
\vdots & \vdots & \vdots & \vdots & \vdots \\
0 & 0 & \cdots & 0 & 0 \\
0 & 0 & \cdots & 0 & -a \pm d_2 \\
0 & 0 & \cdots & a \mp d_2) & 0 \\
0 & 0 & \cdots & 0 & 0 \\
0 & 0 & \cdots & -1 & 0 \\
0 & 0 & \cdots & 0 & -1
\end{bmatrix}
\cdot
\begin{bmatrix}
F_{x1} \\ F_{y1} \\ \vdots \\ P_y \\ P_z
\end{bmatrix}
= [0]_{132\times1} \tag{6.11}$$

It is necessary to identify the set of primary variables $[\Psi_p]$ (known variables), among the variables of Ψ. Once identified, the system of the Eq. (6.10) is rearranged and dividing into two sets, as shown by Eq. (6.12).

$$\left[\widehat{A}_{ns}\right]_{132\times147}[\Psi_s]^T_{147\times1} + \left[\widehat{A}_{np}\right]_{132\times3}[\Psi_p]^T_{3\times1} = [0]_{132\times1} \tag{6.12}$$

where $[\Psi_p]$ is the primary variable vector, $[\Psi_s]$ is the secondary variable vector (unknown variables), $\left[\widehat{A}_{np}\right]$ are the columns corresponding to the primary variables and $\left[\widehat{A}_{ns}\right]$ are the columns corresponding to the secondary variables.

In this case, the primary variable vector is:

$$[\Psi_p]_{3\times1} = \begin{bmatrix} P_x & P_y & P_z \end{bmatrix}^T \tag{6.13}$$

and the secondary variable vector is:

$$[\Psi_s]_{147\times1} = \begin{bmatrix} F_{x1} & F_{y1} & M_{y1} & \cdots & F_{z3} & F_{z17} & F_{z19} \end{bmatrix}^T \tag{6.14}$$

Solving the system in Eq. (6.12) using the Gauss-Jordan elimination method, the last row of the solution system provides the following equation:

$$F_{z3} + \frac{P_1 + t_3}{t_1 \cos\psi} F_{z19} + \frac{P_1}{t_1 \cos\psi} F_{z17}$$

$$- \frac{h_1 + P_1}{t_1 \cos\psi} P_z + \frac{h_2}{t_1 \cos\psi} P_y = 0 \tag{6.15}$$

replacing P_y and P_z:

$$F_{z3} + \frac{P_1 + t_3}{t_1 \cos\psi} F_{z19} + \frac{P_1}{t_1 \cos\psi} F_{z17}$$

$$- \frac{h_1 + P_1}{t_1 \cos\psi} (W \cos\phi \cos\varphi + m a_y \sin\phi)$$

$$+ \frac{h_2}{t_1 \cos\psi} (m a_y \cos\phi - W \sin\phi \cos\varphi) = 0 \tag{6.16}$$

where P_1 is a system variable ($P_1 = (2l_{13}\sin\psi + t_2(\cos\psi - 1))/2$), h_1 is the instantaneous lateral distance between the zero-reference frame and the *CG*, and h_2 is the instantaneous *CG* height, as shown in Figs. 55 and 56 and Table 10. Dividing by $W\cos(\phi)$, making $\tan(\phi) = e$, where e is the tangent of the bank angle, and rearranging the equation, we have:

$$\frac{a_y}{g} = \frac{h_1 \cos\varphi + h_2 e \cos\varphi}{h_2 - (h_1 + P_1)e} \cdot$$

$$\left(1 - \frac{t_1 F_{z3} \cos\psi + P_1 (F_{z17} - W \cos\phi \cos\varphi) + (P_1 + t_3) F_{z19}}{W \cos\phi (h_1 \cos\varphi + h_2 e \cos\varphi)}\right) \tag{6.17}$$

According to the static redundancy problem known as the four-legged table described by Heyman (2008) and Blundell and Harty (2004), a plane is defined by just three points in space and, consequently, a four-legged table has support plane multiplicities. This is why when one leg

loses contact with the ground, the table is supported by the other three legs, as shown in Fig. 60.

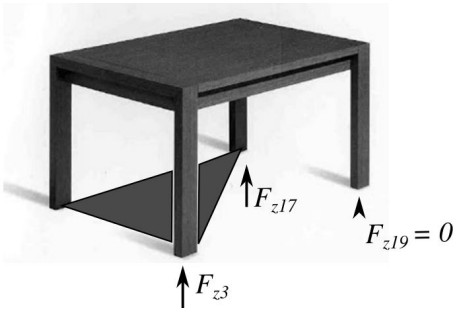

Figure 60 – Problem of redundancy the four-legged table.

The problem of the four-legged table is observed in dynamic rollover tests, when the rear inner tire loses contact with the ground ($F_{z19} = 0$), and the front inner tire (F_{z3}) does not, as show *e.g.* in Fig. 61.

Figure 61 – Dynamic rollover test.
Source: Adapted of Cabral (2008).

Applying this approach to the vehicle stability, and considering the chassis flexibility, fifth-wheel, suspension, tires, and the trailer/trailer angle when a vehicle makes a turn, the vehicle is subjected to an increasing lateral load until it reaches the rollover threshold. During the turning, the rear inner tire is normally the one which loses contact with the ground;

for this condition $F_{z19} = 0$, and thus:

$$SRT_{3D_{\psi\phi\varphi}} = \frac{a_y}{g} = \frac{h_1 \cos\varphi + h_2 e \cos\varphi}{h_2 - (h_1 + P_1)e} \cdot \left(1 - \frac{t_1 F_{z3} \cos\psi + P_1 (F_{z17} - W \cos\phi \cos\varphi)}{W \cos\phi (h_1 \cos\varphi + h_2 e \cos\varphi)}\right) \tag{6.18}$$

where $SRT_{3D_{\psi\phi\varphi}}$ factor is the three-dimensional static rollover threshold for a trailer model with trailer/trailer angle (ψ), bank angle (e), and slope angle (φ).

The normal forces F_{z3} and F_{z17} depend on the *LLT* coefficient in the front and rear axles respectively (RILL, 2011; LUI *et al.*, 1997; KAMNIK *et al.*, 2003). Furthermore, this coefficient depends of the vehicle type, speed, suspension, tires, etc.

Table 12 shows a comparison between the SRT factors of the three-dimensional models presented in the Chapter 2 and the SRT factors of the developed models.

Table 12 shows that the SRT factor of the developed 3D-model (Eq. (6.18)) is more complete, since the model takes into account all the characteristics considered by the other models, and additionally the overweight and the characteristics of the road.

Table 12 also shows that the $SRT_{3D_{\psi\phi\varphi}}$ factor of the developed 3D-model (Eq. (6.18)) is, in general, inferior to the SRT_{2DTM} factor of the developed 2D-model (Eq. (5.22)).

Then, with Eq. (6.18) it is possible to obtain a better vehicle stability representation and the $SRT_{3D_{\psi\phi\varphi}}$ factor value attainments closer to reality.

Figure 62 shows a summary of all characteristics of the vehicle and the road that influence in the $SRT_{3D_{\psi\phi\varphi}}$ factor calculations.

Taking into account the developed model and all characteristics that influence on the $SRT_{3D_{\psi\phi\varphi}}$ factor calculations, Table 13 shows the comparison of the main models developed and the new vehicle stability model.

Table 13 shows that the developed model considered the main characteristics of *LCV's*; additionally, the model includes other characteristics such as the trailer/trailer angle (ψ), longitudinal slope angle (φ), and the trailer overweight.

Table 12 – SRT factors of three-dimensional models.

Models	SRT factors of 3D models
Gillespie model (Eq. (2.28))	$SRT_{3D-G} = \dfrac{\dfrac{t}{2h}}{1+(1-\dfrac{h_0}{h})\left[\dfrac{W(h-h_0)}{k_{\theta f}+k_{\theta r}-W(h-h_0)}\right]}$
Navin model (Eq. (2.30))	$SRT_{3D-N} = \dfrac{\dfrac{t}{2}(1-\dfrac{l_{re}}{L})+h(\phi-\theta)-\dfrac{h_5 l_{re}\phi}{L}+h_0\theta}{\dfrac{t\phi}{2}(\dfrac{l_{re}}{L}-1)+h-h_5\dfrac{l_{re}}{L}}$
Developed 2D (Eq. (5.22))	$SRT_{2DTM} = \dfrac{h_1+h_2 e}{h_2-h_1 e}$
Developed 3D (Eq. (6.18))	$SRT_{3D_{\psi\phi\varphi}} = \dfrac{h_1\cos\varphi+h_2 e\cos\varphi}{h_2-(h_1+P_1)e}\cdot \left(1-\dfrac{t_1 F_{z3}\cos\psi+P_1(F_{z17}-W\cos\phi\cos\varphi)}{W\cos\phi(h_1\cos\varphi+h_2 e\cos\varphi)}\right)$

Figure 62 – Characteristics that influence on the $SRT_{3D_{\psi\phi\varphi}}$ factor calculation.

Table 13 – Stability models comparison.

	Characteristics																							
	2D	3D	Bicycle model	*CG* height (h_2)	*CR* height	Bank angle (ϕ)	Slope angle (φ)	Vehicle track (t)	Suspension	Tires	Steering angle	Trailer/trailer angle (ψ)	Fifth-wheel	Inertial forces	*LLT* coefficient	Longitudinal location of *CG*	Stiffness of the chassis	Active suspension	Liquid loads	Load distribution	Wind force	Roll angle (θ_{all})	Rearward amplification (RA)
Models of SRT factor																							
Gillespie (1992)	x	x		x	x			x	x					x								x	
Winkler *et al.* (1992)	x			x	x			x	x	x				x								x	
Navin (1992)		x		x	x	x		x	x				x	x		x						x	
Ranganathan (1993)	x			x	x			x	x					x					x			x	
Winkler (2000)		x		x	x			x	x	x			x	x	x	x	x		x	x		x	
Chang (2001)	x			x	x	x			x					x								x	
Jung *et al.* (2009)	x			x	x	x		x	x					x	x							x	
Rill (2011)	x			x	x			x	x	x				x	x							x	
Other models of lateral stability																							
Fancher and Winkler (1992)	x		x								x	x	x	x		x						x	x
Rempel (2001)		x		x				x	x		x	x	x	x		x							x
Takano and Nagai (2001)	x		x	x	x			x	x		x			x		x	x					x	
Miege and Cebon (2002)	x			x				x	x					x				x	x			x	
Kamnik *et al.* (2003)		x		x	x			x	x		x	x	x	x	x	x	x					x	
Sampson and Cebon (2003)		x		x				x	x				x	x		x		x				x	
Sanchez *et al.* (2004)		x		x	x			x	x		x	x	x	x		x						x	
Whitehead *et al.* (2004)	x		x	x				x	x		x			x		x						x	
Bouteldja *et al.* (2004)		x		x	x			x	x		x	x	x	x		x						x	
Dahlberg and Wideberg (2004)	x		x								x	x	x	x		x						x	x
Gaspar *et al.* (2005)		x		x	x			x	x		x			x	x	x		x				x	
Prem *et al.* (2006)		x		x		x		x	x	x				x	x	x			x				
Pinxteren (2010)		x		x				x	x		x	x	x	x		x							
Ricalde *et al.* (2008)		x		x	x			x	x		x	x	x	x		x						x	
Hac *et al.* (2008)			x								x	x	x	x		x							x
Chen and Chen (2009)	x			x	x	x		x	x		x			x	x							x	
Ryu *et al.* (2010)		x		x	x			x	x		x			x		x		x				x	
Islam and He (2013)	x		x								x	x	x	x		x						x	

Table 13 – Stability models comparison.

	Characteristics	2D	3D	Bicycle model	*CG* height (h_2)	*CR* height	Bank angle (ϕ)	Slope angle (φ)	Vehicle track (t)	Suspension	Tires	Steering angle	Trailer/trailer angle (ψ)	Fifth-wheel	Inertial forces	*LLT* coefficient	Longitudinal location of *CG*	Stiffness of the chassis	Active suspension	Liquid loads	Load distribution	Wind force	Roll angle (θ_{all})	Rearward amplification (*RA*)
Malviya and Mishra (2014)			x		x		x	x	x						x	x	x					x	x	
Imine *et al.* (2014)		x		x	x	x				x	x	x			x	x	x		x				x	
Huston and Kelly (2014)		x			x	x			x						x							x	x	
He *et al.* (2015)			x		x				x	x	x				x	x	x					x	x	
Developed 2D-model		**x**			**x**	**x**	**x**		**x**	**x**	**x**				**x**	**x**					**x**		**x**	
Developed 3D-model			**x**		**x**	**x**	**x**	**x**	**x**	**x**	**x**	**x**	**x**	**x**	**x**	**x**	**x**	**x**			**x**		**x**	

In order to simplify the solution of the equations system in Eq. (6.12), the following assumptions were applied:

• the load of the trailer is uniformly distributed on the front and rear axles (Eq. (4.27));

• the lateral load transfer of the trailer model is controlled through the torsional moment of the chassis (spherical joints 27 and 28 (Eqs. (4.21) and (4.22)).

Equation (6.19) shows the final static system for the stability analysis.

Solving the system in Eq. (6.19) using the Gauss-Jordan elimination method, all secondary variables of the system being function of the three primary variables (P_x - force acting on the x-axis, P_y - force acting on the y-axis, and P_z - force acting on the z-axis).

For this analysis only the forces acting on the suspension, tires, fifth-wheel, and the chassis are taken into account; the last nineteen rows of the solution of Eq. (6.19) show the forces acting on the mechanism. Rearranging these lines gives the following equations (C_i are system variables):

$$
\begin{array}{l}
\\
\\
\text{Cut 1} \\
\\
\\
\\
\vdots \\
\vdots \\
\\
\\
\\
\text{Cut 10} \\
\\
\\
\\
\vdots \\
\vdots \\
\\
\\
\\
\text{Cut 22} \\
\\
\\
\\
\\
Eq.\ (4.27) \\
Eq.\ (4.21) \\
Eq.\ (4.22)
\end{array}
\begin{bmatrix}
0 & 0 & \cdots & 0 & 0 & -p_1 & 0 & 0 & 0 & 0 & 0 & 0 \\
0 & 0 & \cdots & 0 & 0 & -p_2 & 0 & 0 & 0 & 0 & 0 & 0 \\
p_1 & p_2 & \cdots & 0 & 0 & 0 & 0 & 0 & 0 & 0 & 0 & 0 \\
1 & 0 & \cdots & 0 & 0 & 0 & 0 & 0 & 0 & 0 & 0 & 0 \\
0 & 1 & \cdots & 0 & 0 & 0 & 0 & 0 & 0 & 0 & 0 & 0 \\
0 & 0 & \cdots & 0 & 0 & 1 & 0 & 0 & 0 & 0 & 0 & 0 \\
\vdots & \vdots & \vdots & \vdots & \vdots & \vdots & \vdots & \vdots & \vdots & \vdots & \vdots & \vdots \\
\vdots & \vdots & \vdots & \vdots & \vdots & \vdots & \vdots & \vdots & \vdots & \vdots & \vdots & \vdots \\
0 & 0 & \cdots & -p_{41} & 0 & 0 & 0 & 0 & 0 & 0 & 0 & 0 \\
0 & 0 & \cdots & -p_{44} & 0 & 0 & 0 & 0 & 0 & 0 & 0 & 0 \\
0 & 0 & \cdots & 0 & 0 & 0 & 0 & 0 & 0 & 0 & 0 & 0 \\
0 & 0 & \cdots & 0 & 0 & 0 & 0 & 0 & 0 & 0 & 0 & 0 \\
0 & 0 & \cdots & 0 & 0 & 0 & 0 & 0 & 0 & 0 & 0 & 0 \\
0 & 0 & \cdots & 1 & 0 & 0 & 0 & 0 & 0 & 0 & 0 & 0 \\
\vdots & \vdots & \vdots & \vdots & \vdots & \vdots & \vdots & \vdots & \vdots & \vdots & \vdots & \vdots \\
\vdots & \vdots & \vdots & \vdots & \vdots & \vdots & \vdots & \vdots & \vdots & \vdots & \vdots & \vdots \\
0 & 0 & \cdots & 0 & 0 & 0 & 0 & 0 & 0 & 0 & 0 & 0 \\
0 & 0 & \cdots & 0 & 0 & 0 & 0 & 0 & 0 & h_2 & 0 & -a \pm d_2 \\
0 & 0 & \cdots & 0 & 0 & 0 & 0 & 0 & 0 & -h_1 & -(-a \pm d_2) & 0 \\
0 & 0 & \cdots & 0 & 0 & 0 & 0 & 0 & 0 & 1 & 0 & 0 \\
0 & 0 & \cdots & 0 & 0 & 0 & 0 & 0 & 0 & 0 & -1 & 0 \\
0 & 0 & \cdots & 0 & 0 & 0 & 0 & 0 & 0 & 0 & 0 & -1 \\
0 & 0 & \cdots & 0 & 0 & 0 & 0 & L & L & h_2 & 0 & -(-a \pm d_2) \\
0 & 0 & \cdots & 0 & 0 & 0 & 0 & 0 & 0 & 0 & 0 & 0 \\
0 & 0 & \cdots & 0 & 0 & 0 & 0 & 0 & 0 & 0 & 0 & 0
\end{bmatrix}
\cdot
\begin{bmatrix}
F_{x1} \\ F_{y1} \\ \vdots \\ T_{x5} \\ T_{x11} \\ T_{x21} \\ T_{x27} \\ T_{x28} \\ F_{T2} \\ F_{T4} \\ F_{T18} \\ F_{T20} \\ F_{LS6} \\ F_{LS9} \\ F_{LS22} \\ F_{LS25} \\ F_{FW12} \\ F_{FW15} \\ F_{z1} \\ F_{z3} \\ F_{z19} \\ F_{z17} \\ P_x \\ P_y \\ P_z
\end{bmatrix}
= [0]_{135\times 1} \tag{6.19}
$$

$$T_{x5} = -C_1P_x - C_2P_y - C_3P_z \tag{6.20}$$

$$T_{x11} = -C_4P_x - C_5P_y - C_6P_z \tag{6.21}$$

$$T_{x21} = -C_7P_x - C_8P_y - C_9P_z \tag{6.22}$$

$$T_{x27} = -C_{10}P_x - C_{11}P_y - C_{12}P_z \tag{6.23}$$

$$T_{x28} = -C_{13}P_x - C_{14}P_y - C_{15}P_z \tag{6.24}$$

$$F_{T2} = -C_{16}P_x - C_{17}P_y - C_{18}P_z \tag{6.25}$$

$$F_{T4} = -C_{19}P_x - C_{20}P_y - C_{21}P_z \tag{6.26}$$

$$F_{T18} = -C_{22}P_x - C_{23}P_y - C_{24}P_z \tag{6.27}$$

$$F_{T20} = -C_{25}P_x - C_{26}P_y - C_{27}P_z \tag{6.28}$$

$$F_{LS6} = -C_{28}P_x - C_{29}P_y - C_{30}P_z \tag{6.29}$$

$$F_{LS9} = -C_{31}P_x - C_{32}P_y - C_{33}P_z \tag{6.30}$$

$$F_{LS22} = -C_{34}P_x - C_{35}P_y - C_{36}P_z \tag{6.31}$$

$$F_{LS25} = -C_{37}P_x - C_{38}P_y - C_{39}P_z \tag{6.32}$$

$$F_{FW12} = -C_{40}P_x - C_{41}P_y - C_{42}P_z \tag{6.33}$$

$$F_{FW15} = -C_{43}P_x - C_{44}P_y - C_{45}P_z \tag{6.34}$$

$$F_{z1} = -C_{46}P_x - C_{47}P_y - C_{48}P_z \tag{6.35}$$

$$F_{z3} = -C_{49}P_x - C_{50}P_y - C_{51}P_z \tag{6.36}$$

$$F_{z19} = -C_{52}P_x - C_{53}P_y - C_{54}P_z \tag{6.37}$$

$$F_{z17} = -C_{55}P_x - C_{56}P_y - C_{57}P_z \tag{6.38}$$

From Eqs. (6.20) to (6.38), the instantaneous forces acting on mechanism can be obtained. These forces modifying the configuration of the tires, suspension, fifth-wheel and the chassis systems, as shown in chapter 4.

At the rollover limit condition, the normal load F_{19_z}, reaches zero and on applying this condition in Eq. (6.37) the $SRT_{3D_{\psi\phi\varphi}}$ factor can also be calculated as:

$$SRT_{3D_{\psi\phi\varphi}} = \frac{a_y}{g} = \frac{-C_{52}(\sin\varphi/\cos\phi) - C_{53}e\cos\varphi - C_{54}\cos\varphi}{C_{53} + C_{54}e} \tag{6.39}$$

6.3 PUBLICATIONS

The three-dimensional model of the trailer has the following publications:

• Moreno, G. G., Nicolazzi, L., Vieira, R. S., Martins, D. *Stability of Long Combination Vehicles*. International Journal of Heavy vehicle Systems, (in press). 2016.

• Book chapter. Graph-Based Modelling in Engineering. Ed. Zawiślak, S and Rysiński, J. Chapter 9: *Three-Dimensional Analysis of Vehicle Stability Using Graph Theory*. Moreno, G. G., Barreto, R. L. P., Vieira, R. S., Nicolazzi, L., Martins, D. Springer International Publishing, (in press). Switzerland. 2016. ISBN 978-3319390185. DOI 10.1007/978−3−319−39020−8_9.

• Moreno, G. G., Nicolazzi, L., Vieira, R. S., Martins, D. *Three-Dimensional Analysis of the Rollover Risk of Heavy Vehicles Using Davies Method*. In: 14^{th} World Congress in Mechanical and Machine Science (IFToMM2015). Taipei - Taiwan, 2015. DOI: 10.6567/IFToMM.14TH.WC.PS4.006.

• Moreno, G. G., Nicolazzi, L., Vieira, R. S., Martins, D. *Rollover of heavy truck using Davies method*. In: RS5C 2016 - 17^{th} International Conference Road Safety on Five Continents. Río de Janeiro - Brasil. 2016. DOI: 10.13140/RG.2.2.20805.24807.

Chapter 7

ADAMS® SIMULATION - SEMI-TRAILER 2D

For the validation the two-dimensional model developed in the Chapter 5, a simplified two-dimensional model of a semi-trailer (Figure 63 - SECTION A - A) with the parameters of the Table 14 was analyzed using the software ADAMS® (2016).

Adams simulations allowed us to get different loading conditions to be studied through a finite element method (FEM) analysis, putting to evidence the most critical loading combinations.

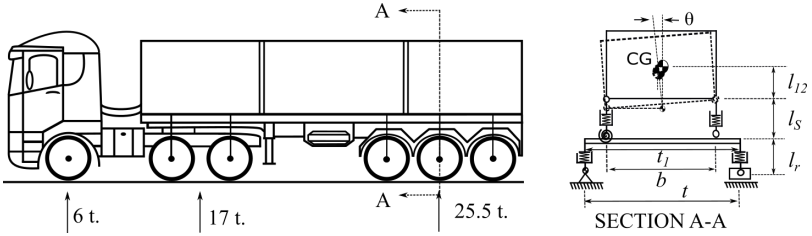

Figure 63 – Model of Semi-trailer.

Table 14 – Parameters of the trailer model - Semi-trailer.

Parameter	**Value**	**Units**
Trailer weight - W	250	kN
Vehicle track - t	1.86	m
Axle width - t_1	1.86	m
Equivalent stiffness of the suspension - k_{Ls}	5400	kN/m
Equivalent tire vertical stiffness - k_T	5040	kN/m
Initial suspension height - l_s	0.205	m
Initial dynamic rolling radius - l_r	0.499	m
Lateral separation between the springs - b	0.95	m
CG height above the chassis - l_{12}	1.346	m

7.1 STATIC ROLLOVER THRESHOLD WITH ADAMS

In this analysis a student license of Adams was used, which is quite limited in regards to the number of bodies to be simulated. The two-dimensional model of the trailer is composed of seven bodies (as shown in

Figure 64). According to the physical parameters of the vehicle in Adams multi-body system dynamics model (Table 14), it can be found that the model consists of following parts: suspension, tires, and frame.

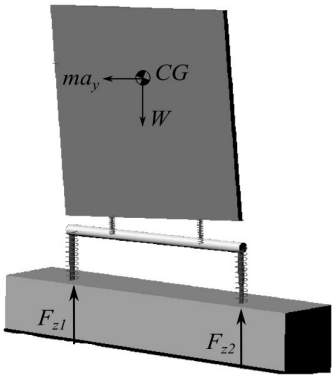

Figure 64 – Semi-trailer - Adams model.

For the SRT factor calculation, the inertial force was applied until the lateral load transfer of the model become complete. At the rollover threshold limit condition, the normal load F_{z2} reaches zero, as shown in Fig. 65.

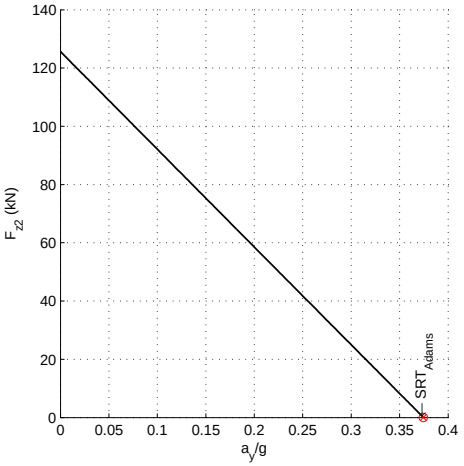

Figure 65 – Normal force in the outer tire (F_{z2}) - SRT factor - Adams model.

The example shows that the SRT factor for a trailer model is 0.374. The reduction in the SRT factor results from the combined action of the trailer systems (suspension and tires), which allows the *CG* movements and a body roll angle of the trailer model of $\theta = 5.75°$, as shown in Fig. 66.

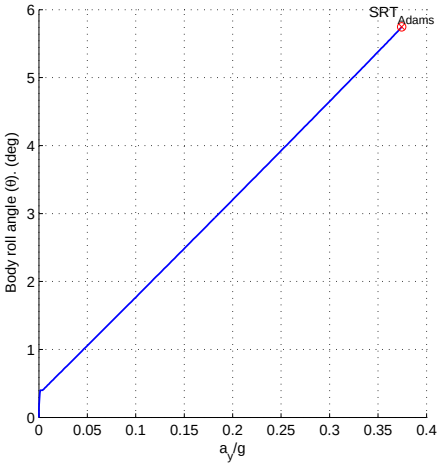

Figure 66 – Body roll angle of the trailer model - Adams model.

7.2 STATIC ROLLOVER THRESHOLD WITH THE DEVELOPED MODEL

Using the two-dimensional model of stability developed in the Chapter 5, the same vehicle of the previous example was analyzed. More details concerning to the developed example are contained in the article "*Suspension and tire: the stability of heavy vehicles*" (MORENO *et al.*, 2016c)

For the SRT factor calculation (Eq. 5.22), the inertial force was applied until the lateral load transfer of the model become complete. At the rollover threshold limit condition, the normal load F_{z2} reaches zero, as shown in Fig. 67.

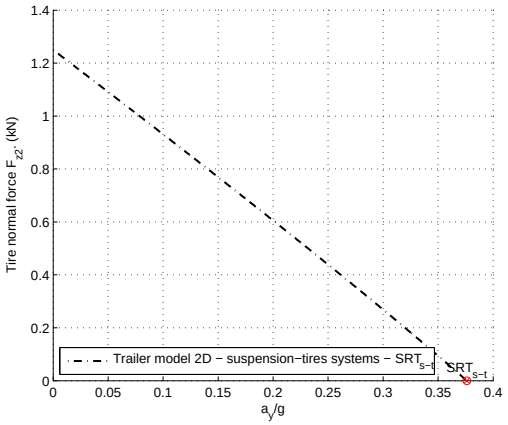

Figure 67 – Normal force in the outer tire (F_{z2}) - SRT factor - Developed model 2D.

The example shows that the SRT factor for a trailer model is 0.376. The reduction in the SRT factor results from the combined action of the trailer systems (suspension and tires), which allows the *CG* movements and a body roll angle of the trailer model of $\theta = 6.1°$, as shown in Fig. 68.

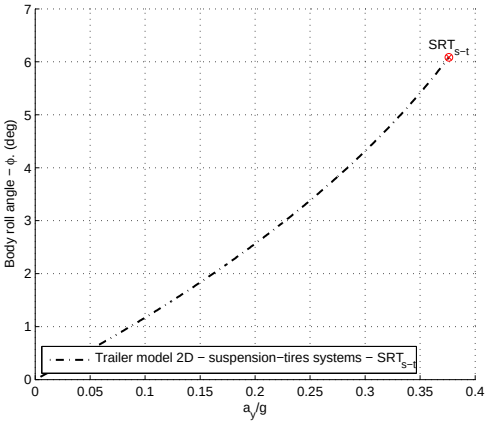

Figure 68 – Body roll angle of the trailer model - Developed model 2D.

7.3 CONCLUSIONS

Figure 69 shows a summary of some SRT factors: the rigid, the Rill and the Winkler models that were presented in the Chapter 2, the proposed two-dimensional model developed in this thesis (Chapter 5), and the developed model with ADAMS® (2016).

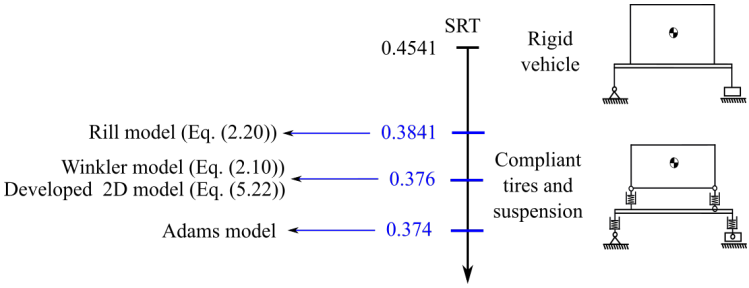

Figure 69 – Developed two-dimensional models.

Figure 69 shows that:

- the developed two-dimensional model presents a difference of 0.5% as compared to the Adams model,
- the developed two-dimensional has a similar SRT factor as the model developed by Winkler *et al.* (1992), and
- the developed two-dimensional presents a difference of 2% as compared to the Rill model (RILL, 2011).

The proposed tires and suspension systems of the developed model allow the determination of their influence on the SRT factor of the vehicle, and the changes on the *CG* of the vehicle positions.

The results obtained with the proposed model were compared with the Adams and the Winkler models, and the reductions in the SRT factor was similar. This guarantee that this approach is coherent and can be well accepted.

The proposed model also shows how several characteristics of the vehicle affect dramatically the SRT factor estimation, and enables a better understanding and interpretation of the rollover phenomenon, becoming closer to reality.

Chapter 8

TRUCKSIM® SIMULATION - SEMI-TRAILER 3D

For the validation the three-dimensional model developed in this work (Chapter 6), a model of a semi-trailer such as shown on Fig. 70 was analyzed using the software TruckSim® (2016). The model is composed by: the truck with one axle on front and one axle on rear, and a trailer with three axles.

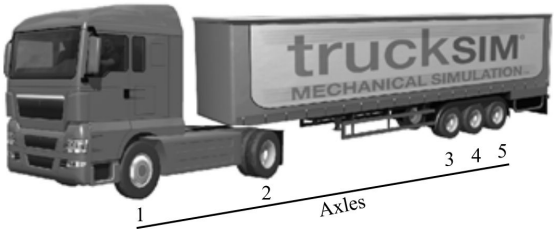

Figure 70 – Semi-trailer - TruckSim® (2016).

TruckSim is a software that is being used in a wide variety of driving simulations. This software allows to evaluate and analyze the performance of a vehicle when making certain manoeuvres on a selected road.

8.1 STATIC ROLLOVER THRESHOLD WITH TRUCKSIM

For the SRT factor calculation, the steady state circular tests (ISO-14792, 2011) were conducted on two path references:

- Test 1: 60 m radius circle with 10 % of bank angle (ϕ), and
- Test 2: 100 m radius circle (flat paved surface), as shown in Fig. 71.

To calculate the SRT factor, the tests were make at constant tangential speed (V), therefore a constant inertial force was applied until the lateral load transfer in the rear axles of the trailer become complete (3^{rd}, 4^{th} and 5^{th} axles).

Table 15 show the parameters of the vehicle and the road used in this analysis.

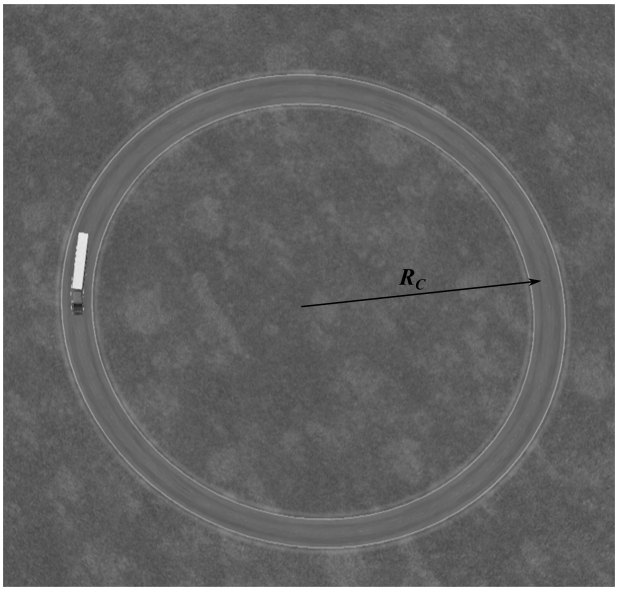

Figure 71 – Circular road - TruckSim® (2016).

Table 15 – Parameters of the trailer model - Semi-trailer.

Parameter	**Value**	**Units**
Trailer weight - W	364.147	kN
Front and rear track widths - $t_{1,3}$	1.815	m
Front and rear axle widths - $t_{2,4}$	1.815	m
Stiffness of the suspension per axle - k_{Ls}	2500	kN/m
Number of axles at the front (trailer) (4 tires per axle)	1	
Number of axles at the rear (trailer) (4 tires per axle)	3	
Vertical stiffness per tire - k_T	980	kN/m
Stiffness of the fifth-wheel - k_f	7500	kN/m
Initial suspension height - $l_s = l_{3,4,9,10}$	0.205	m
Initial dynamic rolling radius - $l_r = l_{1,2,7,8}$	0.51	m
Initial height of the fifth wheel - l_f	0.1	m
Lateral separation between the springs - b	0.95	m
Fifth-wheel width - b_1	0.6	m
CG height above the chassis - l_{12}	1.285	m
Distance between the fifth wheel and the front axle - l_{13}	0.9	m
Wheelbase of the trailer - L	8.7	m
Distance from the front axle to the center of gravity - a	5	m
Trailer/trailer angle (ψ)	0	^{0}
Radius of the circular road (R)	60	m
Bank angle (ϕ)	10	%
Speeds of the tests (V)	50:1 to 60	km/h

8.1.1 Test 1

Using the 60 m radius circle with 10 % of bank angle (ϕ), the test made with vehicle speed of 50 km/h shows that the lateral load transfer (*LLT*) in the 5^{th} axle of the semi-trailer was not complete. Figures 72 shows the normal forces on tires of 5^{th} axle.

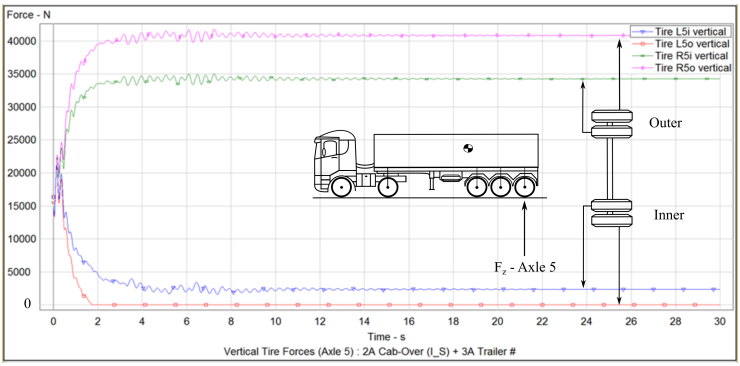

Figure 72 – Normal force on tires of 5^{th} axle - V = 50 km/h.

The test made with vehicle speed of 55 km/h shows that the *LLT* coefficient was completed in the 5^{th} axle, but it was not in the 3^{rd} and 4^{th} axles. Figures 73 to 75 show the normal forces on tires of 3^{rd}, 4^{th} and 5^{th} axles.

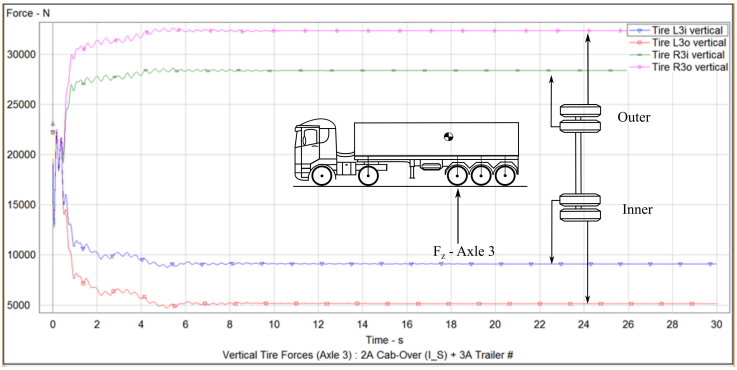

Figure 73 – Normal force on tires of 3^{rd} axle - V = 55 km/h.

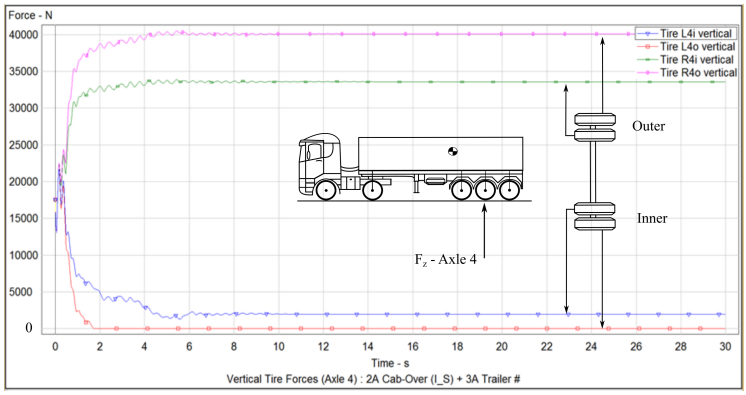

Figure 74 – Normal force on tires of 4^{th} axle - V = 55 km/h.

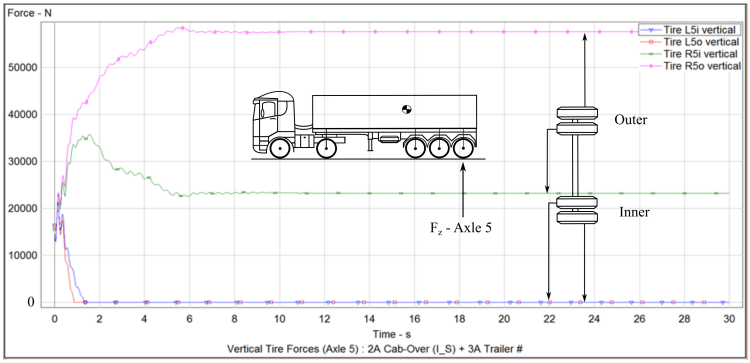

Figure 75 – Normal force on tires of 5^{th} axle - V = 55 km/h.

The test made with vehicle speed of 58 km/h shows that the lateral load transfer (*LLT*) in the 3^{rd}, 4^{th} and 5^{th} axles were complete. Figures 76 to 78 show the normal forces on tires of the axles 3^{rd}, 4^{th} and 5^{th} axles.

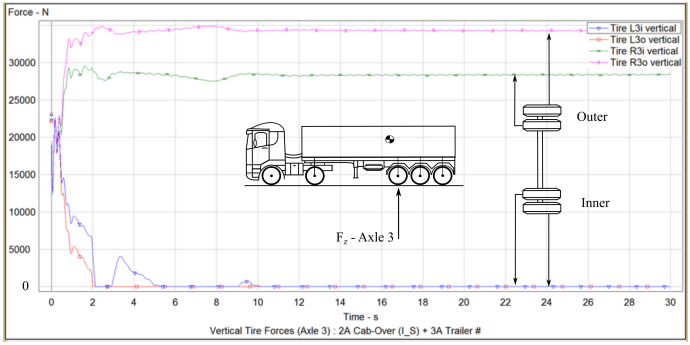

Figure 76 – Normal force on tires of 3^{rd} axle - V = 58 km/h.

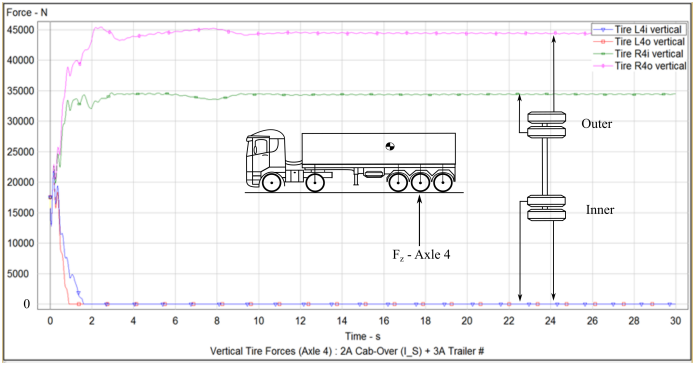

Figure 77 – Normal force on tires of 4^{th} axle - V = 58 km/h.

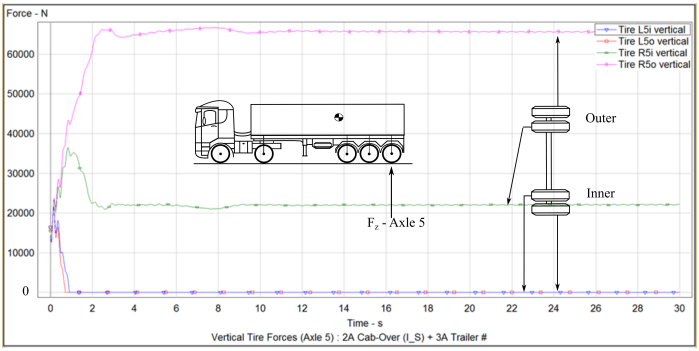

Figure 78 – Normal force on tires of 5^{th} axle - V = 58 km/h.

In this specific case, Fig. 79 shows that the lateral load transfer (*LLT*) in the 2^{nd} axle was not complete. This fact is important, since it corroborated the theory of the four-legged table, proposed in this work.

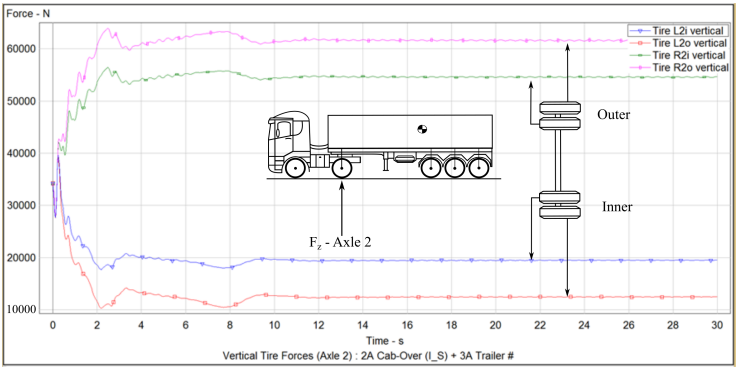

Figure 79 – Normal force on tires of 2^{nd} axle - V = 58 km/h.

Making an analysis of the normal forces on the 2^{nd} axle, the lateral load transfer (Eq. (2.5)) is about 57 %.

Rearranging the Eq. (6.18), and replacing the speed of the vehicle (V) and the radius of curvature (R_c), the SRT factor for the TruckSim model (Test 1) is 0.4409.

$$SRT_{3D_{\psi\phi\varphi}} = \frac{a_y}{g} = \frac{V^2}{R_c \quad g} \tag{8.1}$$

8.1.2 Test 2

Following the same methodology of the previous example, and using the 100 m radius circle (flat paved surface), the test made with vehicle speed of 64 km/h shows that the lateral load transfer (*LLT*) in the 3^{rd}, 4^{th} and 5^{th} axles were complete, but in the 2^{nd} axle was not complete. Figures 80 to 83 show the normal forces on tires of the axles 3^{rd}, 4^{th}, 5^{th} and 2^{nd} axles.

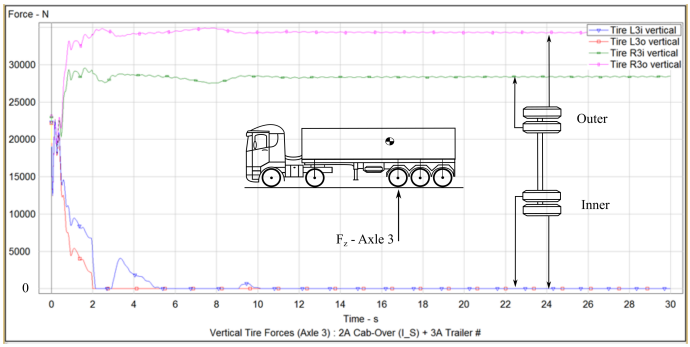

Figure 80 – Normal force on tires of 3^{rd} axle - V = 64 km/h.

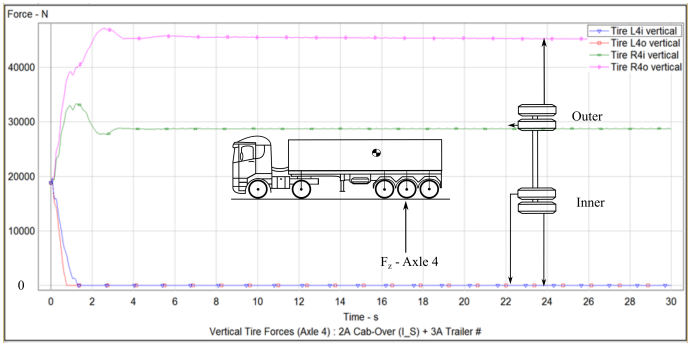

Figure 81 – Normal force on tires of 4^{th} axle - V = 64 km/h.

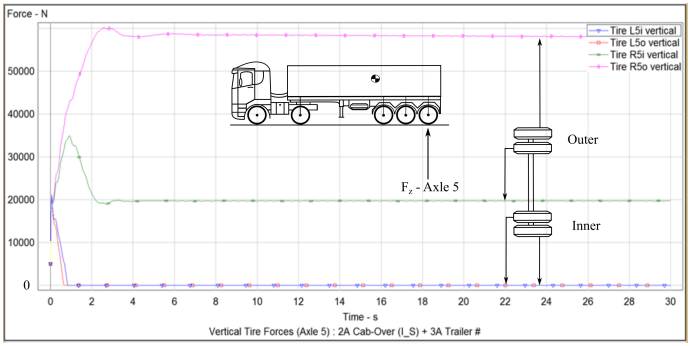

Figure 82 – Normal force on tires of 5^{th} axle - V = 64 km/h.

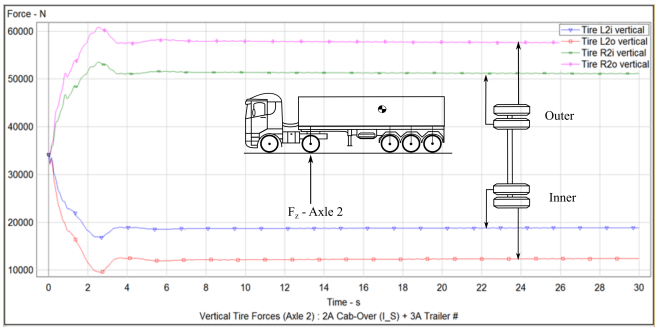

Figure 83 – Normal force on tires of 2^{nd} axle - V = 64 km/h.

Making an analysis of the normal forces on the 2^{nd} axle, the lateral load transfer (Eq. (2.5)) is about 56 %; of the Eq. (8.1) the SRT factor for the TruckSim model (Test 2) is 0.3221.

8.2 STATIC ROLLOVER THRESHOLD WITH THE DEVELOPED MODEL

8.2.1 Test 1

Using the three-dimensional model of stability (Chapter 6), the same vehicle of the previous example (Subsection 8.1.1) is analyzed; Fig. 84 and Table 15 show the parameters of the model used in this analysis.

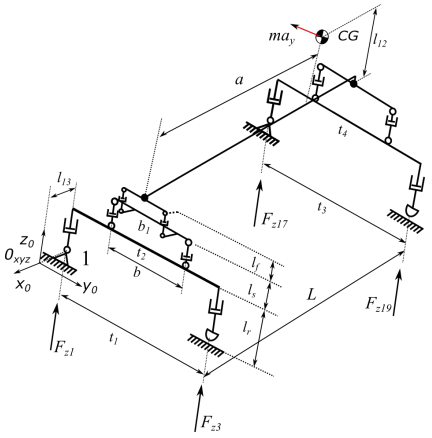

Figure 84 – Parameters of the trailer model.

The SRT factor calculation was obtained using the steady circular test (ISO-14792, 2011), to calculate the SRT factor, the inertial force was increased until the lateral load transfer in the rear axle is complete and the LLT_f coefficient on the front axle is about 57 % (TruckSim model).

At the rollover threshold limit, the normal force in the rear inner tire (F_{z19}) reaches zero (Eqs. (6.17) and (6.39)). Hence, applying this condition, Figs. 85 and 86 show the normal forces on the tires of the trailer model with respect to the increase of the inertial force (SRT factor), F_{z3} and F_{z1} are the inner and outer normal forces on the front axle of the trailer model respectively, and F_{z19} and F_{z17} are the inner and outer normal forces on the rear axle of the trailer model respectively.

The example in the Figs. 85 and 86 show that the reduction in the SRT factor results from the combined action of the trailer systems, the example shows that the proposed model with all systems and considers that LLT_f coefficient on the front axle is about 57 % (TruckSim model), the $SRT_{LLT_f=57\%}$ factor for a model is 0.4353.

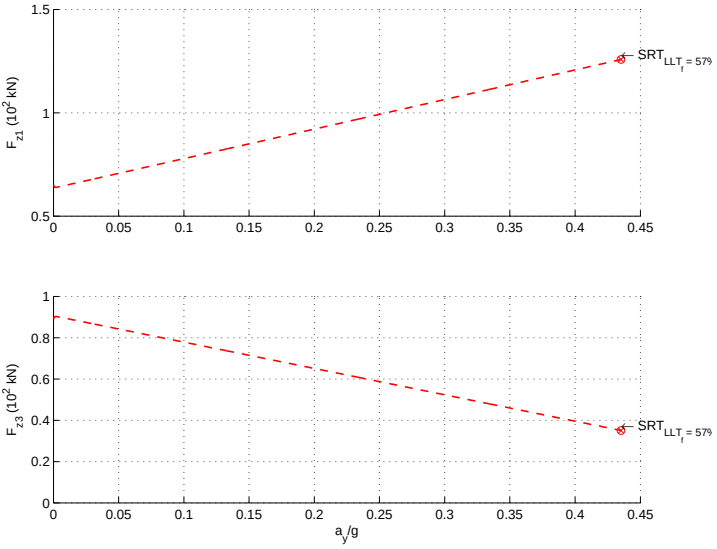

Figure 85 – Normal force on the front axle (F_{z1} and F_{z3})- SRT factor - Semi-trailer.

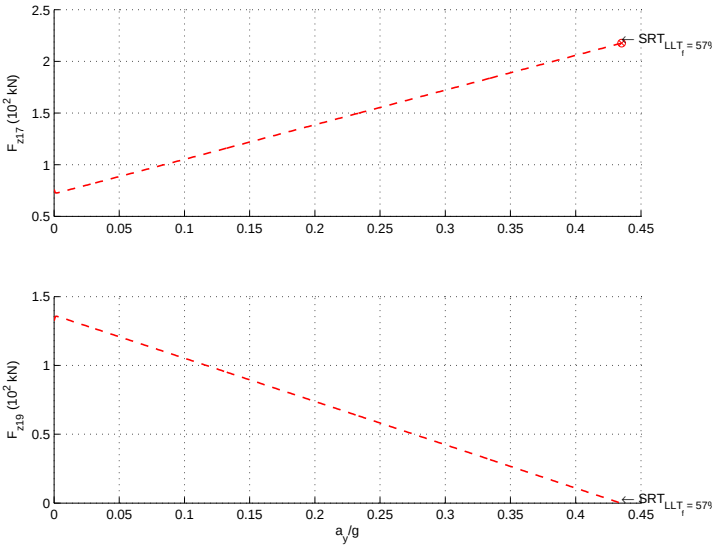

Figure 86 – Normal force on the rear axle (F_{z17} and F_{z19}) - SRT factor - Semi-trailer.

8.2.2 Test 2

Using the three-dimensional model of stability (Chapter 6), the same vehicle of the previous example (Subsection 8.1.2) is analyzed.

The SRT factor calculation was obtained using the steady circular test (ISO-14792, 2011), to calculate the SRT factor, the inertial force was increased until the lateral load transfer in the rear axle is complete and the LLT_f coefficient on the front axle is about 57 % (TruckSim model)

At the rollover threshold limit, the normal force in the rear inner tire (F_{z19}) reaches zero (Eqs. (6.17) and (6.39)). Hence, applying this condition, Fig. 87 show the normal forces on the tires of the trailer model with respect to the increase of the inertial force (SRT factor).

The example in the Fig. 87 show that the reduction in the SRT factor results from the combined action of the trailer systems, the example shows that the proposed model with all systems and considers that LLT_f coefficient on the front axle is about 57 % (TruckSim model), the $SRT_{LLT_f=57\%}$ factor for a model is 0.3231.

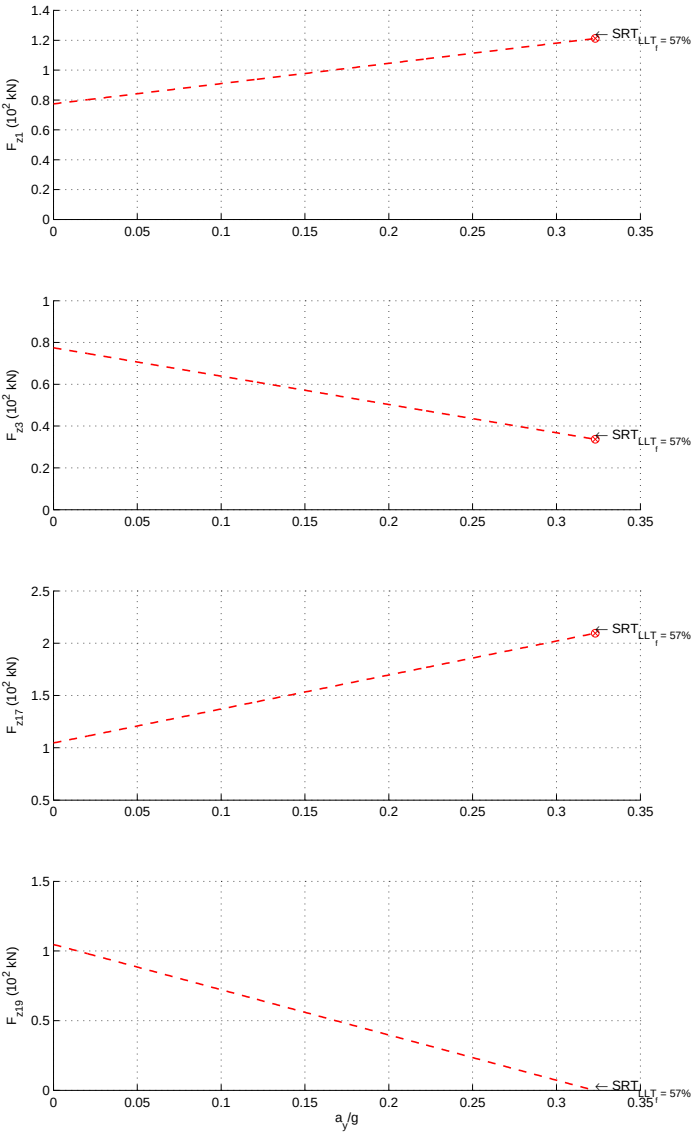

Figure 87 – Normal forces - SRT factor - Semi-trailer.

8.3 CONCLUSIONS

Figures 88 and 89 show a summary of some SRT factor: the rigid, the Gillespie and the Navin three-dimensional model developed in the Chapter 2, the proposed three-dimensional model developed in this thesis (Chapter 6), and the tests of TruckSim model.

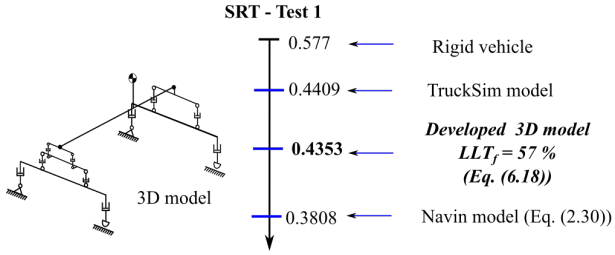

Figure 88 – Developed three-dimensional models - Test 1.

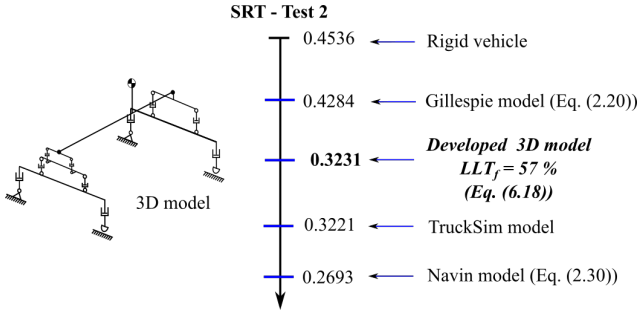

Figure 89 – Developed three-dimensional models - test 2.

Figure 88 and 89 show that:

• the Navin model (NAVIN, 1992) presents a difference of 15.7 % as compared to the TruckSim model (Test 1) and of 19.6 % as compared to the TruckSim model (Test 2),

• the Gillespie model (GILLESPIE, 1992) presents a difference of 33 % as compared to the TruckSim model (Test 2), and

• the developed three-dimensional model presents a difference of 1.2 % as compared to the TruckSim model (Test 1) and of 0.3 % as compared to the TruckSim model (Test 2).

The results of this example demonstrate that the longitudinal characteristics of a trailer model and the road have an important influence on

the SRT factor calculation, which allows that the model provides consistent results.

The results obtained with the proposed model were compared with the TruckSim model, and the reductions in the SRT factor was similar. This guarantee that this approach is coherent and can be well accepted.

Chapter 9

CASE STUDY - B-TRAIN

In this study, a trailer of a B-train with two axles on front (truck) and three axles on rear was analyzed (Fig. 90). In this model a suspension system with a tandem axle is used and the suspension parameters are dependent on the construction materials. Harwood *et al.* (2003) reported that the range of values for the stiffness of the suspension per axle is $k_{Ls} = (1500 - 2400) \quad kN.m^{-1}$. Another important parameter is the dynamic rolling radius or loaded radius l_r; the proposed model considers Michelin XZA® (MICHELIN, 2013) radial tires with $l_r = 0.499$ m. Figure 91 and Table 16 show the parameters of the trailer used in this analysis (ERVIN; GUY, 1986). The proposed model is adaptable to other vehicles, and other examples are shown in appendices B and C.

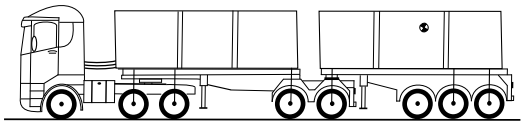

Figure 90 – B-train.

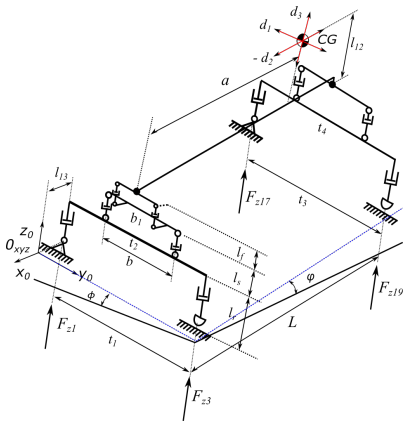

Figure 91 – Parameters of the trailer model.

Table 16 – Parameters of the trailer model - B-train.

Parameter	Value	Units
Trailer weight - W	355.22	kN
Front and rear track widths - $t_{1,3}$	1.86	m
Front and rear axle widths - $t_{2,4}$	1.86	m
Stiffness of the suspension per axle - k_{Ls} (HARWOOD *et al.*, 2003)	1800	kN/m
Number of axles at the front (trailer) (4 tires per axle)	2	
Number of axles at the rear (trailer) (4 tires per axle)	3	
Vertical stiffness per tire - k_T (HARWOOD *et al.*, 2003)	840	kN/m
Stiffness of the fifth-wheel - k_f	7500	kN/m
Initial suspension height - $l_s = l_{3,4,9,10}$	0.205	m
Initial dynamic rolling radius - $l_r = l_{1,2,7,8}$ (MICHELIN, 2013)	0.499	m
Initial height of the fifth wheel - l_f	0.1	m
Lateral separation between the springs - b	0.95	m
Fifth-wheel width - b_1	0.6	m
CG height above the chassis - l_{12}	1.356	m
Distance between the fifth wheel and the front axle - l_{13}	0.15	m
Wheelbase of the trailer - L	4.26	m
Distance from the front axle to the center of gravity - a	3	m
Lateral *CG* displacement, offset of the cargo d_1	$\pm$ 0.04 $\pm$ 0.08 $\pm$ 0.12 $\pm$ 0.16	m
Longitudinal *CG* displacement d_2	$\pm$ 0.5 $\pm$ 1 $\pm$ 1.5	m
Vertical *CG* displacement d_3	$\pm$ 0.1 $\pm$ 0.2	m
Trailer/trailer angle (ψ)	0	$^\circ$

9.1 THREE-DIMENSIONAL STATIC ROLLOVER THRESHOLD

The SRT factor calculation was obtained using the steady state circular test (ISO-14792, 2011), the load conditions include a load laterally centered, load with *CG* displacement and overweight with *CG* displacement.

The simulation model was applied using MATLAB® (2013). To calculate the SRT factor, the inertial force was increased until the lateral load transfer in the rear axle become complete.

At the rollover threshold limit, the normal force in the rear inner tire F_{z19} reaches zero (Eqs. (6.17) and (6.39)). Hence, applying this condition, Fig. 92 shows the normal forces on the tires of the trailer model with respect to the increase of the inertial force (SRT factor).

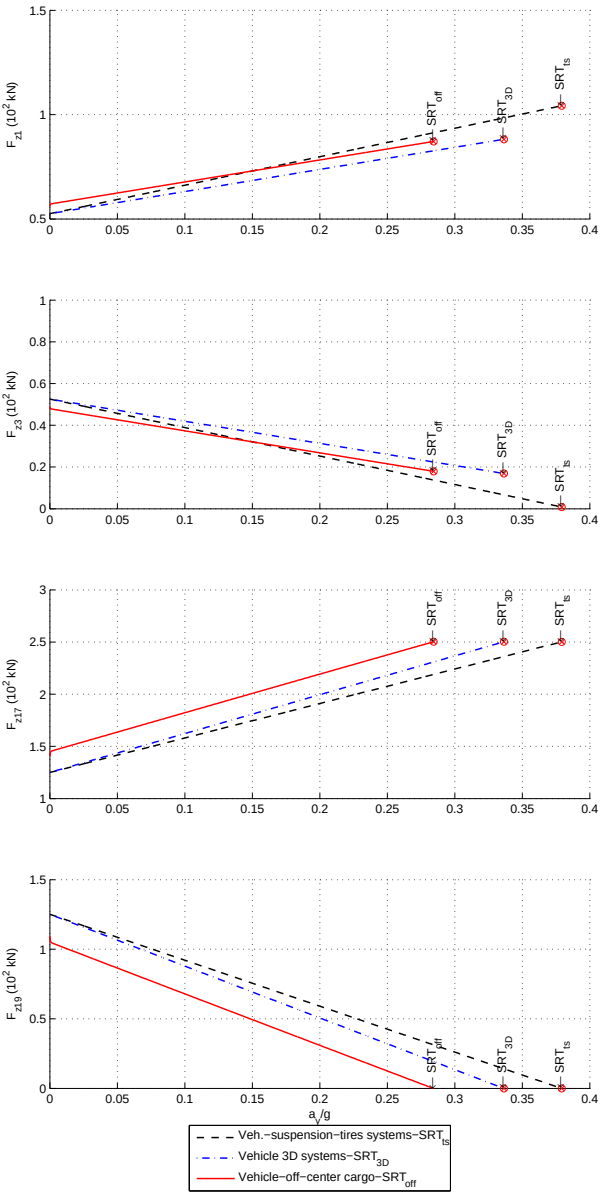

Figure 92 – Normal forces - SRT factor - B-train.

where F_{z3} and F_{z1} are the inner and outer normal forces on the front of the trailer model respectively, and F_{z19} and F_{z17} are the inner and outer normal forces on the rear of the trailer model respectively.

The example of Fig. 92 shows the normal forces on the tires and the following stages of the trailer model: in the first stage, the model considers the tires and suspension systems, SRT_{ts} factor for a model is 0.3792.

In the second stage, the trailer model considers all systems (tires, suspension, fifth-wheel, and the flexibility of the chassis). According to Kamnik *et al.* (2003), they detected that when an articulated vehicle makes a spiral manoeuvre, the LLT_f coefficient on the front axle is approximately 70 % of the LLT_r coefficient on the rear axle (as shown in Fig. 93). Applying this concept, the SRT_{3D} factor reduces to 0.3364.

Finally, the proposed model shows how the lateral offset of the cargo ($d_1 = 0.1$ m) influences the SRT_{off} factor: 2 cm of lateral offset corresponds to a loss of stability of around 0.01 (a reduction similar to that reported by Winkler (2000)).

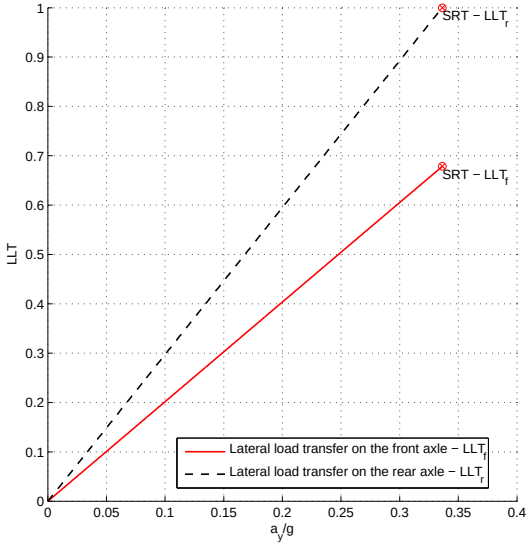

Figure 93 – Lateral load transfer of the trailer model - SRT factor - B-train.

The reduction in the SRT factor results from the combined action of the trailer systems, which allows a body roll angle of the trailer of

$\theta_{3D} = \theta_{17} + \theta_{21} + \theta_{23} + \theta_{27} = 5.8°$, as shown in Fig. 94.

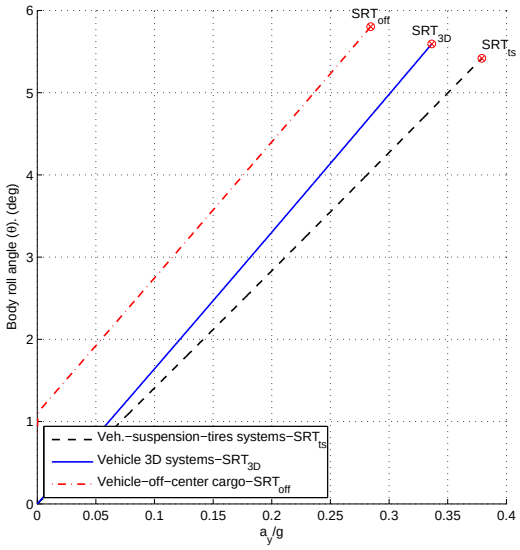

Figure 94 – Total body roll angle of the trailer (θ_{3D}) - SRT factor - B-train.

Additionally, the proposed model shows how a change in the lateral separation between the springs (b) influences the SRT factor. Some *LCV's* with tanker trailers have a grater lateral separation between the springs, which leads to a decrease in the roll angle and thus an increase in the SRT factor: 1 cm of lateral separation between the springs corresponds to an increase or loss of stability of around 0.001, as shown in Fig. 95.

Furthermore, this model also allows the determination of the lateral (h_1 - the instantaneous lateral distance between the zero-reference frame and the center of gravity - as shown in Fig. 96) and the vertical (h_2 - the instantaneous *CG* height - as shown in Fig. 97) *CG* displacements.

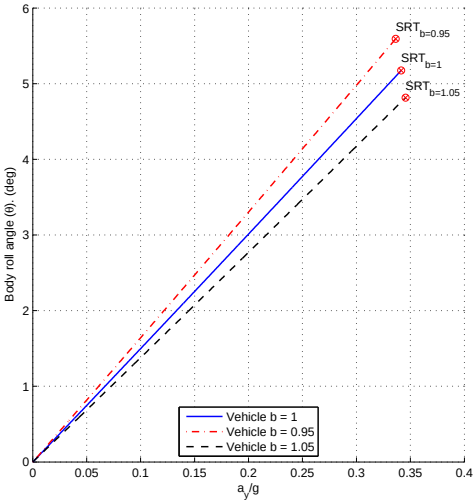

Figure 95 – Total body roll angle of the trailer (θ_{3D}) - SRT factor (lateral separation between the springs (b)) - B-train.

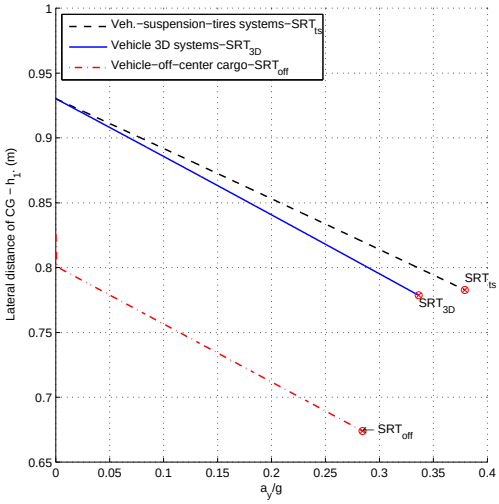

Figure 96 – Lateral movement of *CG* - SRT factor - B-train.

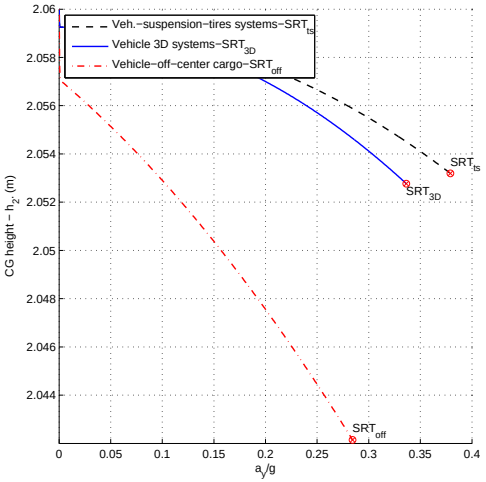

Figure 97 – Vertical movement of *CG* - SRT factor - B-train.

9.2 DOWNHILL AND UPHILL CORNERS

In this case, for the stability analysis is considered the recommended maximum lateral load transfer ratio (LLT_r) for the rear axle of 0.6 (WOODROOFFE *et al.*, 2010; WALKER; PEARSON, 1987), and also include the recommended bank angle and longitudinal slope of the road (AASHTO, 2003) (AASHTO, 2001), we can calculate the SRT factor for a trailer model on uphill (Fig. 98(a)) and downhill corners (Fig. 98(b)).

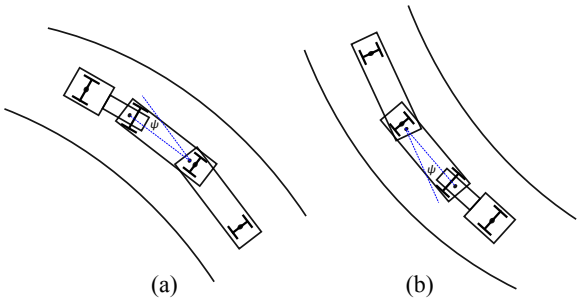

Figure 98 – a - Uphill corner. b - Downhill corner.

As mentioned previously, in this study was analyzed the last trailer of a *LCV's*; for this reason is considered the angle formed by the last units when the *LCV* makes turns (trailer/trailer angle - ψ), as shown in Fig. 98. These manoeuvres are made at relatively low speeds, according to the studies of "Minimum turning paths of design vehicles" (AASHTO, 2001) is assumed that the trailer/trailer angle not be greater than 30°.

Figure 99 shows the behavior of the SRT factor under the influence of the bank angle, longitudinal slope angle, and the trailer/trailer angle.

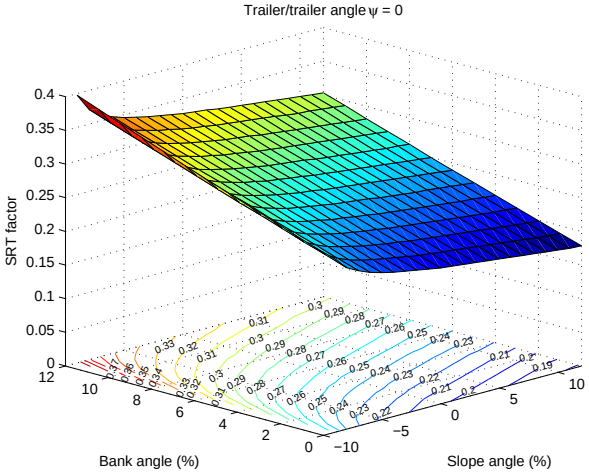

Figure 99 – Trailer/trailer angle ($\psi = 0^0$) - SRT factor - B-train.

Table 17 shows the influence of the bank angle, longitudinal slope angle, and the trailer/trailer angle on the SRT factor calculations.

In the worst case scenario, the trailer model, for a downhill corner with a bank angle of 0 %, longitudinal slope of the road of 12 %, and a trailer/trailer angle of 30°, can reduce the SRT factor of the vehicle by 61.8 %, using 0.451 as a reference.

Table 17 – Static Rollover Threshold (SRT) of *LCV* with trailer/trailer angle - B-train.

Slope angle (φ) - (%)		**Uphill corners**						**Downhill corners**					
Trailer/trailer angle (ψ) – (^{0})	**Bank angle (ϕ) - (%)**	9	8	6	4	2	0	2	4	6	8	10	12
0	0	0.257	0.240	0.223	0.214	0.208	0.202	0.198	0.194	0.190	0.186	0.181	0.178
0	2	0.278	0.261	0.245	0.235	0.228	0.223	0.218	0.214	0.210	0.206	0.202	0.199
0	4	0.302	0.283	0.265	0.256	0.249	0.244	0.239	0.234	0.230	0.226	0.223	0.219
0	6	0.324	0.305	0.286	0.277	0.270	0.265	0.260	0.256	0.252	0.248	0.244	0.240
0	8	0.349	0.327	0.308	0.299	0.292	0.285	0.281	0.276	0.272	0.268	0.264	0.261
0	10	0.373	0.350	0.330	0.320	0.313	0.307	0.303	0.298	0.294	0.290	0.285	0.281
0	12	0.398	0.372	0.352	0.341	0.334	0.328	0.324	0.319	0.315	0.311	0.307	0.303
10	0	0.258	0.241	0.223	0.214	0.207	0.202	0.197	0.193	0.189	0.185	0.180	0.177
10	2	0.280	0.262	0.245	0.234	0.227	0.222	0.217	0.213	0.209	0.205	0.201	0.198
10	4	0.303	0.283	0.265	0.256	0.249	0.243	0.239	0.233	0.229	0.225	0.222	0.218
10	6	0.326	0.306	0.286	0.276	0.270	0.264	0.259	0.255	0.251	0.247	0.243	0.239
10	8	0.351	0.328	0.308	0.298	0.291	0.285	0.280	0.276	0.271	0.267	0.264	0.260
10	10	0.375	0.351	0.330	0.319	0.312	0.307	0.302	0.297	0.293	0.288	0.284	0.280
10	12	0.401	0.373	0.352	0.341	0.333	0.328	0.323	0.318	0.314	0.310	0.306	0.302
20	0	0.259	0.241	0.222	0.212	0.206	0.200	0.195	0.191	0.187	0.182	0.178	0.175
20	2	0.281	0.262	0.244	0.233	0.226	0.220	0.216	0.211	0.207	0.203	0.199	0.196
20	4	0.304	0.283	0.264	0.254	0.247	0.242	0.236	0.232	0.227	0.224	0.220	0.216
20	6	0.327	0.306	0.285	0.275	0.268	0.262	0.257	0.253	0.249	0.245	0.241	0.236
20	8	0.352	0.328	0.307	0.297	0.290	0.283	0.278	0.274	0.270	0.265	0.262	0.258
20	10	0.377	0.351	0.329	0.318	0.311	0.305	0.300	0.295	0.291	0.286	0.282	0.278
20	12	0.403	0.373	0.351	0.339	0.332	0.326	0.321	0.316	0.312	0.308	0.304	0.300
30	0	0.259	0.240	0.220	0.210	0.203	0.197	0.193	0.188	0.183	0.179	0.176	0.172
30	2	0.281	0.261	0.242	0.231	0.223	0.218	0.213	0.208	0.204	0.200	0.197	0.193
30	4	0.305	0.282	0.262	0.252	0.245	0.239	0.233	0.229	0.225	0.221	0.217	0.213
30	6	0.328	0.305	0.283	0.273	0.265	0.260	0.255	0.250	0.246	0.242	0.238	0.233
30	8	0.353	0.327	0.305	0.295	0.286	0.280	0.275	0.271	0.267	0.263	0.259	0.255
30	10	0.378	0.350	0.327	0.316	0.308	0.302	0.297	0.293	0.287	0.283	0.279	0.275
30	12	0.404	0.372	0.349	0.337	0.329	0.323	0.318	0.313	0.309	0.305	0.301	0.297

Making an analysis of Table 17, the following conclusions for the critical conditions of the trailer model are obtained:

• a 1 % bank angle corresponds to a gain in stability of around 0.01;

• when the trailer model is in downhill corners; a 1 % slope angle corresponds to a loss of stability of around 0.0021;

• the trailer/trailer angle is inversely proportional to the SRT factor since, when the trailer model makes a horizontal curve with a small radius, the trailer/trailer angle and the inertial force are large, then the SRT factor is smaller.

9.3 LOAD DISTRIBUTION

Using the same trailer model described in section 9.1, at the rollover threshold limit, the example shows a trailer with relatively low stability, under the action of suspension, tires and the chassis, the SRT_{3D} factor of the model is 0.3364; additionally the trailer model takes into account the *CG* displacement (as it was described in section 4.7), Fig. 100 shows a sensibility analysis of the *CG* displacement, for the simulation of the trailer rollover, the vertical *CG* displacement (d_3) is fixed, and the longitudinal (d_2) and lateral (d_1) *CG* displacement are varied.

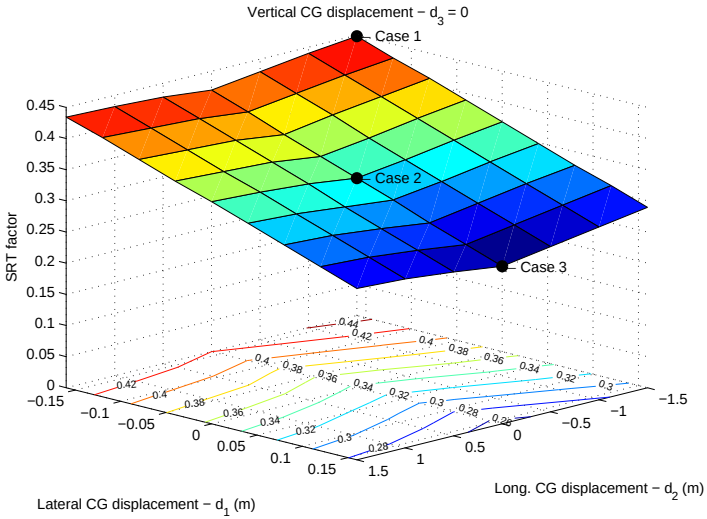

Figure 100 – Lateral and longitudinal *CG* displacement - SRT factor - $d_3 = 0$ - B-train.

Rearranging the Eq. (8.1), the speed limit of the vehicle (V-(km/h))

can be calculated for different radius of roadway curves (R_c-(m)), as shown in Eq. (9.1).

$$V = \sqrt{127 \quad SRT_{3D_{\psi\phi\varphi}} \quad R_c} \tag{9.1}$$

From Eq. (9.1), another example for sensibility analysis of the load distribution and the *CG* displacement is shown; Table 18 shows the speed limits for a vehicle making a curve of radius R_c = 80 m, and taking into account the $SRT_{3D_{\psi\phi\varphi}}$ factor for the three cases highlighted in Fig. 100.

Table 18 – Maximum speed of the trailer model - B-train.

Parameters	$SRT_{3D_{\psi\phi\varphi}}$ factor	Max. speed (km/h)
Case 1 (the best SRT factor)	0.4485	67.5
Case 2 (standard SRT factor)	0.3364	58.5
Case 3 (the worst SRT factor)	0.2528	50.7

Table 18 shows how the SRT factor and the load distribution can influence the speed limits of the vehicles, which make them unstable in the worst case.

Table 19 shows the influence of the *CG* displacement on the SRT factor calculations.

Making the technique interpretation of the result (Table 19), the following conclusions are obtained:

• 2 cm of lateral *CG* displacement (d_1) corresponds to an increase or loss of stability of around 0.01, (a reduction similar to that reported by Winkler (2000);

• 4 cm of vertical *CG* displacement (d_3) corresponds to an increase or loss of stability of around 0.01;

• for the longitudinal *CG* displacement (d_2), the overweight on the front or the rear axle enable an increase of the SRT factor; but, the overweight on the front axle induces the understeer of the vehicle, and the overweight on the rear axle induces the oversteer of the vehicle.

Table 19 – Static Rollover Threshold (SRT) of *LCV* with *CG* displacement - B-train.

Lateral *CG* disp. - (d_1)-(m)		**External side of veh. in the turn**					**Internal side of veh. in the turn**			
Vertical *CG* disp. (d_3)-(m)	**Long. *CG* disp. (d_2)-(m)**	0.16	0.12	0.08	0.04	0	-0.04	-0.08	-0.12	-0.16
0.2	1.5	0.234	0.255	0.273	0.292	0.308	0.326	0.345	0.363	0.381
0.2	1	0.232	0.251	0.269	0.287	0.306	0.324	0.343	0.361	0.379
0.2	0.5	0.226	0.245	0.265	0.283	0.302	0.320	0.338	0.359	0.377
0.2	0	0.218	0.236	0.257	0.275	0.294	0.314	0.332	0.351	0.371
0.2	-0.5	0.230	0.251	0.269	0.287	0.306	0.326	0.345	0.363	0.381
0.2	-1	0.245	0.263	0.281	0.300	0.318	0.336	0.357	0.375	0.393
0.2	-1.5	0.257	0.275	0.294	0.312	0.330	0.349	0.367	0.385	0.404
0.1	1.5	0.255	0.273	0.294	0.312	0.330	0.351	0.369	0.387	0.406
0.1	1	0.251	0.269	0.290	0.308	0.328	0.347	0.367	0.385	0.406
0.1	0.5	0.245	0.263	0.283	0.304	0.322	0.343	0.361	0.381	0.402
0.1	0	0.234	0.255	0.275	0.294	0.314	0.334	0.355	0.373	0.393
0.1	-0.5	0.247	0.267	0.285	0.306	0.326	0.347	0.365	0.385	0.404
0.1	-1	0.259	0.279	0.298	0.318	0.338	0.357	0.377	0.396	0.416
0.1	-1.5	0.273	0.292	0.312	0.330	0.349	0.369	0.387	0.406	0.426
0	1.5	0.275	0.296	0.316	0.336	0.357	0.375	0.396	0.416	0.434
0	1	0.271	0.292	0.312	0.332	0.353	0.371	0.391	0.412	0.432
0	0.5	0.263	0.283	0.304	0.324	0.347	0.367	0.387	0.408	0.428
0	0	0.253	0.273	0.294	0.316	0.336	0.357	0.377	0.400	0.420
0	-0.5	0.265	0.285	0.306	0.326	0.347	0.367	0.389	0.410	0.430
0	-1	0.277	0.298	0.318	0.338	0.359	0.379	0.400	0.420	0.440
0	-1.5	0.290	0.310	0.328	0.349	0.369	0.389	0.410	0.428	0.449
-0.1	1.5	0.300	0.320	0.340	0.363	0.383	0.404	0.424	0.444	0.465
-0.1	1	0.294	0.314	0.336	0.357	0.377	0.400	0.420	0.440	0.463
-0.1	0.5	0.283	0.306	0.328	0.349	0.371	0.393	0.414	0.436	0.457
-0.1	0	0.273	0.294	0.316	0.338	0.361	0.383	0.404	0.426	0.449
-0.1	-0.5	0.283	0.306	0.328	0.349	0.371	0.393	0.414	0.436	0.457
-0.1	-1	0.296	0.316	0.338	0.359	0.381	0.402	0.424	0.444	0.467
-0.1	-1.5	0.308	0.328	0.349	0.371	0.391	0.412	0.432	0.455	0.475
-0.2	1.5	0.324	0.347	0.369	0.391	0.412	0.434	0.457	0.477	0.499
-0.2	1	0.318	0.340	0.363	0.385	0.408	0.430	0.451	0.473	0.495
-0.2	0.5	0.308	0.330	0.353	0.377	0.400	0.422	0.444	0.467	0.489
-0.2	0	0.294	0.318	0.340	0.365	0.387	0.412	0.434	0.457	0.479
-0.2	-0.5	0.306	0.328	0.351	0.375	0.398	0.420	0.442	0.465	0.489
-0.2	-1	0.316	0.338	0.361	0.383	0.406	0.428	0.451	0.473	0.497
-0.2	-1.5	0.326	0.349	0.371	0.393	0.416	0.438	0.461	0.481	0.504

9.4 OVERWEIGHT

Using the same trailer model described in section 9.1, at the rollover threshold limit, the example shows a trailer with relatively low stability, under the action of suspension, tires and the chassis, the SRT_{3D} factor of the model is 0.3364.

Taking into account that the overweight on the front axle induces the understeer of the vehicle, and the overweight on the rear axle induces the oversteer of the vehicle. The SRT factor calculation was obtained using 5 % and 10 % of overweight, load laterally centered, and load with *CG* displacement.

Figures 101 and 102 show the influence of the overweight on the SRT factor calculation; this overweight affects the *CG* height (h_2) and the trailer roll angle (θ), 1 % of overweight corresponds to a loss of stability of around 0.2 %.

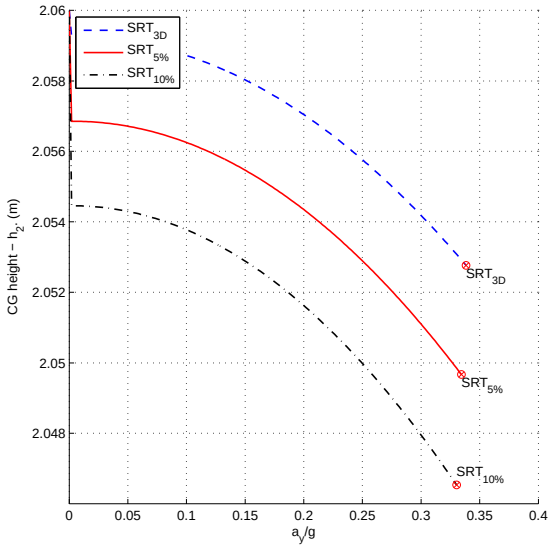

Figure 101 – *CG* height - Overweight - SRT factor - B-train.

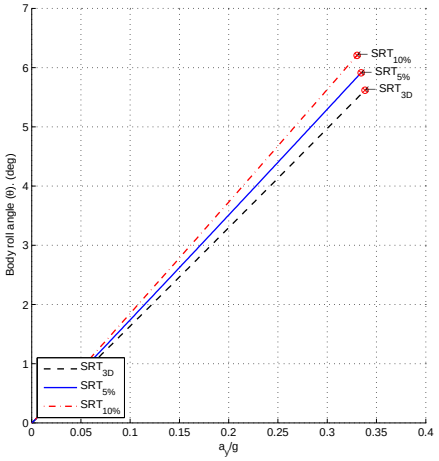

Figure 102 – Total roll angle (θ_{3D}) - Overweight - SRT factor - B-train.

Figure 103 shows the influence of lateral *CG* displacement (d_1) and the overweight on the SRT factor calculation and the trailer roll angle: 2 cm of lateral *CG* displacement and 1 % of overweight corresponds to a loss of stability of around 0.0106.

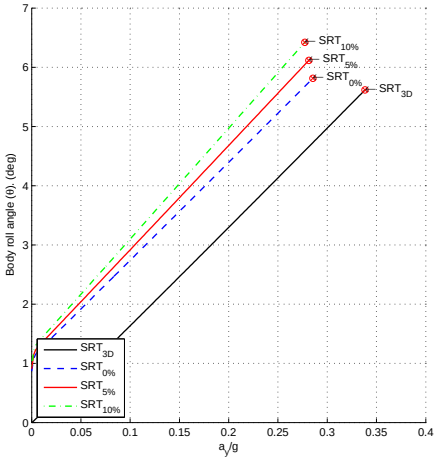

Figure 103 – Lateral *CG* movement - Overweight - SRT factor - B-train.

Figures 104 and 105 show the influence of vertical *CG* displacement (d_3) and the overweight on the SRT factor calculation and the trailer roll angle: Fig. 104 shows that: 4 cm of vertical increase of the *CG* location and 1 % of overweight corresponds to a loss of stability of around 0.0106.

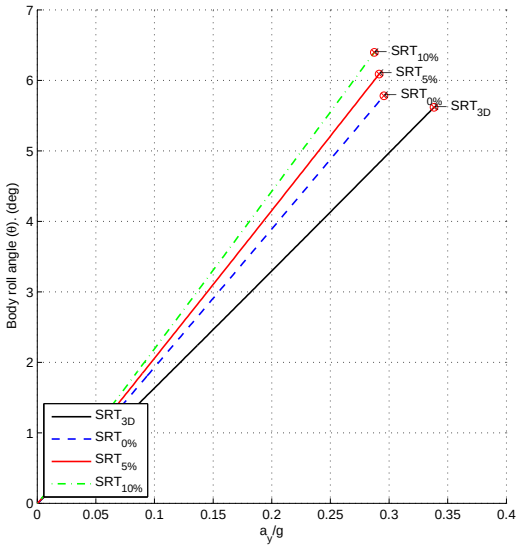

Figure 104 – Vertical *CG* movement - Overweight - SRT factor - B-train.

Fig. 105 shows that: 4 cm of vertical decrease of the *CG* location corresponds to an increase of stability of around 0.01, and 1 % of overweight corresponds to a loss of stability of around 0.0006.

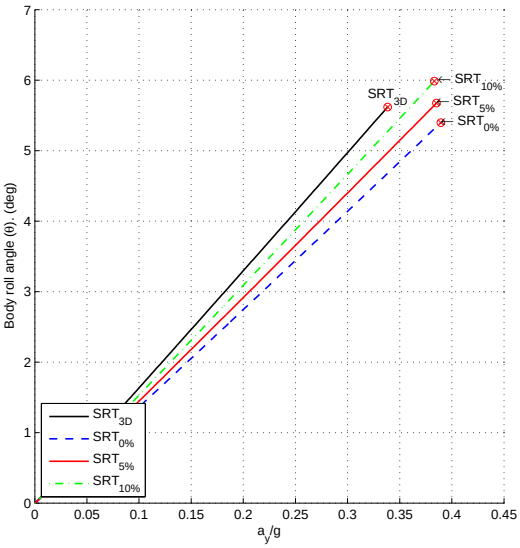

Figure 105 – Vertical *CG* movement - Overweight - SRT factor - B-train.

9.5 STABILITY MODELS COMPARISON

Using the same trailer model described in the section 9.1, the results were compared with the models exposed in the Chapter 2.

Additionally, for the stability analysis is considered the recommended maximum lateral load transfer ratio (LLT_r) for the rear axle of 0.6 (WOODROOFFE *et al.*, 2010; WALKER; PEARSON, 1987); this value is compared with the SRT factors used in USA (SRT = 0.23) (BAKER *et al.*, 2001) and New Zealand (SRT = 0.22) (NZTA, 2008).

Figure 106 shows the summary of all stages of the model, and the influence of its characteristics in the SRT factor calculation.

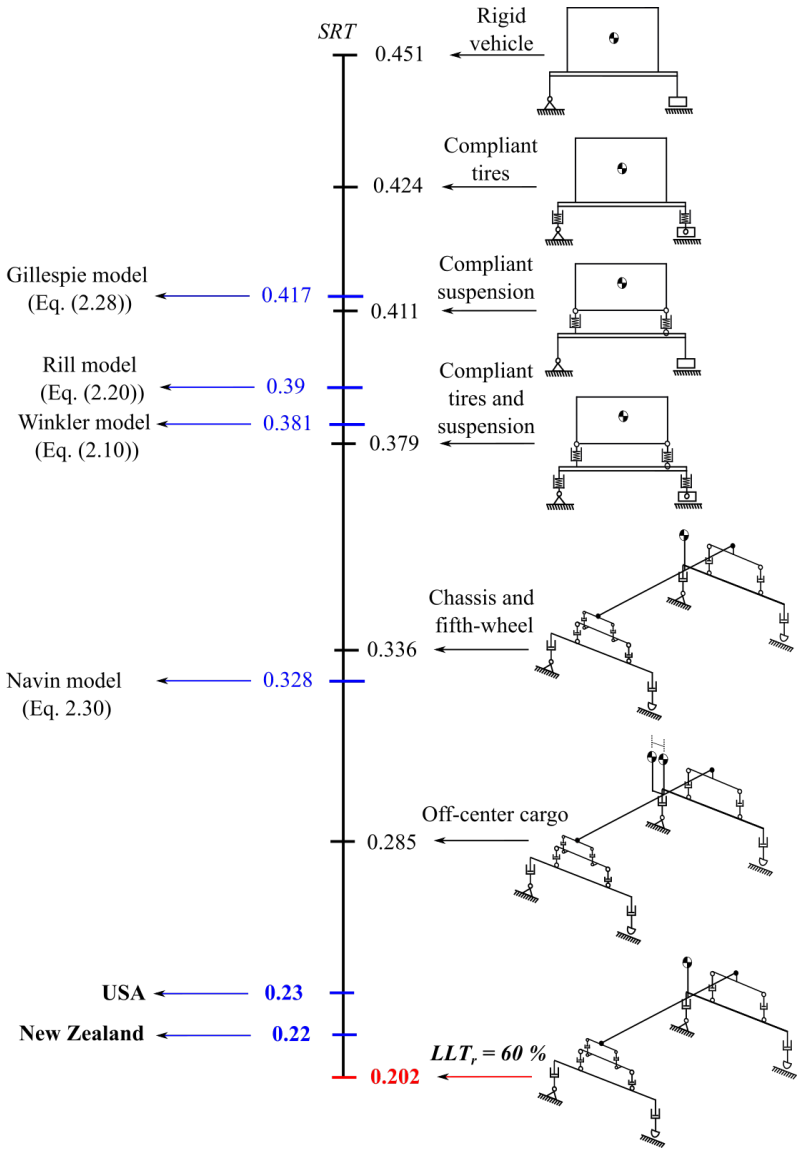

Figure 106 – Stability models comparison.

Figure 106 shows that the differences between the developed model and the models cited are small, which indicates that the proposed model provides consistent results.

Figure 106 shows that the SRT factor for the developed model is less than the ones currently used in the world, this fact would make that the road safety greater

On the other hand, using the Eq. (9.1), an example for sensibility analysis of the SRT factor is shown; Table 20 shows the speed limits for a vehicle making a curve of radius R = 120 m, and taking into account the SRT factor for the three cases highlighted in Fig. 106 and the SRT factor for the vehicle in downhill corner with 12 % of slope angle and 0 % of bank angle (Table 17).

Table 20 – Maximum speed of the trailer model - B-train.

Parameters	$SRT_{3D_{\psi\phi\varphi}}$ factor	Max. speed (km/h)
USA	0.23	59.2
New Zealand	0.22	57.9
Proposed model	0.202	55.5
Proposed model Downhill corners Slope angle ($\varphi = 12\%$) Bank angle ($\phi = 0\%$)	0.172	51.2

Table 20 shows how the SRT factor can influence the speed limits of the vehicles. The velocity of the proposed model (Case 3) has a decrease of around 6.3 % with respect to the velocity in USA, and the velocity of the proposed model (Case 4) has a decrease of around 13.5 % with respect to the velocity in USA.

9.6 ROAD DESIGN MINIMUM RADIUS FOR *LCV*

According to AASHTO (2001), AASHTO (2003), DNER (1999) and DNIT (2009): "The minimum radius is a limiting value of curvature for a given design speed and is determined from the maximum rate of superelevation (bank angle) and the maximum side friction factor selected for design (limiting value of f). Using a sharper curvature for that design speed would call for superelevation beyond what is considered comfortable by many drivers, or both. Although based on a threshold of driver comfort, rather than safety, the minimum radius of curvature is also an important control value for determination of superelevation rates for flatter curves. The minimum radius of curvature, R_{min} (m), can be calculated directly from the next simplified curve formula":

$$R_{min} = \frac{V^2}{127(0.01e_{max} + f_{max})} \tag{9.2}$$

where V is the vehicle speed (km/h), e is the rate of roadway superelevation or bank angle (percent), and f_{max} is the side friction (demand) factor. Table 21 shows the recommended friction factors in relation to speed limits on roads:

Table 21 – Speed limits and friction factors.

Speed limits - (V) (km/h)	Friction factor (f)
30	0.17 - 0.28
40	0.17 - 0.23
50	0.16 - 0.19
60	0.15 - 0.17
70	0.14 - 0.15
80	0.14
90	0.13 - 0.14
100	0.12 - 0.13
110	0.11 - 0.12
120	0.09 - 0.11

Source: Adapted from AASHTO (2003), DNER (1999) and DNIT (2009)

However, this method is based on using the limiting values of e and f (or as mentioned above, the minimum radius of curvature is based on the driver comfort threshold, rather than safety); this is a problem, because, the vehicle has two accident possibilities: slide out and rollover, as shown in Fig. 107.

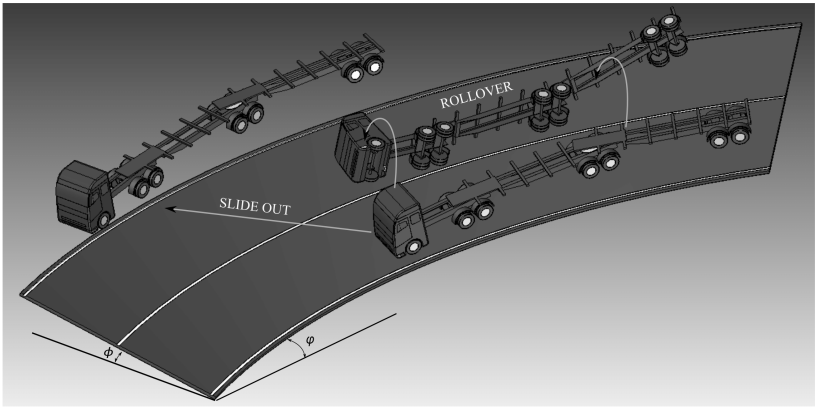

Figure 107 – Accident possibilities of *LCV's*.

Then, taking into account the second possibility, and using the $SRT_{3D_{\psi\phi\varphi}}$ factor (Eq. (8.1)) for the minimum radius calculation, the next

equations are defined:

$$R_{min} = \frac{V^2}{127 \quad SRT_{3D_{\psi\phi\varphi}}} \tag{9.3}$$

Using the same trailer model described in section 9.2, and taking into account the theory mentioned above, Figures 108 to 114 compared the minimum radius given by the Eq. (9.2) and the minimum radius given by the Eq. (9.3); in these equations the bank angle and the slope angle are varied. These figures show that for certain situations and using the classical minimum radius given by the Eq. (9.2), the trailer is prone to rollover. This shows that the SRT factor plays an important role in road design and the speed limits of vehicles.

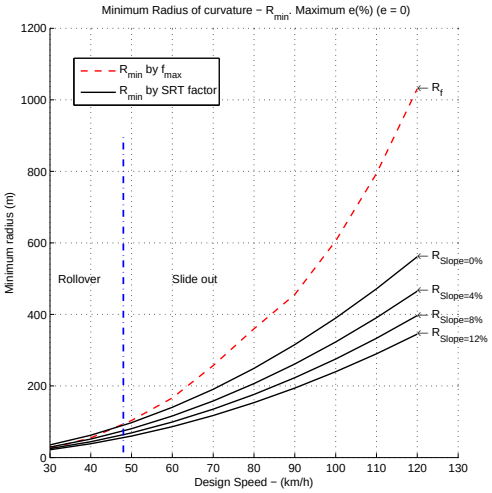

Figure 108 – Minimum radius of curvature R_{min}. Bank angle (e = 0 %) - B-train.

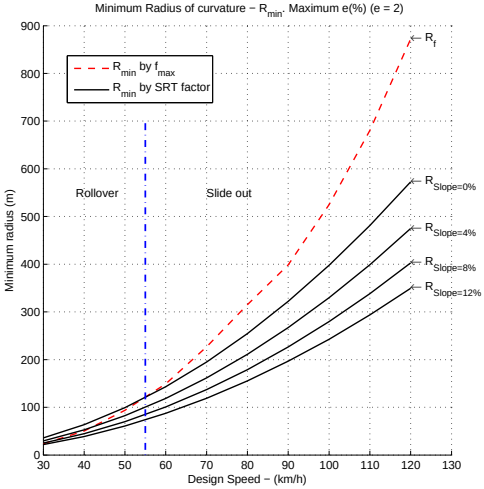

Figure 109 – Minimum radius of curvature R_{min}. Bank angle (e = 2 %) - B-train.

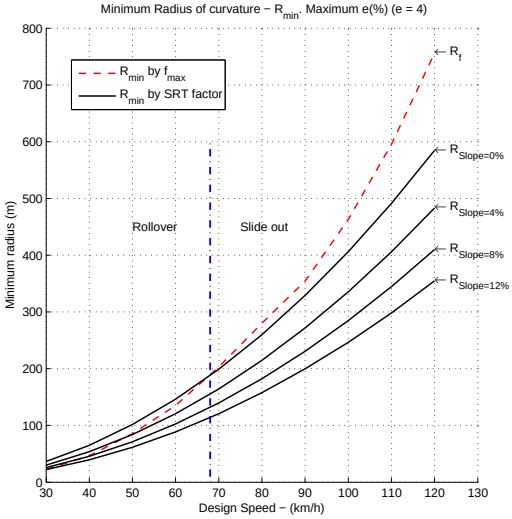

Figure 110 – Minimum radius of curvature R_{min}. Bank angle (e = 4 %) - B-train.

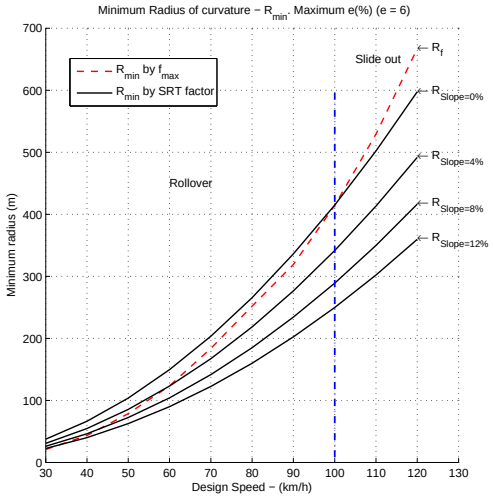

Figure 111 – Minimum radius of curvature R_{min}. Bank angle (e = 6 %) - B-train.

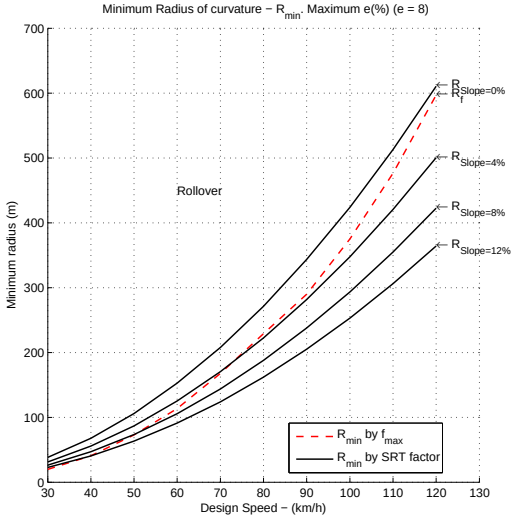

Figure 112 – Minimum radius of curvature R_{min}. Bank angle (e = 8 %) - B-train.

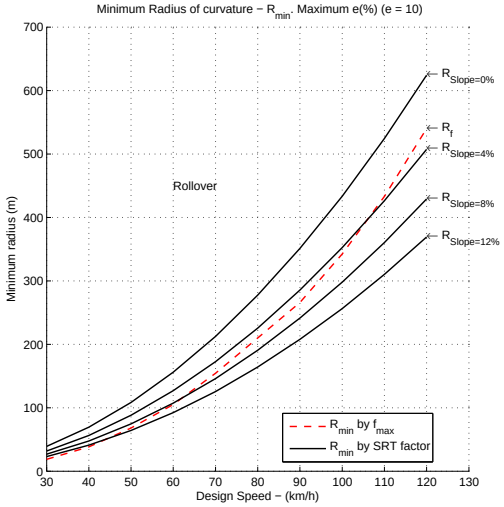

Figure 113 – Minimum radius of curvature R_{min}. Bank angle (e = 10 %) - B-train.

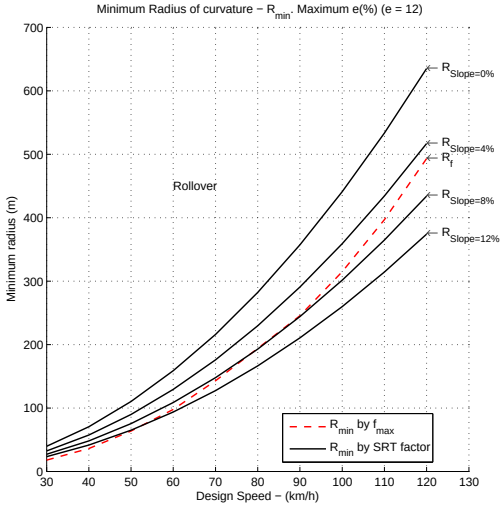

Figure 114 – Minimum radius of curvature R_{min}. Bank angle (e = 12 %) - B-train.

Chapter 10

CONCLUSIONS

From the technique of analysis, the following conclusions are given:

- The developed technique, which used the Virtual Joint Method (*VJM*) along with the theory of buckling, allows the modeling of mechanical components where the linear deformation and the shear deformation plays an important role for the stiffness analysis of the mechanism.
- The developed technique can be applied in different types of mechanisms and mechanical structures; the deformation model provides consistent results and it enables a better design and selection of mechanical components.

Important conclusions were reached comparing the SRT factor in two dimensional and three-dimensional models:

- When the vehicle length is considered, the SRT factor becomes smaller, and this is a real problem. If we use the SRT_{2D} factor as an important feature to characterize the vehicle stability, we are neglecting the longitudinal effects. Which means that the vehicle load distribution and the *LLT* coefficient have important role on the calculation of SRT factor of the vehicle, and not only the track (t) and gravity center height (h).
- The theory of the four legged table described by Heyman (2008) allowed a better understanding of vehicles stability, this theory is possible due to different vehicle characteristics, such as suspension, tires, fifth wheel, and chassis flexibility. This important analysis allows the development of more complex models, in different types of vehicles, allowing better rollover phenomenon representations.
- The results of this study demonstrate that the longitudinal characteristics of a trailer model have an important influence on the SRT factor calculation. In the case study, when the proposed model makes a horizontal curve the $SRT_{3D_{\psi\phi\varphi}}$ factor is approximately 38 % lower than the reported value for a rigid vehicle. This value is very close

to that reported by Winkler (2000) (*i.e.,* 40 %), which suggests that the proposed model provides consistent results.

From the technical analysis of the simulations, the following conclusions are given:

- The proposed model shown that the change in the lateral separation between the springs (b) plays an important role and thus it should be considered in the design and construction of vehicles. A greater lateral separation between the springs will increase the vehicle stability.
- We also found that the parameters of the road, such as the bank angle and the longitudinal slope angle, can affect the vehicle stability. This situation is closer to the actual problem: when the road is not planar, the lateral and the longitudinal load transfer play an important role in reducing the stability. On the other hand, this provides a very important warning, because some simplifications carried out when estimating the SRT factor can lead to a considerably higher stability value. This is a point of concern, leading to the perception that our roads are safer than they really are.
- In the worst case scenario, when the vehicle is in downhill corners, and if it is considered the recommended maximum lateral load transfer ratio for the rear axle of 0.6, it can reduce the SRT factor of the vehicle by 61.8 %
- The results demonstrate that the load distribution and the overweight have an important role on the SRT factor calculation of *LCV's*. The case study showed that the lateral and vertical *CG* displacement can reduce or increase the SRT factor.
- In the same way the longitudinal *CG* displacement of the vehicle enables an increase of the SRT factor; but the overweight on the front axle induces the understeer of the vehicle, and the overweight on the rear axle produces the oversteer of the vehicle.

From the case study of the road design, the following conclusions are given:

- The study showed that for certain situations and using the classical minimum radius given by the Eq. (9.2), the trailer is prone to rollover. This shows that the SRT factor plays an important role in road design and the speed limits of vehicles.

- Therefore, when road design studies are made, it is important to take into account that the vehicle has two accident possibilities: slide out and rollover.
- The SRT factor decrease is important, as it allows to set new road speed limits, which contributes with road safety and decreases vehicle stability related to accidents, which are very high nowadays.

10.1 CONTRIBUTION OF THIS WORK

The original contributions of this work can be summarized as shown below:

(i) Development a technique that allows the modeling of mechanical components where the linear deformation and the shear deformation play an important influence for the stiffness analysis of the mechanism.

(ii) Development of a three-dimensional trailer model for the stability analysis of *LCV's*.

(iii) Inclusion of the load distribution, slope angle, trailer/trailer angle, and the overweight on the static rollover threshold of the *LCV's*.

(iv) The model proposed allows the calculation of the speed limits of the vehicles and the minimum radius of curvature of the road; these make an important contribution to the road safety and to the new road design studies

Chapter 11

RECOMMENDATIONS FOR FUTURE WORK

Based on the results obtained in this thesis, some recommendations for further investigations in vehicle stability and road safety can be made, especially concerning the software development. The following activities are suggested as future research topics:

1. **Vehicle assessment**: In this topic the proposed model allows the following sub topics:

    a) Evaluation of stability in different vehicles.

    b) Evaluation of vehicle implements, such as the suspension, tires, chassis, among others.

    c) Development of new vehicle models and anti-rollover equipments.

2. **Road infrastructure safety assessment**: In this topic the proposed model allows the following sub topics:

    a) Evaluation of speed limit for different types of roads.

    b) Evaluation of new road projects.

3. **Transport logistics assessment**: In this topic the proposed model allows the following sub topics:

    a) Evaluation of the load distribution and the overweight on *LCV*.

    b) Route type evaluations.

BIBLIOGRAPHY

AASHTO. **A Policy on Geometric Design of Highways and Streets**. 4th. ed. Washington, D.C.: American Association of State Highway and Transportation Officials, 2001. ISBN 1-56051-156-7.

AASHTO. **Recommendation for AASHTO Superelevation Design**. Desing Quality Assurance Bureau, NYSDOT. Washington, D.C., 2003.

ADAMS®. **Multibody Dynamics Simulation**. Newport Beach, CA., 2016.

ADMAN, R.; SAIDANI, M. Elastic buckling of columns with end restraint effects. **Journal of Constructional Steel Research**, v. 87, p. 1–5, 2014.

ANTT. **Registro Nacional de Transportadores Rodoviarios de Cargas (RNTRC)**. 2016. Available at: <http://www.antt.gov.br/index.php/content/view/38870/Estatisticas.html>. Accessed on: 17/08/2016.

ANTT. **Transportadores - Frota/Tipo de Veiculo**. 2016. Available at: <http://www.antt.gov.br/index.php/content/view/20271/Transportadores__Frota___Tipo_de_Veiculo.html>. Accessed on: 19/09/2016.

ARAUJO, M. P.; CAMPOS, V.; BANDEIRA, R. An Overview of Road cargo Transport in Brazil. **International Journal of Industrial Engineering and Management**, v. 4, n. 3, p. 151–160, 2013.

BAKER, D.; BUSHMAN, R.; BERTHELOT, C. Effectiveness of truck rollover warning systems. **Transportation Research Record: Journal of the Transportation Research Board**, Transportation Research Board of the National Academies, n. 1779, p. 134–140, 2001.

BAKHSHESH, M.; BAKHSHESH, M. Optimization of steel helical spring by composite spring. **International Journal of Multidisciplinary Science and Engineering**, v. 3, n. 6, 2012.

BARICKMAN, F.; ELSASSER, D.; ALBRECHT, H.; CHURCH, J.; XU, G. **Tractor Semi-Trailer Stability Objective Performance Test Research - Roll Stability**. National Highway Traffic Safety Administration - NHTSA - DOT HS 811 467. Washington, D.C., 2011.

BENNETT, S. **Heavy Duty Systems**. 5th. ed. Clifton Park, New York: Cengage Learning, 2011. ISBN 13:9781435483828.

BIDAUD, P.; BENAMAR, F.; POULAIN, T. Kineto-static analysis of an articulated six-wheel rover. In: **Climbing and Walking Robots**. Berlin, Heidelberg: Springer, 2006. p. 475–484.

BLUNDELL, M.; HARTY, D. **The Multibody System Approach to Vehicle Dynamics**. 1st. ed. Burlintong, MA 01803.: ELSEVIER, 2004. ISBN 0 7506 5112 1.

BONNESON, J. A. **Superelevation distribution methods and transition designs**. Washington, D.C.: National Cooperative Highway Research Program, NCHRP Report 439, 2000.

BOUTELDJA, M.; M'SIRDI, N. K.; GLASER, S.; DOLCEMASCOLO, V. Stability Analysis and Rollover Scenario Prediction For Tractor Semi-Trailer. 2004.

CABRAL, J. C. **Randon e Wabco desenvolvem sistema electrónico anti-tombamento para bitrens - Agência Intelog Notícias**. 2008. Available at: <http://www.newslog.com.br>. Accessed on: 19/08/2008.

CAIXETA, J. V. **Transportation and logistics in Brazilian agriculture**. United States Department of Agriculture, Agricultural Outlook Forum. Arlington, USA, 2003. Available at: <http://EconPapers.repec.org/RePEc:ags:usaoth:33141>.

CAZANGI, H. R. **Aplicação do Método de Davies para Análise Cinemática e Estática de Mecanismos com Múltiplos Graus de Liberdade**. Master's Thesis (Master's Thesis) — Universidade Federal de Santa Catarina, Florianópolis-Brasil, 2008.

CHANG, T. Effect of Vehicles´ Suspension on Highway Horizontal Curve Design. **Journal of Transportation Engineering**, v. 127, n. 1, p. 89–91, 2001.

CHEN, C.; TOMIZUKA, M. Dynamic modeling of articulated vehicles for automated highway systems. In: IEEE. **American Control Conference, Proceedings of the 1995**. Seattle,Washington, 1995. v. 1, p. 653–657.

CHEN, F.; CHEN, S. Assessment of vehicle safety behavior under adverse driving conditions. In: **11th American Conference of wind engineering**. San Juan, Puerto Rico.: American Conferences on Wind Engineering (ACWE), 2009.

CNT. **Confederação Nacional do Transporte - Boletim Estatistíco**. 2016. Available at: <http://www.cnt.org.br/Boletim/boletim-estatistico-cnt>. Accessed on: 16/01/2017.

CONTRAN. **Legislação de pesos e dimensões, Resoluções 210 e 211**. 2011.

COSTA, F. L. Turning the Right Corner Towards a Low-Emission Transport Sector - Transport Sector Emissions in Brazil A Brief Overview. In: **International Transport Forum.** Berlin, Germany: Federal Ministry of Transport, Building and Urban Developmant., 2012.

CROSSLEY, F. R. E. A Contribution to Grübler´s Theory in Number Synthesis of Plane Mechanisms. **ASME Journal of Engineering Industry**, v. 86, n. 2, p. 1–8, 1964.

DAHLBERG, E.; WIDEBERG, J. Influence of the fifth-wheel location on heavy articulated vehicle handling. In: **8th International Symposium on Heavy Vehicle Weights and Dimensions.** Johannesburg, South Africa.: International Forum for Road Transport Technology, 2004.

DAVIES, T. H. Kirchhoff´s circulation law applied to multi-loop kinematic chains. **Mechanism and Machine Theory**, v. 16, n. 3, p. 171–183, 1981.

DAVIES, T. H. Mechanical networks-I Passivity and redundancy. **Mechanism and Machine Theory**, v. 18, n. 2, p. 95–101, 1983.

DAVIES, T. H. Mechanical networks-III wrenches on circuit screws. **Mechanism and Machine Theory**, v. 18, n. 2, p. 107–112, 1983.

DAVIES, T. H. Couplings, coupling network and their graphs. **Mechanism and Machine Theory**, v. 30, n. 7, p. 1001–1012, 1995.

DAVIES, T. H. The 1887 committee meets again. Subject: freedom and constraint. **Ball 2000 Conference, Cambridge University Press, Trinity College, Cambridge, UK.**, p. 56, 2000.

DELANNE, Y.; SCHMITT, V.; DOLCEMASCOLO, V. Heavy trucks rollover simulation. In: **Proceedings of 18th International Technical Conference on the Enhanced Safety of Vehicles.** Held Nagoya, Japan.: National Highway Traffic Safety Administration - NHTSA., 2003.

DENATRAN. **Portaria 63/09 - Composições homologadas para o transporte de carga**. 2009. Available at: <http://www.denatran.gov.br/download/Portarias/2009/PORTARIA_DENATRAN_63_09_ANEXOS.pdf>. Accessed on: 19/09/2016.

DHOSHI, N. P.; INGOLE, N. K.; GULHANE, U. D. Analysis and Modification of Leaf Spring of Tractor Trailer Using Analytical and Finite Element Method. **International Journal of Modern Engineering Research**, v. 1, n. 2, p. 719–722, 2011.

DNER. **Manual de Projeto Geométrico de Rodovias Rurais**. Departamento Nacional de Estradas de Rodagem - DNER. Rio de Janeiro - Brasil, 1999.

DNIT. **Manual de Projeto Geométrico de Travessias Urbanas**. Departamento Nacional de Infraestrutura de Transportes - DNIT. Rio de Janeiro - Brasil, 2009.

ERTHAL, J. **Modelo Cinestático para Análise de Rolagem em Veículos**. Phd Thesis (PhD Thesis) — Universidade Federal de Santa Catarina, Florianópolis - Brasil, 2010.

ERVIN, R. D.; GUY, Y. **The Influence of Weights and Dimensions on the Stability and Control of Heavy Duty Trucks in Canada**. UMTRI - The University of Michigan Transportation Research Institute, Final Report UMTRI-86-35/III. Ann Arbor, Detroit, 1986.

FANCHER, P.; WINKLER, C. A methodology for measuring rearward amplification. In: **Proceedings: International Technical Conference on the Enhanced Safety of Vehicles**. USA: National Highway Traffic Safety Administration, 1992. v. 1992, p. 352–358.

FANG, W.; TSAI, H.-C.; LO, C.-Y. Determining thermal expansion coefficients of thin films using micromachined cantilevers. **Sensors and Actuators A: Physical**, Elsevier, v. 77, n. 1, p. 21–27, 1999.

FARLEY, C. T.; MORGENROTH, D. C. Leg stiffness primarily depends on ankle stiffness during human hopping. **Journal of Biomechanics**, Elsevier, v. 32, n. 3, p. 267–273, 1999.

GARCIA-POZUELO, D.; DIAZ, V.; BOADA, M. New tyre-road contact model for applications at low speed. **International Journal of Automotive Technology**, Springer, v. 15, n. 4, p. 553–564, 2014.

GASPAR, P.; SZASZI, I.; BOKOR, J. Reconfigurable control structure to prevent the rollover of heavy vehicles. **Control Engineering Practice**, Elsevier, v. 13, n. 6, p. 699–711, 2005.

GILLESPIE, T. D. **Fundamentals of Vehicle Dynamics**. 7th. ed. Warrendale, PA.: SAE International, 1992. ISBN 1560911999.

GONCALVES, N. R. **Bitrem e outras questões: em defesa do consenso**. 2006. Available at: <http://www.guiadotrc.com.br/pdfiles/artigoneuto.pdf>. Accessed on: 17/08/2016.

HAC, A. Rollover Stability Index Including Effects of Suspension Design. **SAE International - SAE 2002 World Congress**, Detroit-USA, March 4–7., 2002.

HAC, A.; FULK, D.; CHEN, H. Stability and control considerations of vehicle-trailer combination. **SAE International Journal of Passenger Cars-Mechanical Systems**, v. 1, n. 2008-01-1228, p. 925–937, 2008.

HART, P. **Rollover of Heavy Vehicles**. ARTSA - Australian Road Transport Suppliers Association, Hawthorn LPO Vic 3122, Australia, 2012. Available at: <http://www.artsa.com.au/assets/articles/2012_06.pdf>.

HARWOOD, D. W.; TORBIC, D. J.; RICHARD, K. R.; GLAUZ, W. D.; L, E. **Review of Truck Characteristics as Factors in Roadway Design**. Washington, D.C.: National Cooperative Highway Research Program, 2003. ISBN 0-309-08779-1.

HE, Y.; YAN, X.; CHU, D.; WU, C.; CHEN, Z. Contribution of wind forces to rollover stability of heavy duty vehicle. In: IEEE. **2015 International Conference on Transportation Information and Safety (ICTIS)**. Wuhan, China, 2015. p. 173–176.

HEYMAN, J. **Basic Structural Theory**. 1st. ed. New York: Cambridge University Press, 2008. ISBN 13 978-0-511-39692-2.

HIBBELER, R. C. **Mechanics of Materials**. 8th. ed. Boston: Pearson - Higher Education, 2011. ISBN 13 9780136022305.

HU, Z.-Q.; FU, Z.-G.; FANG, H.-R. Study of singularity robust inverse of Jacobian matrix for manipulator. In: **Proceedings. 2002 International Conference on Machine Learning and Cybernetics**. Beijing, China.: IEEE, 2002. v. 1, p. 406–410.

HUANG, Y.; QU, S.; HWANG, K.; LI, M.; GAO, H. A conventional theory of mechanism-based strain gradient plasticity. **International Journal of Plasticity**, Elsevier, v. 20, n. 4, p. 753–782, 2004.

HUSTON, R. L.; KELLY, F. A. Another look at the static stability factor (SSF) in predicting vehicle rollover. **International journal of crashworthiness**, Taylor & Francis, v. 19, n. 6, p. 567–575, 2014.

IMINE, H.; BENALLEGUE, A.; MADANI, T.; SRAIRI, S. Rollover risk prediction of heavy vehicle using high order sliding mode observer: experimental results. **IEEE Transactions on Vehicular Technology**, v. 63, n. 6, p. 2533–2543, 2014.

IPEA. **Estimativa dos Custos dos Acidentes de Trânsito no Brasil com Base na Atualização Simplificada das Pesquisas Anteriores do Ipea**. IPEA - Instituto de Pesquisa Econômica Aplicada. Brasilia., 2015.

ISLAM, M. M.; HE, Y. Design of a Preview Controller for Articulated Heavy Vehicle. **Journal of Mechanics Engineering and Automation**, p. 661–676, 2013.

ISO-14792. **Heavy commercial vehicles and buses - Steady state circular tests**. International Organization for Starndardization. Geneva, Switzerland, 2011.

JABOUR, C. C. **Custos dos Acidentes de Trânsito nas Rodovias Federais**. Publicação IPR - 733. Instituto de Pesquisas Rodoviárias - DNTI. Brasilia, 2004.

JAZAR, R. N. **Vehicle Dynamics: Theory and Application**. 2nd. ed. New York: Springer, 2014. ISBN 978-1-4614-8544-5.

JINDRA, F. Handling Characteristic of Tractor-Trailer Combinations. **SAE**, 1966.

JUNG, J.; SHIM, T.; GERTSCH, J. A vehicle roll-stability indicator incorporating roll-center movements. **IEEE Transactions on Vehicular Technology**, IEEE, v. 58, n. 8, p. 4078–4087, 2009.

KAMNIK, R.; BOETTIGER, F.; HUNT, K. Roll dynamics and lateral load transfer estimation in articulated heavy freight vehicles. **Proceedings of the Institution of Mechanical Engineers, Part D: Journal of Automobile Engineering**, Sage Publications Sage UK: London, England, v. 217, n. 11, p. 985–997, 2003.

KIM, S.-G.; RYU, J. New dimensionally homogeneous jacobian matrix formulation by three end-effector points for optimal design of parallel manipulators. **IEEE Transactions on Robotics and Automation**, IEEE, v. 19, n. 4, p. 731–736, 2003.

KURDI, O.; RAHMAN, R. A.; SAMIN, P. M. Optimization of Heavy Duty Truck Chassis Design by Considering Torsional Stiffness and Mass of the Structure. **Applied Mechanics and Materials**, v. 554, p. 459–463, 2014.

KUTZBACH, K. Mechanische Leitungsverzweigung, ihre Gesetze und Anwendungen. **Maschinenbau. Betrieb**, v. 8, n. 8, p. 710–716, 1929.

LAMBERT, K. **A Study of Vehicle Properties that Influence Rollover and their Effect on Electronic Stability Controllers**. Master's Thesis (Master's Thesis) — Auburn University, Auburn - Alabama, USA, 2007.

LEDESMA, R.; SHIH, S. Heavy and Medium Duty Vehicle Suspension-Related Performance Issues and Effective Analytical Model for System Design Guide. **SAE International**, 1999.

LEE, U. **A Study on a Method for Predicting the Vehicle Controllability and Stability Using the Screw Axis Theory**. Phd Thesis (PhD Thesis) — Hanyang University, Seoul-South Korea, 2001.

LEE, U.; HAN, C. A method for predicting dynamic behaviour characteristics of a vehicle using the screw theory-part 1. **Proceedings of the Institution of Mechanical Engineers, Part D: Journal of Automobile Engineering**, Sage Publications, v. 222, n. 1, p. 65–77, 2008.

LIMA, V.; GARBIN, L.; SANTOS, C. Simulação de dinâmica lateral de um caminhão com suspensão traseira modificada. **SAE - Brasil**, 2011.

LOPES, S. S.; CARDOSO, M. P.; PICCININI, M. S. O Transporte Rodoviário de Carga e o Papel do BNDES. **Revista do BNDS**, Rio de Janeiro, v. 14, n. 29, p. 35–60, 2008.

LUI, P.; RAKHEJA, S.; AHMED, A. Detection of Dynamic Roll Instability of Heavy Vehicles for Open-Loop Rollover Control. In: **1997 International Truck and Bus Meeting**. Cleveland, Ohio.: SAE Special Publications 1308 - SAE Paper No. 973263, 1997. p. 105–112.

MALVIYA, V.; MISHRA, R. Development of an analytical multi-variable steady-state vehicle stability model for heavy road vehicles. **Applied Mathematical Modelling**, Elsevier, v. 38, n. 19, p. 4756–4777, 2014.

MATLAB®. **Version R2013a**. MathWorks, São Paulo, Brazil., 2013.

MEJIA, L.; SIMAS, H.; MARTINS, D. Force Capability Maximization of a 3RRR Symmetric Parallel Manipulator by Topology Optimization. In: **22nd International Congress of Mechanical Engineering (COBEM 2013)**. Ribeirão Preto, SP, Brazil: ABCM - Associação Brasileira de Engenharia e Ciências Mecânicas, 2013.

MELO, R. P. **Avaliação da Estabilidade Lateral de CVCs**. Master's Thesis (Master's Thesis) — Pontifical University Catholic of Parana, Brasil, 2004.

MERLET, J.-P. Jacobian, manipulability, condition number, and accuracy of parallel robots. **Journal of Mechanical Design**, American Society of Mechanical Engineers, v. 128, n. 1, p. 199–206, 2006.

MICHELIN. **Michelin XZA Tire**. Michelin North America, INc. Greenville, SC 29615, 2013.

MIEGE, A.; CEBON, D. Design and implementation of an active roll control system for heavy vehicles. In: **Proceedings of the 6th International Symposium on Advanced Vehicle Control (AVEC)**. Hiroshima - Japan: Advanced Vehicle Control (AVEC), 2002. p. 9–13.

MIRZAEIFAR, R.; DESROCHES, R.; YAVARI, A. A combined analytical, numerical, and experimental study of shape-memory-alloy helical springs. **International Journal of Solids and Structures**, Elsevier, v. 48, n. 3, p. 611–624, 2011.

MORENO, G.; BARRETO, R. L. P.; VIEIRA, R. S.; NICOLAZZI, L.; MARTINS, D. **Three-Dimensional Analysis of Vehicle Stability Using Graph Theory**. Switzerland: Springer International Publishing, 2016. 117–129 p. ISBN 978-3319390185.

MORENO, G.; NICOLAZZI, L.; VIEIRA, R. S.; MARTINS, D. Three-Dimensional Analysis of the Rollover Risk of Heavy Vehicles Using Davies Method. In: **14th World Congress in Mechanical and Machine Science (IFToMM2015)**. Taipei - Taiwan: IFToMM -International Federation for the Promotion of Mechanism and Machine Science, 2015.

MORENO, G.; NICOLAZZI, L.; VIEIRA, R. S.; MARTINS, D. Modeling and analysis of solid axle suspension and its impact on the heavy vehicles stability. In: **CONEM 2016 Congresso Nacional de Engenharia Mecânica**. Fortaleza - Brasil: ABCM - Associação Brasileira de Engenharia e Ciências Mecânicas, 2016.

MORENO, G.; NICOLAZZI, L.; VIEIRA, R. S.; MARTINS, D. Stability of Long Combination Vehicles. **International Journal of Heavy vehicle Systems, (in press)**, 2016.

MORENO, G.; NICOLAZZI, L.; VIEIRA, R. S.; MARTINS, D. Suspension and tyres: the stability of heavy vehicles. **International Journal of Heavy vehicle Systems, (in press)**, 2016.

NAKAMURA, Y.; HANAFUSA, H. Inverse Kinematic Solutions with Singularity Robustness for Robot Manipulator Control. **ASME. Journal of Dynamic System, Measurement, and Control**, v. 108(3), p. 163–171, 1986.

NAVIN, F. Estimating Truck's Critical Cornering Speed and Factor of Safety. **Journal of Transportation Engineering**, 1992.

NZTA. **Heavy vehicle stability guide**. 2008. Available at: <https://www.nzta.govt.nz/assets/resources/heavy-vehicle-stability-guide/docs/heavy-vehicle-stability-guide.pdf>. Accessed on: 17/08/2016.

PACEJKA, H. **Tire and Vehicle Dynamics**. 3rd. ed. Netherlands: Published by Elsevier Ltd, 2012. ISBN 9780080970165.

PASHKEVICH, A.; KLIMCHIK, A.; CHABLAT, D. Enhanced stiffness modeling of manipulators with passive joints. **Mechanism and Machine Theory**, v. 46, p. 662–679, 2011.

PETRASSI, P. **Estudo dos Impactos do Bitrem nas rodovias Federais Brasileiras**. DNTI - Instituto de Pesquisas Rodoviárias. Brasilia, Brasil, 2010.

PINXTEREN, M. **Brake and roll-over performance of longer heavier vehicle combinations**. Master's Thesis (Master's Thesis) — Eindhoven University of Technology, 2010.

POPOV, E. **Engineering Mechanics of Solids**. New Jersey, USA.: Prentice-Hall, Inc., 1998. ISBN 10:0137261598.

PREM, H.; MAI, L.; BRUSZA, L. Tilt testing of two heavy vehicles and related performance issues. In: **International Symposium on Heavy Vehicle Weights and Dimensions, 9th**. Pennsylvania State University, State College, Pennsylvania.: Transportation Research Board, 2006.

RANGANATHAN, R. Rollover threshold of partially filled tank vehicles with arbitrary tank geometry. **Proceedings of the Institution of Mechanical Engineers, Part D: Journal of Automobile Engineering**, Sage Publications Sage UK: London, England, v. 207, n. 3, p. 241–244, 1993.

REMPEL, M. R. **Improving the Dynamic Performance of Multiply-Articulated Vehicles**. Master's Thesis (Master's Thesis) — The University of British Columbia, Vancouver - Canada., 2001.

RICALDE, L. J.; SANCHEZ, E. N.; LANGARI, R.; SHAHMIRZADI, D. Rollover control in heavy vehicles via recurrent high order neural networks. 2008.

RILL, G. Vehicle modeling by subsystems. **Journal of the Brazilian Society of Mechanical Sciences and Engineering**, SciELO Brasil, v. 28, n. 4, p. 430–442, 2006.

RILL, G. **Road Vehicle Dynamics: Fundamentals and Modeling**. Boca Ratón, Florida: CRC Press, 2011. ISBN 978-1-4398-3898-3.

RILL, G.; KESSING, N.; LANGE, O.; J, M. Leaf Spring Modelling for Real Time Applications. In: **18th IAVSD-Symposium**. Atsugi-Japan.: IAVSD-The International Association for Vehicle System Dynamics, 2003.

ROCHA, C.; TONETTO, C.; DIAS, A. A comparison between the denavit–hartenberg and the screw-based methods used in kinematic modeling of robot manipulators. **Robotics and Computer-Integrated Manufacturing**, Elsevier, v. 27, n. 4, p. 723–728, 2011.

RYU, Y. I.; KANG, D. O.; HEO, S. J.; IN, J. H. Rollover Mitigation for a Heavy Commercial Vehicle. **International Journal of Automotive Technology**, 2010.

SAF-HOLLAND. **About Fifth Wheels**. SAF-HOLLAND Group. Germany, 2006.

SAMPSON, D. J.; CEBON, D. Achievable roll stability of heavy road vehicles. **Proceedings of the Institution of Mechanical Engineers, Part D: Journal of Automobile Engineering**, Sage Publications Sage UK: London, England, v. 217, n. 4, p. 269–287, 2003.

SANCHEZ, E. N.; RICALDE, L. J.; LANGARI, R.; SHAHMIRZADI, D. Rollover prediction and control in heavy vehicles via recurrent neural networks. In: **Decision and Control, 2004. CDC. 43rd IEEE Conference on**. Atlantis, Paradise Island, Bahamas: Proceedings of the IEEE International, 2004. v. 5, p. 5210–5215.

SARIYILDIZ, E.; UCAK, K.; OKE, G.; TEMELTAS, H. A Trajectory Tracking Application of Redundant Planar Robot Arm via Support Vector Machines. In: **Proceedings of the Second International Conference on Adaptive and Intelligent Systems**. Berlin, Heidelberg: Springer-Verlag, 2011. (ICAIS'11), p. 192–202. ISBN 978-3-642-23856-7.

SMITH, N. D. Understanding Parameters Influencing Tire Modeling. **Formula SAE Platform - Colorado State University**, 2004.

TAKANO, S.; NAGAI, M. Dynamics control of large vehicles for rollover prevention. In: **Vehicle Electronics Conference, 2001. IVEC 2001.** Thailand: Proceedings of the IEEE International, 2001. p. 85–89.

TAYLOR, R. K.; BASHFORD, L. L.; SCHROCK, M. D. Method for Measuring Vertical Tire Stiffness. **American Society of Agricultural Engineers**, v. 42, n. 6, p. 1415–1419, 2000.

TRUCKSIM®. **Mechanicla Simulation**. Virtual CAE, São Caetano do Sul-SP, Brazil., 2016.

TSAI, L. W. **Robot Analysis - The Mechanism of Serial and Parallel Manipulators**. New York: John Wiley & Sons, 1999. ISBN 0-471-32593-7.

TSAI, L. W. **Mechanism Desing: Enumeration of Kinematic Structures Acording to Function**. Boca Ratón, Florida: CRC press, 2001. ISBN 0849309018.

WALKER, H.; PEARSON, J. **Recommended Regulatory Principles for Interprovincial Heavy Vehicle Weights and Dimensions**. CCMTA/RTAC Vehicle Weights and Dimensions Study Implementation Committee Report - Transportation Association of Canada. Ottawa, Ontario, 1987.

WANG, J.; HOWARD, I. The torsional stiffness of involute spur gears. **Proceedings of the Institution of Mechanical Engineers, Part C: Journal of Mechanical Engineering Science**, SAGE Publications, v. 218, n. 1, p. 131–142, 2004.

WHITEHEAD, R.; TRAVIS, W.; BEVLY, D. M.; FLOWERS, G. **A study of the effect of various vehicle properties on rollover propensity**. Department of Mechanical Engineering, Auburn University, 2004.

WINKLER, C. **Experimental Determination of the Rollover Threshold of Four Tractor-Semitrailer Combination Vehicles**. UMTRI Research Review, The University of Michigan Transportation Research Institute. Ann Arbor, Detroit, 1987.

WINKLER, C. Rollover of Heavy Commercial Vehicles. **UMTRI Research Review, The University of Michigan Transportation Research Institute**, v. 31, n. 4, p. 1–20, 2000.

WINKLER, C.; FANCHER, P.; BAREKET, Z.; BOGARD, S.; JOHNSON, G.; KARAMIHAS, S.; MINK, C. **Heavy Vehicle Size and Weight - Test Procedure for Minimum Safety Performance Standards**. UMTRI Research Review, The University of Michigan Transportation Research Institute. Ann Arbor, Detroit, 1992.

WINKLER, C. B.; ERVIN, R. **Rollover of heavy commercial vehicles**. University of Michigan, Transportation Research Institute Ann Arbor, Michigan, USA, 1999.

WOOD, R. Effective lengths of columns in multi-storey buildings Part II. **The Structural Engineer**, v. 52, n. 8, p. 295–302, 1974.

WOODROOFFE, J.; BLOWER, D.; GORDON, T.; GREEN, P.; LIU, B.; SWEATMAN, P. **Safety Benefits of Stability Control System for Tractor-Semitrailers**. National Highway Traffic Safety Administration - NHTSA - DOT HS 811 205. Washington, D.C., 2009.

WOODROOFFE, J.; SWEATMAN, P.; ARBOR, A.; MIDDLETON, D.; JAMES, R.; BILLING, J. R. **National Cooperative Highway Research Program -** *NCHRP***. Report 671. Review of Canadian Experience with the Regulation of Large Commercial Motor Vehicles**. Washington, D.C.: Ed. National Academy of Sciences, 2010. ISBN 978-0-309-15518-2.

ZHOU, S.; ZHANG, S. Assessing the effect of chassis torsional stiffness on tractor semi-trailer rollover. **Appl. Math**, v. 7, n. 2, p. 633–637, 2013.

LIST OF PUBLICATIONS

PAPERS IN PEER-REVIEWED JOURNALS

1. Moreno, G. G., Nicolazzi, L., Vieira, R. S., Martins, D. *Suspension and tyres: the stability of heavy vehicles*. International Journal of Heavy vehicle Systems, (in press). 2016.

2. Moreno, G. G., Nicolazzi, L., Vieira, R. S., Martins, D. *Stability of Long Combination Vehicles*. International Journal of Heavy vehicle Systems, (in press). 2016.

BOOK CHAPTER

1. Book chapter. Graph-Based Modelling in Engineering. Ed. Zawiślak, S and Rysiński, J. Chapter 9: *Three-Dimensional Analysis of Vehicle Stability Using Graph Theory*. Moreno, G. G., Barreto, R. L. P., Vieira, R. S., Nicolazzi, L., Martins, D. Springer International Publishing, (in press). Switzerland. 2016. ISBN 978-3319390185. DOI $10.1007/978-3-319-39020-8\_9$.

TECHNICAL REPORT

1. Moreno G. G. and Nicolazzi L. and Vieira R. S. and Martins D. (2016c). *Modeling and Analysis of the Trailer Model Davies Method*. Technical Report. Available at: <https://www.research gate.net/publication/313472027_Modeling_and_analysis_of_a_trailer_vehicle_using_Davies_Method>. DOI: 10.13140/RG.2.2.30396.64645. Florianpolis - Brazil.

PAPERS SUBMITTED TO JOURNALS

1. Moreno, G. G., Manenti, V., Nicolazzi, L., Vieira, R. S., Martins, D. *Stability of heavy vehicles: effect of load distribution*. Submitted to Proceedings of the Institution of Mechanical Engineers, Part D: Journal of Automobile Engineering.

2. Moreno, G. G., Nicolazzi, L., Vieira, R. S., Martins, D. *Stiffness and deformation of mechanisms locally flexible bodies: a general method using expanded passive joints*. Submitted to Mechanism and Machine Theory.

PAPERS IN CONFERENCE PROCEEDINGS

1. Moreno, G. G., Vieira, R., Martins, D. *Stability and Road Safety of Long Combination Vehicles (LCV): Issues and Models*. In: 22^{nd} International Congress of Mechanical Engineering (COBEM 2013). Riberão Preto, Es. São Paulo, Brazil, 2013. ISSN 2176-5480. DOI: 10.13140/2.1.1151.2007
2. Moreno, G. G., Vieira, R., Martins, D. *Estabilidad de Combinaciones de Vehículos de Carga (Long Combination Vehicles - LCV): Estudios y Modelos*. In: 11^0 Congreso Iberoamericano de Ingeniería Mecánica - CIBIM11. La Plata - Argentina. 2013. DOI: 10.13140/2.1.3068.1289.
3. Moreno, G. G., Nicolazzi, L., Vieira, R. S., Martins, D. *Three-dimensional Analysis of the Rollover Risk of Heavy Vehicles Using Davies Method*. In: 14^{th} World Congress in Mechanical and Machine Science (IFToMM2015). Taipei - Taiwan, 2015. DOI: 10.6567/IFToMM.14TH.WC.PS4.006.
4. Moreno, G. G., Nicolazzi, L., Vieira, R. S., Martins, D. *Rollover of heavy truck using Davies method*. In: RS5C 2016 - 17^{th} International Conference Road Safety on Five Continents. Río de Janeiro - Brasil. 2016. DOI: 10.13140/RG.2.2.20805.24807.
5. Moreno, G. G., Nicolazzi, L., Vieira, R. S., Martins, D. *Modeling and analysis of solid axle suspension and its impact on the heavy vehicles stability*. In: CONEM 2016 Congresso Nacional de Engenharia Mecânica. Fortaleza - Brasil. 2016. DOI: 10.13140/RG.2.2.32141.33766.

PAPERS SUBMITTED TO CONGRESS

1. Moreno, G. G., Nicolazzi, L., Vieira, R. S., Martins, D. *Rollover of long combination vehicles: effect of overweight*. Submitted to 6^{th} International Symposium on Multibody Systems and Mechatronics - MuSMe. Federal University of Santa Catarina, Florianopolis, Brazil. October 24-28, 2017.

Appendix A

DAVIES METHOD

A.1 SCREW THEORY

Screw theory enables the representation of the instantaneous position of the mechanism in a coordinate system (successive screw displacement method) and the representation of the forces and moments (wrenches), replacing the traditional vector representation. All these fundamentals are presented in this section.

A.1.1 Method of successive screw displacements

The screw displacement of all points of a rigid body are represented by a rotation (θ) around a screw axis (s) followed by a translation (d) along the same axis (TSAI, 1999; LEE, 2001; ROCHA *et al.*, 2011), as shown in Fig. 115.

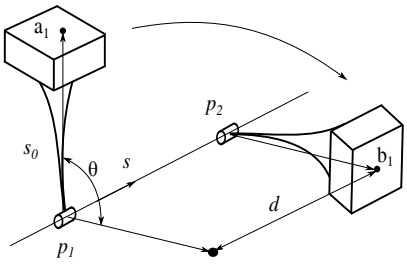

Figure 115 – General displacement of a rigid body in space by screw representation.
Source: Adapted from Lee (2001).

After establishing these concepts, the body instantaneous position matrix (p_2) in a screw displacement is given by the Eq. (A.1):

$$p_2 = Ap_1 \tag{A.1}$$

where p_1 is the reference position matrix,

$$p_1 = \begin{bmatrix} 1 & 0 & 0 & s_{0x} \\ 0 & 1 & 0 & s_{0y} \\ 0 & 0 & 1 & s_{0z} \\ 0 & 0 & 0 & 1 \end{bmatrix} \tag{A.2}$$

and the transformation matrix A is a 4×4 matrix, which includes the rotation matrix whose elements are:

$$\begin{aligned} a_{11} &= (s_x^2 - 1)(1 - \cos\theta) + 1 \\ a_{12} &= s_x s_y (1 - \cos\theta) - s_z \sin\theta \\ a_{13} &= s_x s_z (1 - \cos\theta) + s_y \sin\theta \\ a_{21} &= s_y s_x (1 - \cos\theta) + s_z \sin\theta \\ a_{22} &= (s_y^2 - 1)(1 - \cos\theta) + 1 \\ a_{23} &= s_y s_z (1 - \cos\theta) - s_x \sin\theta \\ a_{31} &= s_z s_x (1 - \cos\theta) - s_y \sin\theta \\ a_{32} &= s_z s_y (1 - \cos\theta) + s_x \sin\theta \\ a_{33} &= (s_z^2 - 1)(1 - \cos\theta) + 1 \end{aligned} \tag{A.3}$$

and the translation vector is given by the last column of the matrix:

$$\begin{aligned} a_{14} &= d s_x - s_{0x}(a_{11} - 1) - s_{0y} a_{12} - s_{0z} a_{13} \\ a_{24} &= d s_y - s_{0x} a_{21} - s_{0y}(a_{22} - 1) - s_{0z} a_{23} \\ a_{34} &= d s_z - s_{0x} a_{31} - s_{0y} a_{32} - s_{0z}(a_{33} - 1) \end{aligned} \tag{A.4}$$

where $s = \begin{bmatrix} s_x & s_y & s_z \end{bmatrix}^T$ denotes a unit vector along the direction of the screw axis, and $s_0 = \begin{bmatrix} s_{0x} & s_{0y} & s_{0z} \end{bmatrix}^T$ denotes the position vector of a point lying on the screw axis. The angle of rotation (θ_i) and the translation (d_i) are known as the screw parameters. The elements $a_{41} = a_{42} = a_{43} = 0$ and $a_{44} = 1$ complete the matrix.

A.1.2 Wrench - forces and moments

In the static analysis, all mechanism forces and moments are represented by wrenches ($\$^A$), according to Eq. (A.5).

$$\$^A = \left\{ \begin{array}{c} s_{0i} \times F_i \\ F_i \end{array} \right\} \tag{A.5}$$

where F_i is the force applied on joint i of the mechanism, and $s_{0i} = \left[\begin{array}{ccc} s_{0ix} & s_{0iy} & s_{0iz} \end{array} \right]^T$ is the instantaneous position vector of the wrench i, related to the inertial reference point of the mechanism. The vector s_{0i} is obtained from the first three terms of the last column of Eq. (A.1).

The wrench decomposition (Eq. (A.5)) provides the Eq. (A.6), in which (s_i) is the wrench orientation vector i,

$$\$^A = \left\{ \begin{array}{c} s_{0i} \times s_i \\ s_i \end{array} \right\} F_i \tag{A.6}$$

for pure moment (M), the wrench has the form presented by Eq. (A.7),

$$\$^A = \left\{ \begin{array}{c} s_i \\ 0 \end{array} \right\} M \tag{A.7}$$

in a more compact form, the wrench can be represented by Eq. (A.8)

$$\$^A = \widehat{\$}^A . \Psi \tag{A.8}$$

where $\widehat{\$}^A$ is the normalized wrench (screw) and Ψ is its magnitude.

A.2 GRAPH THEORY

Kinematic chains and mechanisms are constituted by links and joints, which can be represented in a more abstract approach by graphs, whose vertices correspond to the links and edges correspond to the joints and external forces(CROSSLEY, 1964; TSAI, 2001).

This methodology is explained with a four-bar mechanics; Fig. 116 illustrates the kinematic structure and the graph of a four-bar mechanism, which contains four revolute joints "R" identified by letters *a, b, c* and *d*, and the four links are identified by numbers 1, 2, 3 and 4.

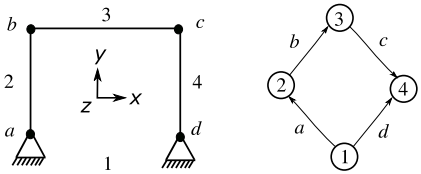

Figure 116 – Four-bar mechanism and the corresponding graph.

The direct coupling graph can be represented by the incidence matrix $[I]$ (DAVIES, 1995), as indicated in Eq. (A.9).

$$I_{4\times4} = \begin{bmatrix} 1 & 0 & 0 & 1 \\ -1 & 1 & 0 & 0 \\ 0 & -1 & 1 & 0 \\ 0 & 0 & -1 & -1 \end{bmatrix} \tag{A.9}$$

The incidence matrix provides the mechanism cut-set matrix $[Q_{INT}]$, Eq. (A.10), where each line represents a cut graph and the columns represent the mechanism joints (DAVIES, 1995). In addition, this matrix allows defining three graph branches (edges *a, b* and *c* - identity matrix) and a chord (edge *d*), as shown in Fig. 117(a).

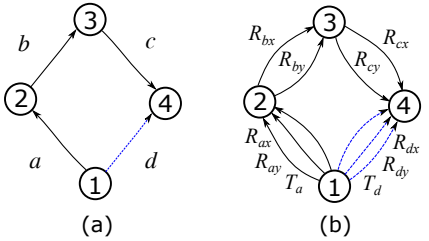

Figure 117 – a) - Direct coupling graph with branch and chord. b) - Direct coupling graph expanded.

$$[Q_{INT}]_{3\times4} = \left[\begin{array}{ccc|c} 1 & 0 & 0 & 1 \\ 0 & 1 & 0 & 1 \\ 0 & 0 & 1 & 1 \end{array}\right] \tag{A.10}$$

For planar mechanisms, a revolute joint "*R*" allows a rotation (*z*-axis) and constrains two translations (R_x, R_y) (TSAI, 2001). Figure 117b

shows the direct coupling graph expanded with the constraints of each joint. Additionally, the external forces in the mechanism are also included: input torque (joint a - T_a) and output torque (joint d - T_d).

Equation (A.11) presents the expanded cut-set matrix $[Q]$, where each line represents a cut graph (Fig. 118), and the columns represent the joint constraints and the external forces present on the mechanism.

$$[Q]_{3\times 10} = \begin{array}{c} \\ Cut1 \\ Cut2 \\ Cut3 \end{array} \begin{array}{c} \begin{array}{cccccccccc} R_{ax} & R_{ay} & T_a & R_{bx} & R_{by} & R_{cx} & R_{cy} & R_{dx} & R_{dy} & T_d \end{array} \\ \begin{bmatrix} 1 & 1 & 1 & 0 & 0 & 0 & 0 & 1 & 1 & 1 \\ 0 & 0 & 0 & 1 & 1 & 0 & 0 & 1 & 1 & 1 \\ 0 & 0 & 0 & 0 & 0 & 1 & 1 & 1 & 1 & 1 \end{bmatrix} \end{array} \tag{A.11}$$

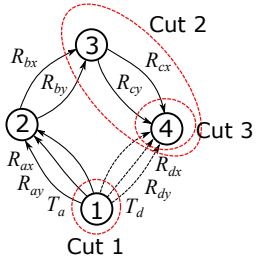

Figure 118 – Cut-set graph.

A.3 KIRCHHOFF'S LAWS

The Kirchhoff's laws for electric circuits were adapted by Davies (1981) to be used on mechanical systems.

Adapting the Kirchhoff-Davies cut-set law, it was possible to establish the relationship between actions belonging to the same partition or node, which contributed to the static analysis. Davies states that the wrench algebraic sums belonging to the same partition or cut is zero, which is the *Cut-set Law*.

According to *Cut-set Law*, the algebraic sum of the normalized wrenches (Eq. (A.8)) belonging to the same cut (Fig. 118) or each line of the expanded cut-set matrix $[Q]$ (Eq. (A.11)) is zero.

The solution of the equations given by the *Cut-set Law* enables the static solution of the proposed mechanism.

Appendix B

CASE STUDY - TRUCK

In this study, a truck with an axle on front and two axles on rear was analyzed (Fig. 119). Figure 120 and Table 22 show the parameters of the truck used in this analysis.

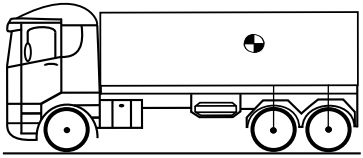

Figure 119 – Truck.

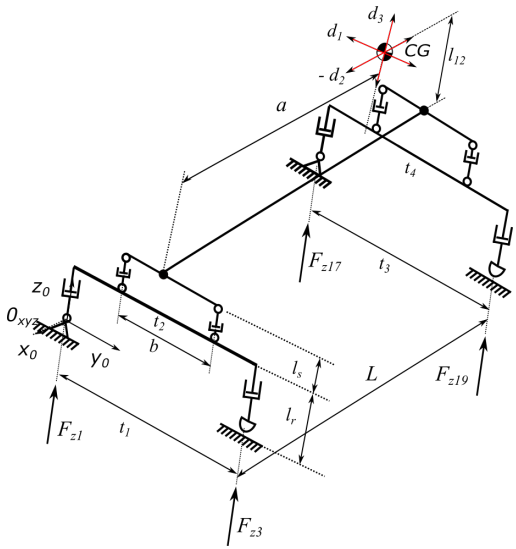

Figure 120 – Parameters of the truck.

Table 22 – Parameters of the truck model.

Parameter	Value	Units
Truck weight - W	255	kN
Front and rear track widths - $t_{1,3}$	1.86	m
Front and rear axle widths - $t_{2,4}$	1.86	m
Stiffness of the suspension per axle - k_{Ls} (HARWOOD *et al.*, 2003)	1800	kN/m
Number of axles at the front (2 tires per axle)	1	
Number of axles at the rear (4 tires per axle)	2	
Vertical stiffness per tire - k_T (HARWOOD *et al.*, 2003)	840	kN/m
Initial suspension height - $l_s = l_{3,4,9,10}$	0.205	m
Initial dynamic rolling radius - $l_r = l_{1,2,7,8}$ (MICHELIN, 2013)	0.499	m
Lateral separation between the springs - b	0.95	m
CG height above the chassis - l_{12}	1.41	m
Wheelbase of the truck - L	7.62	m
Distance from the front axle to the center of gravity - a	5.63	m
Lateral *CG* displacement, offset of the cargo d_1	$\pm$ 0.1	m
Longitudinal and vertical *CG* displacement d_2 - d_3	0	m
Steer angle (ψ)	0	$^\circ$

B.1 THREE-DIMENSIONAL STATIC ROLLOVER THRESHOLD

The SRT factor calculation was obtained using the steady state circular test (ISO-14792, 2011), the load conditions include a load laterally centered and load with *CG* displacement.

The simulation model was applied using MATLAB® (2013). To calculate the SRT factor, the inertial force was increased until the lateral load transfer in the rear axle become complete.

At the rollover threshold limit, the normal load F_{z19} reaches zero (Eqs. (6.17) and (6.39)). Hence, applying this condition Fig. 121 shows the decrease of the normal force in the rear inner tire (F_{z19}) with respect to the increase of the inertial force (SRT factor).

The example shows the normal force on the rear inner tire with respect to the inertial force: in the first stage, the model considers the tires and suspension systems, SRT_{ts} factor for the model is 0.3593.

In the second stage, the truck model considers all systems and the LLT_f coefficient on the front axle is approximately 90 % of the LLT_r coefficient on the rear axle (as shown in Fig. 122). Applying this concept, the SRT_{3D} factor reduces to 0.3456.

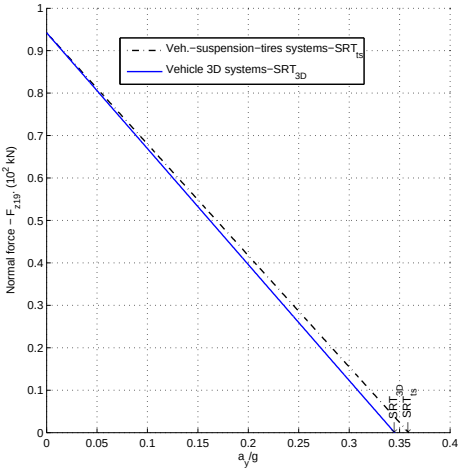

Figure 121 – Normal load F_{z-19} - SRT factor - Truck.

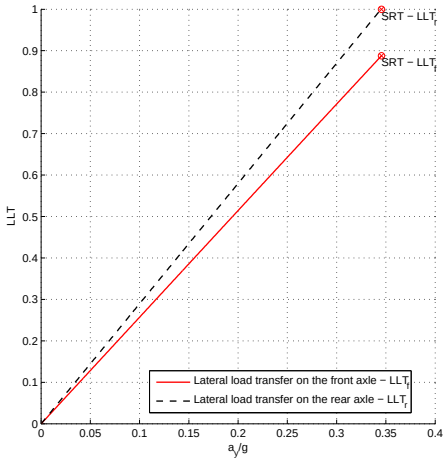

Figure 122 – Lateral load transfer - SRT factor - Truck.

The reduction in the SRT factor results from the combined action of the truck systems, which allows a body roll angle of the truck of $\theta_{3D} = 6.3°$, as shown in Fig. 123.

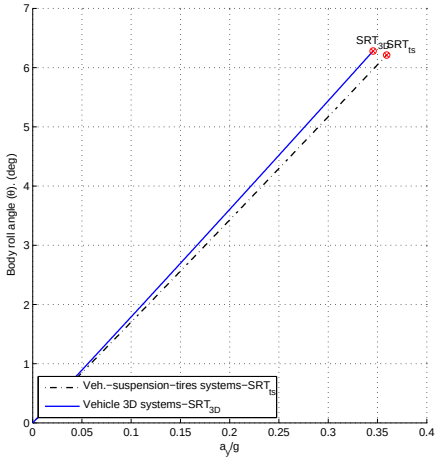

Figure 123 – Total body roll angle (θ_{3D}) - SRT factor - Truck.

Furthermore, this model also allows the determination of the lateral (h_1) and vertical (h_2) *CG* displacements.

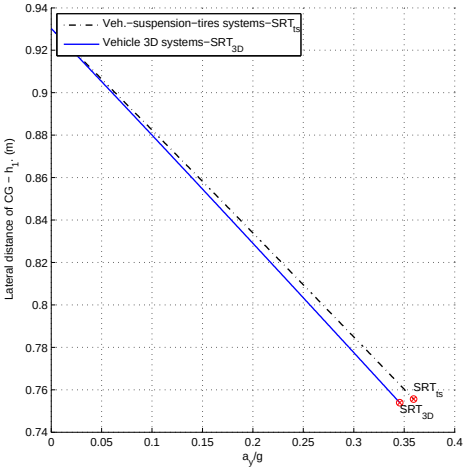

Figure 124 – Lateral movement of *CG* - SRT factor - Truck.

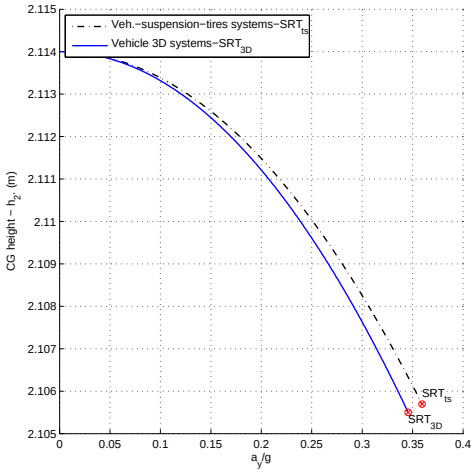

Figure 125 – Vertical movement of *CG* - SRT factor - Truck.

Appendix C

CASE STUDY - SEMI-TRAILER

In this study, the trailer of a semi-trailer with two axles on front (truck) and three axles on rear was analyzed (Fig. 126). Figure 127 and Table 23 show the parameters of the trailer used in this analysis.

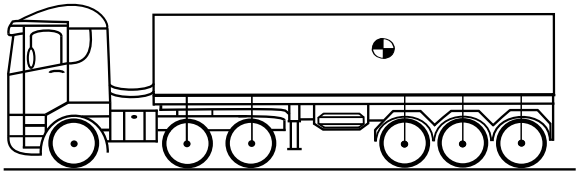

Figure 126 – Semi-trailer.

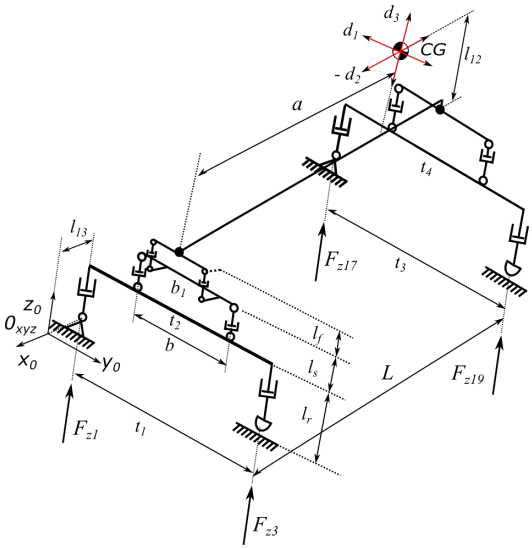

Figure 127 – Parameters of the trailer model.

Table 23 – Parameters of the trailer model - Semi-trailer.

Parameter	Value	Units
Trailer weight - W	392.13	kN
Front and rear track widths - $t_{1,3}$	1.86	m
Front and rear axle widths - $t_{2,4}$	1.86	m
Stiffness of the suspension per axle - k_{Ls} (HARWOOD *et al.*, 2003)	1800	kN/m
Number of axles at the front (trailer) (4 tires per axle)	2	
Number of axles at the rear (trailer) (4 tires per axle)	3	
Vertical stiffness per tire - k_T (HARWOOD *et al.*, 2003)	840	kN/m
Stiffness of the fifth-wheel - k_f	7500	kN/m
Initial suspension height - $l_s = l_{3,4,9,10}$	0.205	m
Initial dynamic rolling radius - $l_r = l_{1,2,7,8}$ (MICHELIN, 2013)	0.499	m
Initial height of the fifth wheel - l_f	0.1	m
Lateral separation between the springs - b	0.95	m
Fifth-wheel width - b_1	0.6	m
CG height above the chassis - l_{12}	1.21	m
Distance between the fifth wheel and the front axle - l_{13}	0.2	m
Wheelbase of the trailer - L	8.7	m
Distance from the front axle to the center of gravity - a	5.55	m
Lateral *CG* displacement, offset of the cargo d_1	$\pm$ 0.1	m
Longitudinal and vertical *CG* displacement d_2 - d_3	0	m
Trailer/trailer angle (ψ)	0	$^\circ$

C.1 THREE-DIMENSIONAL STATIC ROLLOVER THRESHOLD

The SRT factor calculation was obtained using the steady state circular test (ISO-14792, 2011), the load conditions include a load laterally centered and load with *CG* displacement.

The simulation model was applied using MATLAB® (2013). To calculate the SRT factor, the inertial force was increased until the lateral load transfer in the rear axle become complete.

At the rollover threshold limit, the normal load F_{z19} reaches zero (Eqs. (6.17) and (6.39)). Hence, applying this condition Fig. 128 shows the decrease of the normal force in the rear inner tire (F_{z19}) with respect to the increase of the inertial force (SRT factor).

The example shows the normal force on the rear inner tire with respect to the inertial force: in the first stage, the model considers the tires and suspension systems, SRT_{ts} factor for the model is 0.4179.

Finally, in the second stage, the trailer model considers all systems and the LLT_f coefficient on the front axle is approximately 70 % of the LLT_r coefficient on the rear axle. Applying this concept, the SRT_{3D} factor reduces to 0.3629.

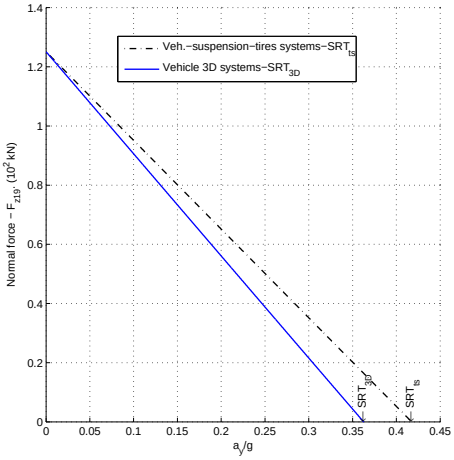

Figure 128 – Normal load F_{z-19} - SRT factor - Semi-trailer.

The reduction in the SRT factor results from the combined action of the trailer systems, which allows a body roll angle of the trailer of $\theta_{3D} = 5.48^0$, as shown in Fig. 129.

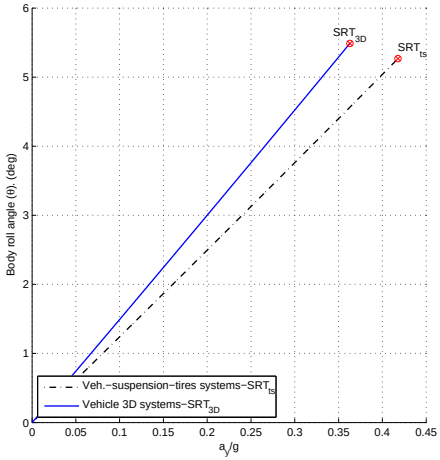

Figure 129 – Total body roll angle of the trailer (θ_{3D}) - SRT factor - Semi-trailer..

Furthermore, this model also allows the determination of the lateral (Fig. 130) and vertical (Fig. 131) *CG* displacements.

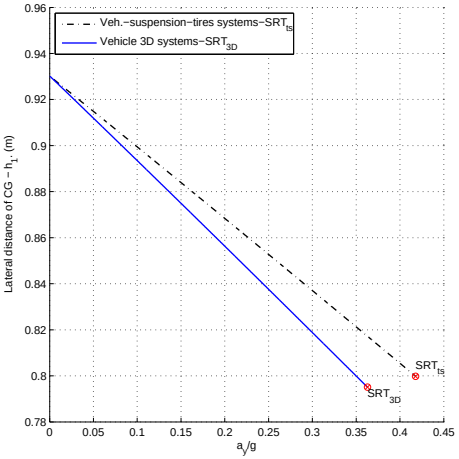

Figure 130 – Lateral movement of *CG* - Semi-trailer.

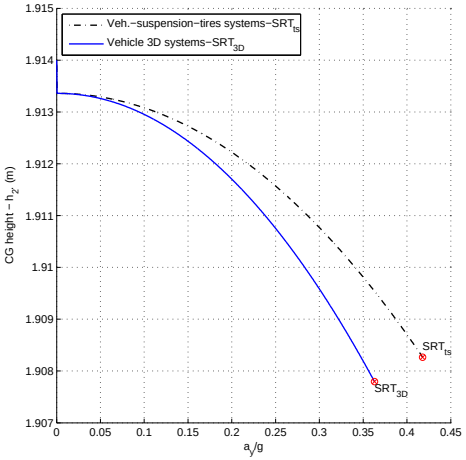

Figure 131 – Vertical movement of *CG* - SRT factor - Semi-trailer.

AUTHOR BIOGRAPHY

Gonzalo Guillermo Moreno Contreras: Mechanical Engineering degree from Francisco de Paula Santander University - Colombia (1999), master's in Mechanical Engineering from the University of the Andes - Colombia (2004) and currently a doctoral student at the Mechanical Engineering Department at Federal University of Santa Catarina (2016). Lecturer of Mechanical Engineering Department at University of Pamplona - Colombia. He has experience in Mechanical Engineering, focusing on machine design, acting in the following areas: statics and dynamics of mechanical systems with emphasis on mechanical design.

Email addresses: gmoren@unipamplona.edu.co, gmoren@gmail.com, gmoren@hotmail.com.